MOLECULAR BEAM SCATTERING

by

JOHN HAY KERR

THESIS PRESENTED FOR THE DEGREE OF

DOCTOR OF PHILOSOPHY

UNIVERSITY OF EDINBURGH

MARCH 1975

A B S T R A C T

The subject of this thesis is the chemical information which can be obtained from molecular beam experiments in the superthermal energy region. In the introduction, the importance of intermolecular potential surfaces and of the beam method of determining them are discussed. The possibility of obtaining information on inelastic events from the observation of the elastic differential cross section is noted, with reference to recent results for ion scattering. In Chapter 2 the apparatus used in the experiments is described. An innovation is a device to monitor the cross beam intensity. The advantages of using a computer for real time collection and analysis of data from a molecular beam experiment and the implementation and performance of such a system is the subject of Chapter 3. In Chapter 4, experimental values of the elastic differential cross sections of potassium from Ar, N_2, SF_6 and CH_3I at energies between 100 and 500eV are reported. These are used to obtain the form of the potential surfaces in the repulsive region, and the anomalous results for SF_6 and, to a lesser extent, CH_3I and N_2 are attributed to chemiionisation. Simple theoretical calculations are performed to illustrate how potential curve crossings could give rise to interference structure, and the absence of such structure in the experimental results is discussed and tentatively attributed to the effect of crossings to the ionic surface. In Chapter 5 results of classical trajectory calculations for the system K/I_2 are presented. The mechanisms for the various effects are deduced from their impact parameter and collision energy dependence and certain observables are calculated.

CONTENTS

CHAPTER 1

INTRODUCTION

This thesis describes some investigations of collisions between neutral species in the 100 - 500eV region by the method of crossed molecular beams. The effects accessible for atomic collisions in this energy range are chemical reaction, ionisation, electronic excitation and elastic scattering. If one of the colliding partners is a molecule, vibrational and rotational excitation are also possible. In addition to their intrinsic interest, these processes are important in understanding the bulk properties of matter, chemical kinetics, space chemistry and plasmas and also for developing theories which will allow the evaluation of cross sections in experimentally inconvenient or inaccessible regions.

Collision phenomena can be understood in terms of movement across potential energy surfaces. The potential energy of a two atom system is defined for a fixed internuclear separation, but an adiabatic potential surface so calculated is applicable to collisions only if the Born-Oppenheimer approximation is valid - ie if the nuclear motion is slow enough for the electron distribution to adjust almost instantaneously. This only breaks down in the keV region (THO 63) except in cases where the energy separation between two states is small, when the nuclear motion can induce transitions between the states.

The form of diatomic potentials is well understood. At separations, R, large enough for orbital overlap to be negligible, the instantaneous correlation between electron distributions produces net attraction. This can be expressed as an expansion in I/R by

second order perturbation theory (MAR 69). The leading (dipole - dipole) term, proportional to R^{-6}, is dominant and may be calculated accurately for many electron atoms as unperturbed core electron wave functions can be used (DAL 67). For small internuclear separations, the internuclear repulsion is augmented by the strong repulsion caused by the impending violation of the Pauli exclusion principle for the united atom. Since all orbitals are strongly perturbed, exact calculations have only been carried out for systems with a small number of electrons (KRA 65, BER 73). Calculations for many electron atoms using a statistical model for the electronic distribution have been carried out by A.A. Abrahamson (ABR 63) who points out the paucity of experimental results against which to test his calculations. These results suggest that an exponential form is the best analytical representation of the repulsive potential.

The classical method of determining intermolecular potentials experimentally is from bulk properties themselves as reviewed by D.D. Fitts (FIT 66). Bulk properties such as the virial coefficients, transport properties of gases and properties of crystals are related to the intermolecular potentials through complex integral formulae which cannot be inverted to give the potentials directly from the data. Forward calculations are therefore performed using parameterised forms and the parameters estimated by fitting methods. Unfortunately, no 2 or 3 parameter form fits all the data over the whole experimental temperature range. Although all analytical forms have an R^{-6} attractive term in accord with the theoretical results for dispersion

forces, the repulsive term has been variously represented by inverse power repulsion (Lennard Jones), inverse power repulsion with impenetrable core (Kihara), and the slightly differing exponential forms of Morse, Buckingham-Corner and exp (α, 6). It appears that the process of averaging the assumed potential over impact parameter and velocity during the forward calculation makes evaluation of unique parameters impossible. In addition, the experimentally feasible temperature range limits the region over which the potential can be evaluated in the repulsive region.

Numerical values of the potential for diatomic molecules in the well region may be obtained from vibration rotation spectroscopy by the R.K.R. method (GIN 65). In certain cases vacuum ultra-violet spectroscopy can be used to determine the potentials of excited states, including purely repulsive ones.

In recent years the molecular beam method has become increasingly used for investigating collision phenomena and determining intermolecular potentials (FLU 73). The method consists of producing a well collimated stream of molecules sufficiently tenuous and in a sufficiently good vacuum that collisions within the beam and with the background gas are negligible. This beam is then allowed to intersect with a target which may be another beam or a stationary gas. The total cross section may be determined from the attenuation of the primary beam, the differential cross section from the variation of scattered intensity with angle. The experimental results are related to collision phenomena and intermolecular potentials by scattering

theory originally developed for nuclear scattering (NEW 66). For molecular beam experiments it is often valid and convenient to use semiclassical approximations (FOR 59) in which the nuclei move along classical trajectories and there is associated with each particle, a phase shift related to the classical action integral which determines the quantum mechanical effects. The principal advantages of the method are the observation of the results of single collisions, possibly with preservation of angular information and the ability to determine the velocity and quantum states of the colliding molecules before and after collision. Determination of potentials from elastic scattering has been reviewed at thermal energies (PAU 65) and above (AMD 66). At thermal energies, the form of the potential in the attractive region and around the minimum may be obtained by the semi-classical theory of Ford and Wheeler (FOR 59), either from the rainbow structure in the differential cross section (MOR 62) or from the glory undulations in the velocity dependence of the total cross section (ROT 63). These methods determine two parameters of an analytical form, corresponding to the depth and position of the potential minimum. Recently Buck (BUC 71) has shown that provided the high frequency structure resulting from the repulsive branch is resolved in addition to the rainbow structure, relative differential cross sections may be used to construct a deflection function which in turn may be invented by the method of Firsov (FIR 53) to give the potential directly. The potentials for some mercury/alkali metal systems have been determined by this method (BUC 71).

At superthermal energies, most information for neutral systems has come from the measurement of absolute total cross sections as a function of collision energy (AMD 66). The data is interpreted using the result of Kennard (KEN 38) for the classical differential cross section at small angles and yields the short range repulsive form of the potential. This is generally expressed as an inverse power form and a wide range of powers are reported. More recently Politiek, Schiffer and Los (POL 70) have reported total cross section measurements for pottasium-rare gas systems from thermal energies up to several eV. Both Lennard Jones (7, 6) and exp (α, 6) forms are found to fit the data. Also, Malerich and Cross (MAL 70) have measured total cross sections for alkali-rare gas systems at energies from 6 to 1,000 eV. They fitted their data to an inverse power form of the potential and also showed that an exponential form did not fit. This work also underlines a weakness in commonly used parameterised forms first pointed out by Buckingham (BUC 47), namely that the long range attractive term should not simply be added to the repulsive term at small separations where it is invalid. Malerich and Cross propose using a switching function to connect the two branches. The potentials from the above experiments, although determined accurately, are valid over a rather small range of potential energy relative to the collision energies used. This is because the results are insensitive to the form of the potential in the region which results in scattering away from the detector. The advantage of this fact is that the increased intensity of high energy beams (as ion beams which

diverge less at high energies are used to produce the high energy neutrals) can be used to make very accurate determinations of the potentials in the chemically interesting region.

Electronic excitation or ionisation may be important if the trajectory passes through the region of an avoided crossing (COU 72) during the collision. According to the theory of Landau and Zener (LAN 32, ZEN 32) transitions between electronic states occur only in narrow regions where there is a pseudocrossing of the potentials corresponding to the two states. The transition probability is a function of the slopes of the potentials at the crossing point, the coupling potential and the relative velocity. The results of such crossings are observed in chemi-ionisation experiments and in molecular beam chemiluminescence (KEM 70, LAC 70) in which a fast alkali beam is passed through a vapour cell and light of a wavelength corresponding to emission from excited atomic states is observed. The threshold energies are much higher and the cross sections much smaller for the inert gases than for certain molecular targets. This indicates that the curve crossing responsible, which must be well up the repulsive wall for the inert gases, occurs at much larger separations for the molecules investigated. An intermediate ionic surface connecting initial and final states has been postulated. Several systems have been investigated in the time of flight experiments of Pauly (GER 73) in which the energy loss spectrum of the alkali beam is measured for various energies and scattering angles. The distinction between the alkali and molecular cases is confirmed.

In systems where there is a curve crossing at internuclear separation, Rc, a trajectory with impact parameter less than Rc leading to either exit channel may traverse either potential surface between the two crossing points.

According to the Landau-Zener theory, there is an equal probability of transition at either crossing. Thus a high probability of exiting in the upper state must be accompanied by a significant probability of exiting in the lower state after traversing the upper state between crossing points. As wavelength changes with energy loss, there can be no interference between upper and lower exit states but the two possible routes to exit in one state will have different phase shifts associated with them. This suggests that interference structure in the differential cross section for one channel may be used to obtain information about crossings to excited states during the collision. Such structure has been observed in a number of experiments. The differential cross section for sodium atoms ionised on collision with bromine at a few eV has been measured by Delvigne and Los (DEL 74) and shows much structure which can be predicted by the concept of interfering branches with crossing probabilities given by the Landau-Zener theory. Fluendy, Lawley and Reddington (RED 73) have performed a two state quantum calculation which illustrates the effect of crossings to and from the ionic surface on the differential cross section of neutral potassium scattered from iodine. Again much interference structure is predicted.

Interference effects which can be expected in atom scattering have been reviewed by Nikitin (NIK 72). In the case of resonant change transfer, interference patterns have been observed (SIS 70) and in the case of identical bosons, structure due to interference between scattered and knocked on particles is predicted and has been observed for He/He scattering (KEN 69). This data has been inverted by semiclassical methods and gives a potential in good agreement with theory. The wealth of information which can be obtained from differential cross sections in ion/atom scattering experiments has prompted the use of the term 'collision spectroscopy' (SMI 67). The observed structure is interpreted as due to crossings to electronically excited states on the repulsive wall, and the scaling law suggested by the high energy expansion of the differential cross section allows data for a range of energies to be plotted on one curve. In addition, features occurring at the same value of energy times scattering angle ($E\theta$) originate at a common area of the interaction potential. The anomalously large peaks appearing at the onset of structure have been explained as having a similar origin to the rainbow effect in thermal energy scattering, ie a minimum in the value of scattering angle as a function of impact parameter. This is not caused by a minimum of the potential as in the thermal case however, but by the abrupt change in gradient at the crossing (OLS 71).

Other effects expected in molecular collisions have been investigated by molecular beams techniques. The state selection method has been used to measure rotational excitation (TOE 65) and

energy loss measurements have been used to investigate rotational excitation (BLY 64) and vibrational excitation (USD71, DAV 71).

The application of molecular beams to chemical reaction has been extensive and fruitful (HER 73). However the reactive channel closes rapidly for energies much above the endothermicity of the reaction as has been shown by Monte-Carlo calculations in the case of K/I_2 (McD 73). This is essentially a consequence of the conservation of momentum and is the subject of Chapter 5.

To summarise, the molecular beam method appears to be most useful in determining potential energy functions directly and in investigating in detail the various elastic and inelastic collision processes over a wide range in energy. The experiments described in the following chapters were designed to look for structure in the small angle elastic differential scattering of potassium scattered from various molecular targets arising from the possible accessibility of two or more compound states during the collision.

CHAPTER 2

APPARATUS

The apparatus used to obtain the results reported in this thesis was designed to measure the differential scattering cross sections of alkali metals at energies from 10 to 1000eV from various molecular targets. The measurements are confined to a small angular range because of low scattered intensity and since the beam energy can be varied to explore different regions of impact parameter. To date experiments have been performed only with potassium as the main beam and for energies between 100 and 500eV. The initial construction of the apparatus has been described by Duchart (DUC 71) and subsequent alterations by Reddington (RED 73). The apparatus will therefore be described briefly with particular attention given to alterations made since the last report.

2.1 General Description

The main beam of high energy potassium atoms is produced by ionisation, electrostatic acceleration and neutralisation. This beam is collimated and allowed to intersect at right angles with a target beam produced by thermal effusion from a slit or capillary array. The scattered potassium atoms are detected in a plane at right angles to the cross beam by surface ionisation on a tungsten/platinum filament. The ions produced are focussed into an electron multiplier whose output pulses are amplified, discriminated and counted. The changes made since the last report are the installation of a cross beam monitor, the introduction of a capillary array in the cross beam source and the removal of mass selection of the detected ions. A diagram of the apparatus is given in Figure 2.1.

FIGURE 2.1

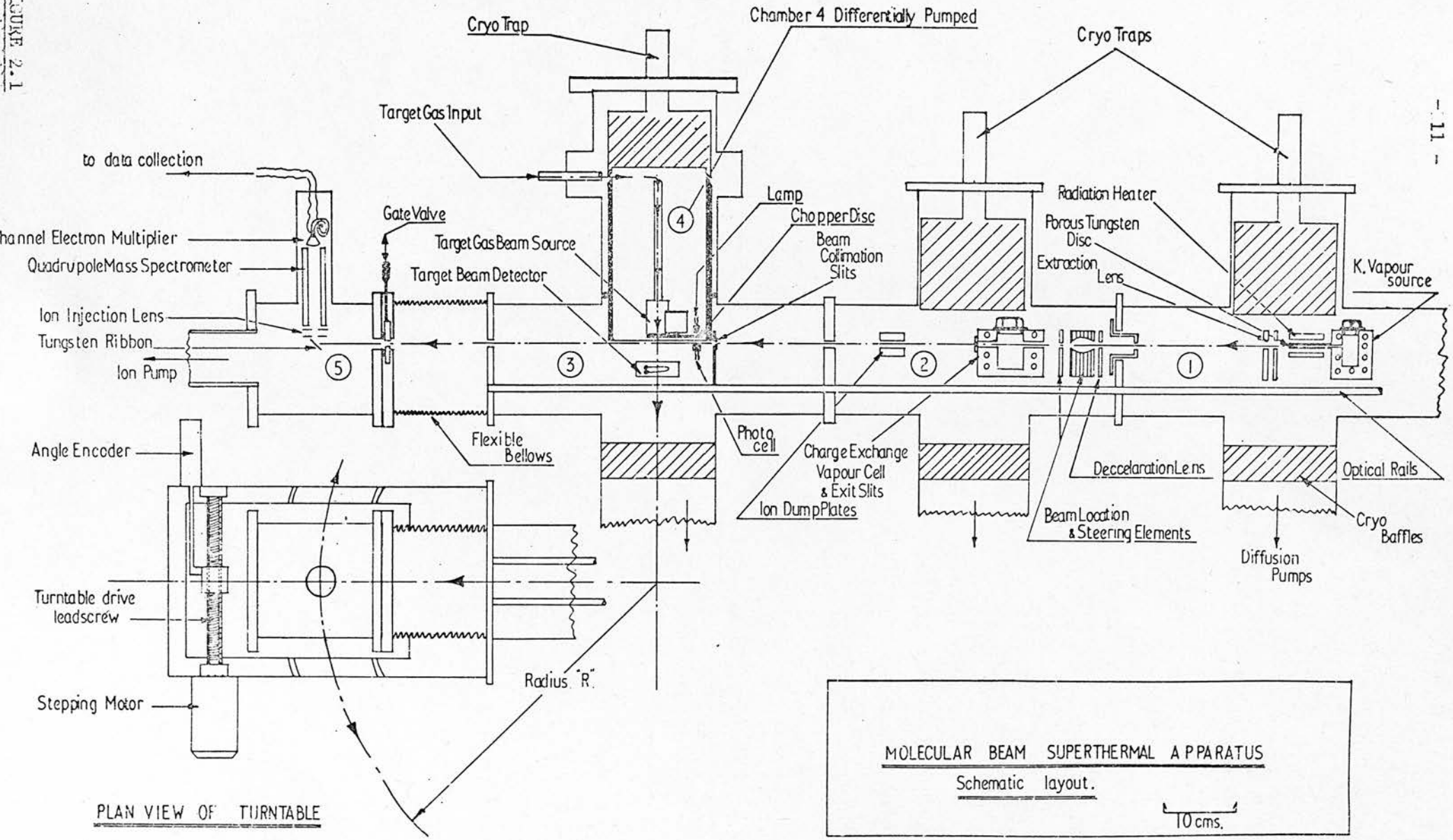
Cryo Trap
Chamber 4 Differentially Pumped
Cryo Traps
Target Gas Input
to data collection
Lamp
Chopper Disc
Radiation Heater
Porous Tungsten Disc
Gate Valve
Target Gas Beam Source
Beam Collimation Slits
Extraction Lens
K. Vapour source
Channel Electron Multiplier
Quadrupole Mass Spectrometer
Target Beam Detector
Ion Injection Lens
Tungsten Ribbon
Ion Pump
5
3
4
2
1
Flexible Bellows
Photo cell
Charge Exchange Vapour Cell & Exit Slits
Ion Dump Plates
Deceleration Lens
Optical Rails
Angle Encoder
Beam Location & Steering Elements
Cryo Baffles
Diffusion Pumps
Turntable drive leadscrew
Radius "R"
Stepping Motor
PLAN VIEW OF TURNTABLE
MOLECULAR BEAM SUPERTHERMAL APPARATUS
Schematic layout.
10 cms.

2.2 Vacuum System

The various components are contained in a vacuum system consisting of five differentially pumped chambers. The first four contain the main beam ion source, the neutralisation chamber, the cross beam source and the intersection region respectively. These chambers are pumped by oil diffusion pumps with liquid nitrogen cooled cryo-baffles. These are supported by three rotary pumps on a common backing line sections of which may however be valved off to help in locating leaks. The fifth chamber contains the detection filament and electron multiplier. It is connected to the collision chamber by flexible stainless steel bellows and may be rotated up to 5^{o} on either side of the main beam line. The only aperture in the detection chamber is a slit which allows the filament to 'see' a narrow cone containing the intersection region. The chamber is initially pumped down through this slit which is then valved shut and an ion pump is used to bring it down to a high vacuum. The ion source and charge exchange chambers are maintained at around 10^{-6} torr during an experiment, the cross beam source at about 2×10^{-5} torr and the collision chamber at 7×10^{-6} torr. The ion pump is kept off during data collection to eliminate noise but is switched on periodically during an experiment to maintain the detector chamber at around 10^{-6} torr on average.

2.3 Main Beam Source

Potassium ions are produced in chamber one by surface ionisation on hot tungsten. This is achieved by allowing potassium vapour to pass through a porous tungsten disc which is maintained at $1200^{o}C$ by a radiation heater. Backlash heating from the nozzle keeps the potassium

resevoir at around 230°C which produces a sufficiently high vapour pressure. To obtain a beam of intermediate energy the ions are accelerated to a high potential then focussed and decelerated to the energy required. This minimises loss of intensity due to divergence of the ion beam. The ion source is kept at a positive voltage corresponding to the final beam energy and the two component acceleration lens is also in the first chamber. The acceleration voltages used are around 1kV. An equipotential region is maintained at the acceleration voltage through the bulkhead separating chambers 1 and 2 where the deceleration, focussing and neutralisation is carried out.

The ions are decelerated and focussed by a Lindholm Gustafsson lens (HAS 62) whose modification to suit the apparatus by calculation and experiment is fully described by Reddington. To allow for slight misalignments or perturbations of the field a three element steering plate was added to guide the beam into the entrance aperture. The lens itself contains four more steering plates and care is required in setting the steering voltages to avoid working with a 'zig-zag' beam. Since the last lens element is at earth potential, the beam emerges at its final energy and enters the neutralisation chamber.

Neutralisation takes place by resonant charge transfer, the cross section for which is around 200A_o^2 for potassium in this energy region (MAH 68). Because of the large separations at which charge transfer takes place and the small mass of the electron, the ions are almost undefelcted in the process (HAS 62). The charge exchange

chamber is loaded with distilled potassium and kept at a temperature of around 150°C by a three term controller. The exit slits from the charge exchange chamber are used to collimate the beam and any remaining ions are deflected by a transverse field of 100 volts. The ion current on the dump plates is monitored while setting the variable lens potentials.

2.4 Cross Beam Source

The cross beam material is delivered from an external gas line although provision is made for an internal oven in the case of insufficiently volatile materials. The cross beam is chopped at 70hz by a slotted disc. The light from a bulb falling on a photo-cell is also chopped and the resulting electrical signal is used to gate the two channel detection system. The cross beam emerges from chamber four to chamber three via a narrow collimation slit.

The collision chamber is thus free from beam sources and can be pumped to around 10^{-7} torr while the cross beam is valved off. With a simple orifice in the cross beam nozzle however, the pumps were only able to maintain a pressure of 2×10^{-5} torr in the collision chamber with the cross beam on. In an attempt to improve this situation, a multichannel array was inserted in the nozzle. The forward intensity to gas load ratio is greater for a multichannel array than for a simple orifice by the factor $3\ell/8r$ where ℓ and r are the length and radius of the channels respectively (FLU 73) provided the mean free path is less than the channel length. A glass capillary array with

r = 5μm and l = 1mm is used. This is fixed in place with araldite and masked to the correct orifice size with gold foil. The delivery pipe can be broken directly above the orifice so that the alignment can be checked optically. The working pressure with this system is around 7×10^{-6} torr. The improvement is limited by the pressure required to achieve sufficient forward intensity. This makes the mean free path, λ, shorter than the channel length and the improvement in forward intensity to gas load ratio is given by $3\lambda/8r$.

2.5 Cross Beam Monitor

An innovation since previous reports is a device to monitor the cross beam intensity. There are two reasons for its introduction, to give the experimenter a more direct indication of the presence and intensity of the cross beam than is provided by the degree of attenuation of the main beam and to allow correction of the data for any cross beam intensity fluctuations. A typical cross beam pressure is 10^{-4} torr which is measurable by conventional electron impact ionisation techniques. The design can therefore be based on a conventional ionisation gauge except that the sampling volume is limited. The cross beam emerges from a slit .15" by .012" and it is desirable to sample it as close to the main beam as possible. In order that the measured signal be directly proportional to the beam intensity so that it can be used for normalisation, it is necessary to subtract the contribution from background gas pressure. This can be done approximately by having a second, identical ionisation region

away from the beam, the signal from which is subtracted from that taken in the beam. To avoid differences in electron emission efficiency, a symmetrical arrangement using one filament is used and a drawing of the device is shown in Figure 2.2.

To achieve maximum electron density in the region of interest and to cut down the size of that region the electrons are focussed through a hole in the grid plate. It was found by field plotting techniques that the focussing effect is substantially improved by the presence of the V shaped grounded plates - see Figure 2.3. To prevent the electrons from simply falling to these plates, the filament is biased with a positive voltage and the grid voltages and distances are such that the electrons coming through the hole cascade back to the grid and only positive ion currents are recorded on the earthed collector plates. To prevent variations in electron emission due to filament ageing, the electron current on the grid plates is maintained at a constant value by a servo mechanism which drives the filament power supply.

The filament, grid and collector plates are mounted in a box of .008" stainless steel sheet. The grid and collector plates are made of the same material and are light enough to be supported by single electrical lead throughs, thus minimising insulation problems Distortion due to the heat from the filament over a period of days was found to be minimal. The filament is an Edwards IG2MA and is held under tension by a small spring. It is mounted on a removable cartridge for ease of replacement as although it normally lasts for the duration of one experiment it becomes brittle and has to be

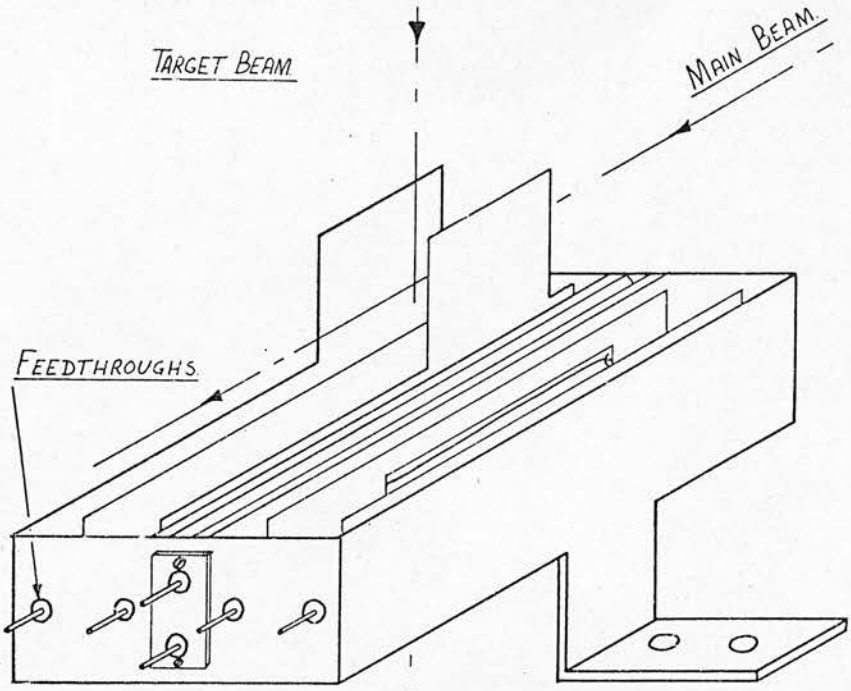

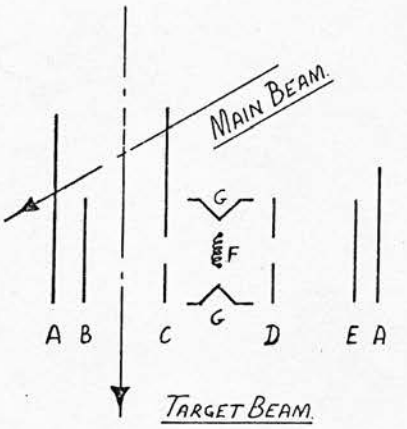

END VIEW OF PLATES.
(SCHEMATIC)

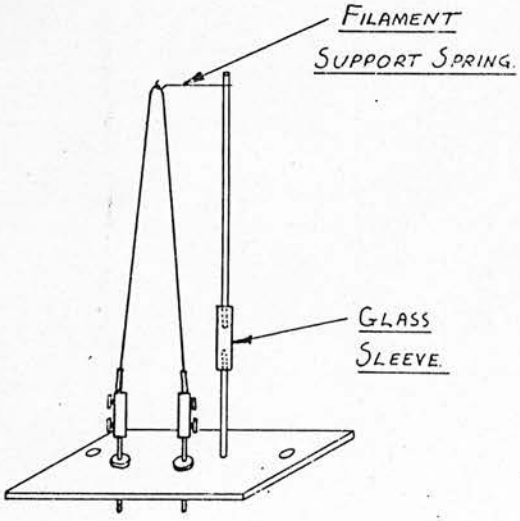

FILAMENT CARTRIDGE.
(FILAMENT : EDWARDS - IG - 2MA)

A	SHIELD	O.V.
B	COLLECTOR (SIG + NOISE)	O.V.
C	GRID	+150V.
F	FILAMENT	−20V.
D	GRID	+150V.
E	COLLECTOR (NOISE)	O.V.
G	FOCUS PLATE	O.V.

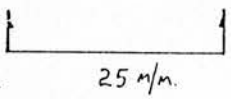

TARGET BEAM MONITOR.

FIGURE 2.2

Electrostatic Field in Cross Beam Monitor

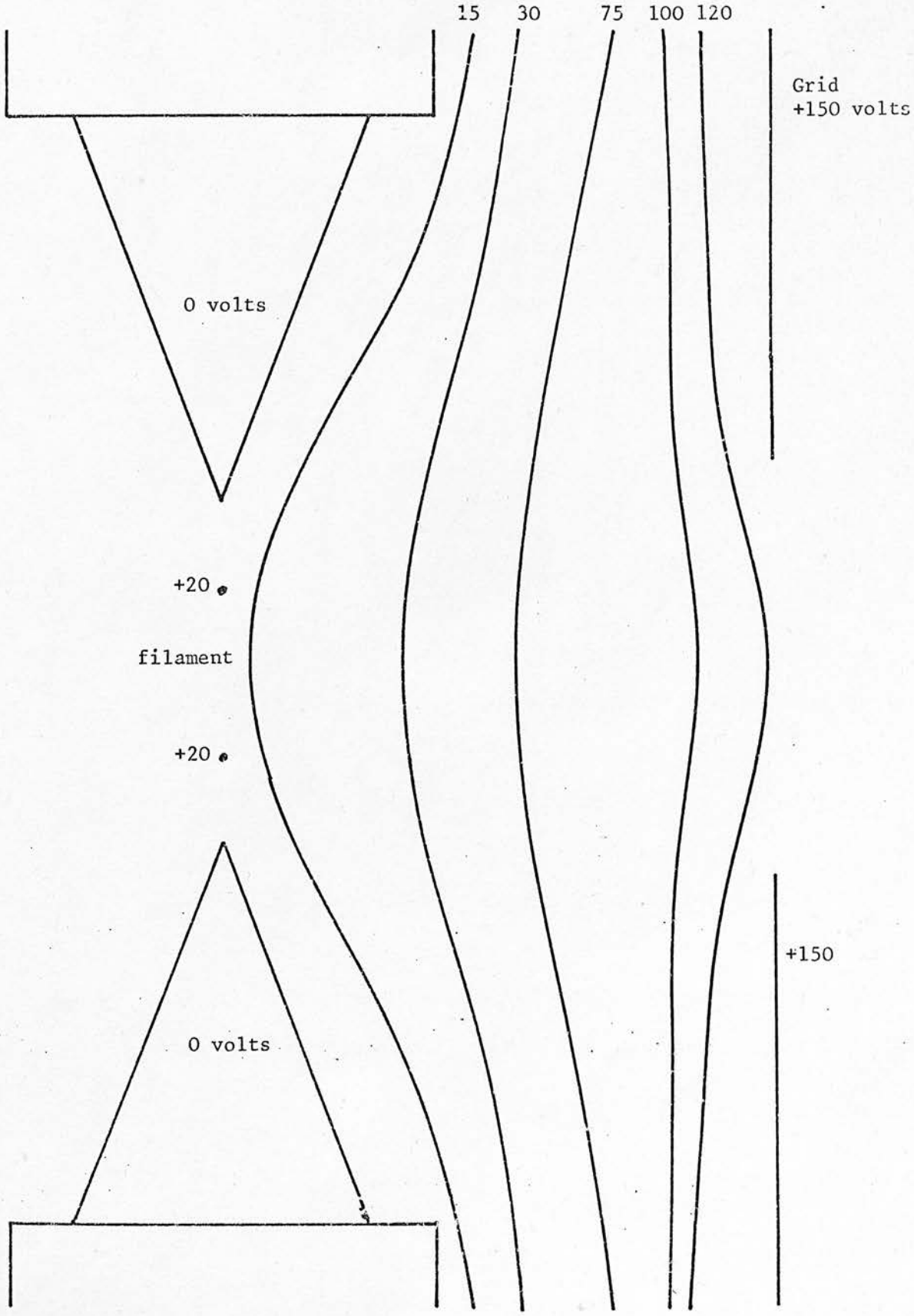

FIGURE 2.3

replaced if disturbed. The whole assembly is bolted to the base of the cross beam mount just below the line of the main beam. The grid and collector plates on the cross beam side are extended up around the main beam to deflect any ions from the source or created on the collision region. The filament bias and grid voltages were determined approximately by field plotting and finally optimised in experimental conditions.

The output of the device is two ion currents in the microamp region. These are led via shielded cables to a difference amplifier where the background current is subtracted. The output has approximately the square wave form of the optical signal from the photocell and the blurring of the edges caused by leakage round the edge of the slotted disc and the energy spread in the cross beam can be seen. This signal is displayed on an oscillosocpe and used to set the widths and phase delay of the counter gating signals. This signal is then amplified in a phase lock amplifier to which is fed the optical signal with a small delay to allow for the flight time. This system reduces noise due to fluctuations in the background pressure not removed by subtraction. The output is now in the form of a DC level which is displayed directly on a meter and fed to an analogue to digital converter whose output is read by the computer as described in Chapter 3. A block diagram of the signal processing electronics is shown in Figure 2.4.

The performance of the device was compared with than of an Elliot PVE 66 ion gauge whose output was 20μA ion current per milliamp

Cross Beam Monitor Detector Electronics

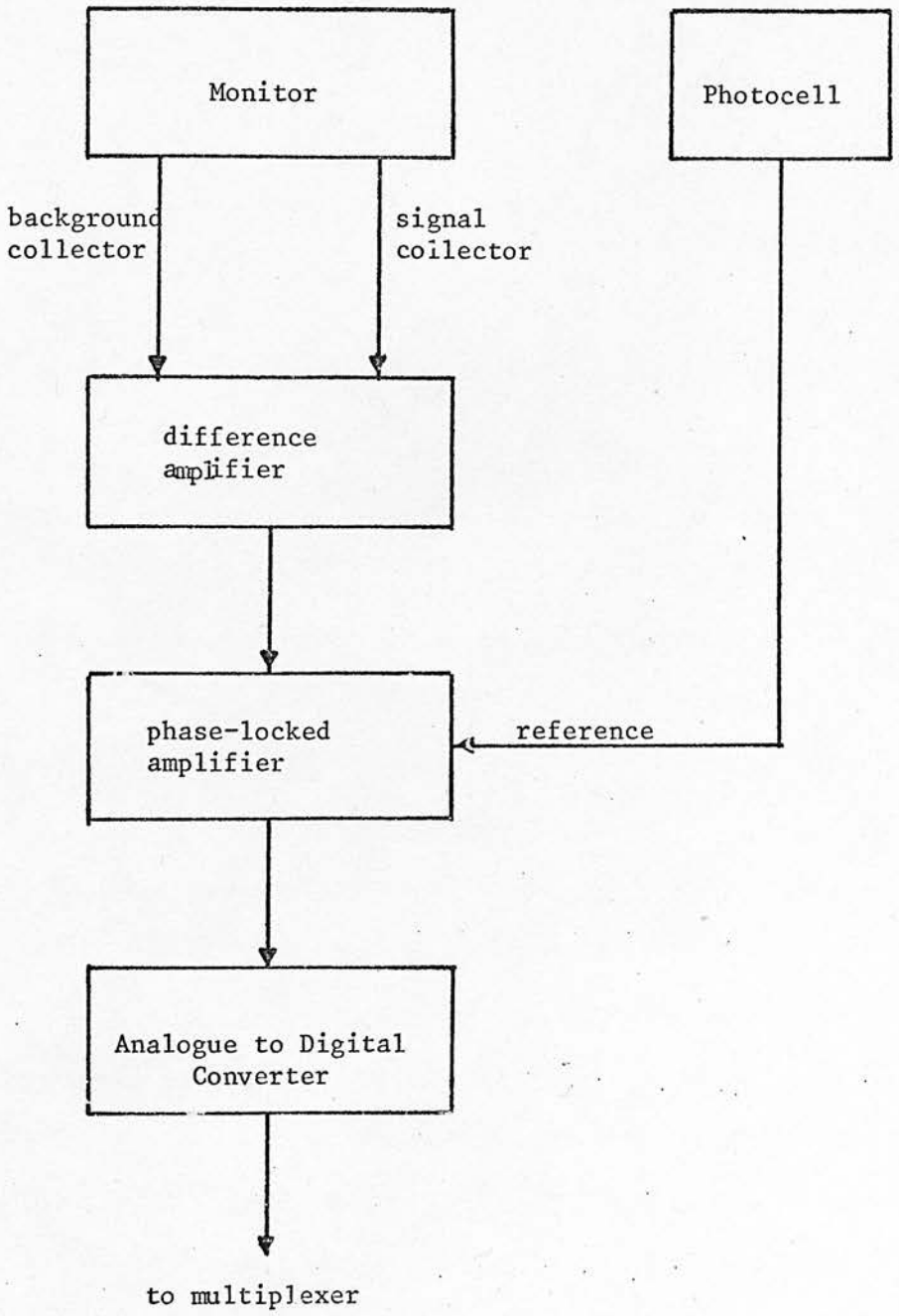

FIGURE 2.4

of emission in a pressure of 10^{-3} torr of air. The cross beam monitor gave ~1μA but when a correction is made for the small volume in which ionisation takes place, the cross beam monitor is about 3 times more efficient showing the effect of the focussing arrangements. The monitor is very successful in showing the presence and relative intensity of the cross beam. The effect of the normalisation process depends on the stability of the beam during the experiment and on the method of covering the angle range. In the set of potassium nitrogen experiments reported in Chapter four, the scatter in the shapes of the envelopes was reduced by half when cross beam normalisation was applied.

2.6 Detector

The present detector arrangement is shown in Figure 2.5. The filament is a 0.2" tungsten/8% platinum ribbon maintained at a temperature just below that necessary to ionise thermal potassium. The high energy potassium atoms are however ionised and focussed onto a Mullard B419BL channel electron multiplier. This device has a gain of about 10^8 but saturation occurs at count rates of above 10^5 sec^{-1} due to the limit on the total amount of current which can flow. The pulses are reduced in amplitude and an increased proportion fail to reach the minimum level accepted by the discriminator. The filament bias is therefore switched from its optimum setting of +150 volts when measurements are taken close to the main beam centre as described in Chapter 3. Since the aperture of the multiplier is at -2.5kV, the

Scattered K atom detector

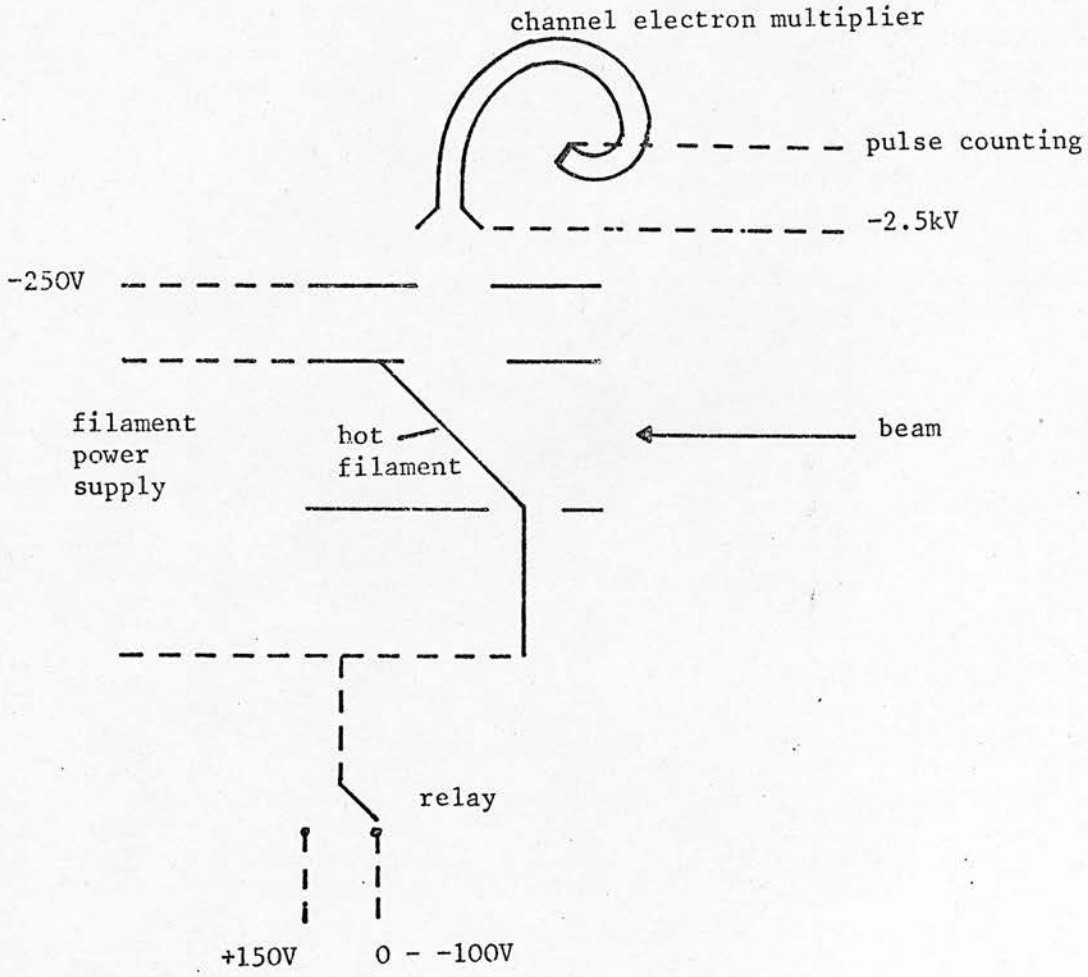

FIGURE 2.5

count rate is not very sensitive to the focus plate voltage which is set at -125 volts.

The apparatus originally had a quadrupole mass filter between the grid and the C.E.M. Its purpose was to discriminate between knocked on and scattered particles in alkali/alkali experiments and to allow detection of reaction products such as KI. The observed transmission of the quadrupole was 8% (DUC 71) and it was felt desirable to abandon the flexibility it offered in favour of improved counting statistics. The count rate for beams of 100eV potassium atoms has been increased from 2×10^5 sec^{-1} to 10^7 sec^{-1} since the previous report. The increase is greater than that expected to result from having removed the quadrupole alone due to slight improvements in alignment and operating technique.

2.7 Dimensions and Alignment

The total path length of the main beam is 50" and since the beam width is ~.02" careful alignment is obviously necessary. The main beam ion source, lens system, neutralisation chamber and cross beam source are mounted on a pair of optically aligned rails in the apparatus. The alignment of each component separately is checked with the help of an identical pair of rails on an optical bench. The final check and positioning of the detector filament and entrance slit is performed in situ with a laser. Small adjustments to the relative detector filament/entrance slit position can be made from

outside the vacuum system while an experiment is in progress.

2.8 Angular Resolution

The principal factors governing the angular resolution of the apparatus are the main beam and detector dimensions. The energy spread in both beams is negligible because of the high energy of the main beam. A procedure for calculating the effect of main beam and detector size on a theoretical differential cross section has been given by Duchart. Since this involves numerical evaluation of the convolution integrals, it does not provide a way of obtaining the differential cross section from the experimental data directly. To make this possible, a much simpler procedure was devised.

The effect of the apparatus resolution on the observed shape of the cross section has been considered by Smith (SMI 67). If the angle defining the detector position is Θ, contributions to the observed signal are obtained from a range of scattering angles θmin to θmax. In the case of tall narrow beams and detectors, θ is much closer to θmin than to θmax. Since the envelope of the high energy differential cross section falls off approximately as θ^{-2}, the result is that the observed cross section is significantly lower than the theoretical value corresponding to θ. This effect increases with decreasing θ. By comparing their experimental results with theory, Smith derived the following correction factor to apply to the data

$$\log_{10} (J(\theta)) = -B/\theta$$

where

$$\sigma_{th}(\theta) = J(\theta) \times \sigma_{obs}(\theta)$$

and δ_{th} and δ_{obs} are the theoretical and observed cross sections. The constant, B, was determined empirically. Since we are denied the luxury of exact theoretical cross sections, an approximation to $J(\theta)$ for the apparatus is derived.

Beck (BEC 62) has given a method for calculating the angular resolution correction in total cross section experiments which involves integrating those segments of circles centred on area elements in the beam image in the detector plane which intersect with the detector, over the beam image area. It is sufficiently accurate to replace the trapezoidal beam intensity distribution with a rectangular one of width, a, where

$$a = \text{top} + (\text{base} - \text{top})/2$$

Beck's method is however extremely complicated in the case of differential cross sections and the following much simplified analysis is felt to be sufficiently accurate.

A diagram of the beam image in the detector plane (a rectangular intensity distribution is assumed) and the detector filament is given in Figure 2.6. Letting

$$d = (a + b)/2$$

Detector Filament and beam image in detector plane

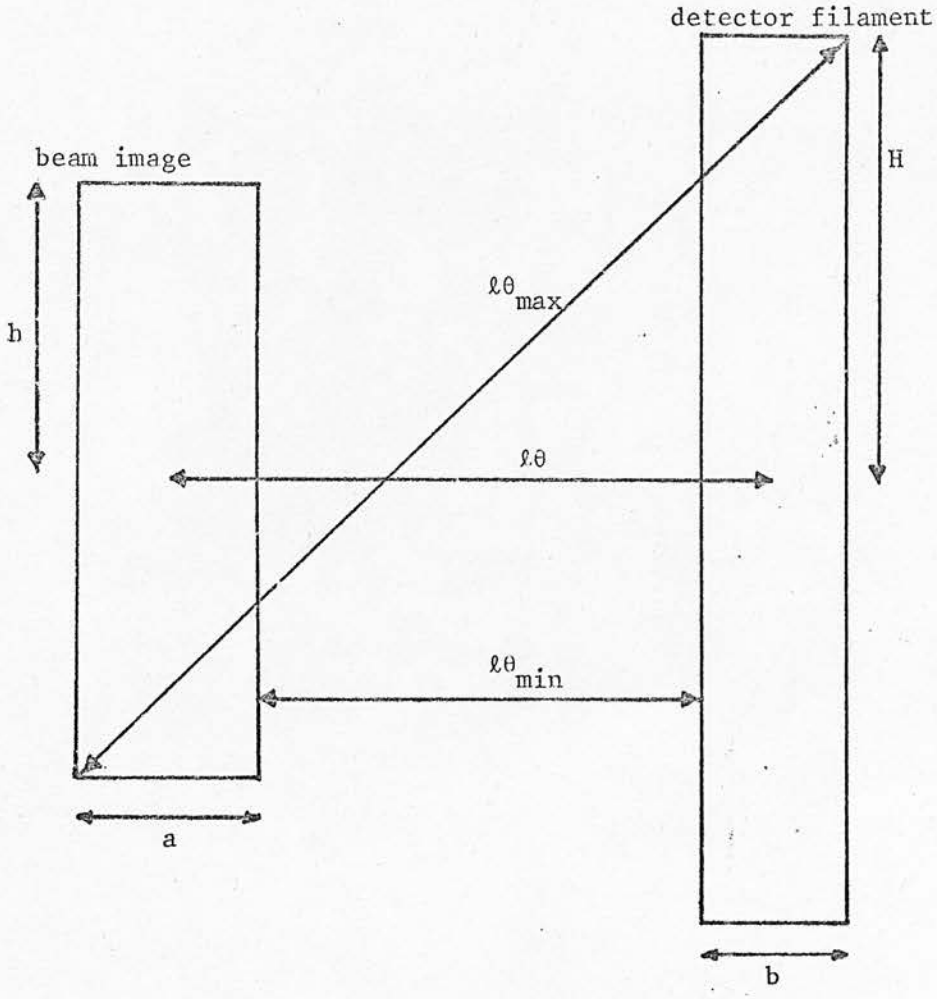

ℓ = scattering centre to detector distance

θ = angular displacement of detector

FIGURE 2.6

For any detector position θ, a range of angles $\Delta\theta$ contribute to the observed signal where

$$\Delta\theta = \theta_{max} - \theta_{min}$$

From the diagram

$$\theta_{max} = \frac{1}{\ell}\{(\ell\theta+d)^2 + (H + h)^2\}^{\frac{1}{2}}$$

$$\theta_{min} = \frac{1}{\ell}(\ell\theta-d)$$

Let $\eta(\theta,\theta+\delta\theta)$ be the detection efficiency for material scattered through the angle $\theta+\delta\theta$ while the detector is at θ. Then

$$\sigma_{obs}(\theta) = \int_{\theta_{min}-\theta}^{\theta_{max}-\theta} \sigma_{th}(\theta+\delta\theta)\eta(\theta,\theta+\delta\theta)d\delta\theta$$

As an approximation, we assume η independent of $\delta\theta$.

$$\eta(\theta,\theta+\delta\theta) \simeq \frac{1}{\theta_{max} - \theta_{min}}$$

as the area of the detector is constant.

The integral may be rewritten

$$\sigma_{obs}(\theta) = \frac{1}{\theta_{max} - \theta_{min}} \int_{\theta_{min}-\theta}^{\theta_{max}-\theta} \{\sigma_{th}(\theta+\delta\theta)(\theta+\delta\theta)^2\}\frac{d\delta\theta}{(\theta+\delta\theta)^2}$$

From the small angle formula

$$\sigma_{th}(\theta+\delta\theta)(\theta+\delta\theta)^2 \simeq \sigma_{th}(\theta)\theta^2 \simeq \text{constant}$$

and may be taken outside the integration. The integral is then

evaluated and the result is

$$\sigma_{obs}(\theta) = \sigma_{th}(\theta)\frac{\theta^2}{\theta_{max}\ \theta_{min}}$$

ie, the approximation for $J(\theta)$ is

$$J(\theta) = \frac{\theta_{max}\ \theta_{min}}{\theta^2}$$

For the apparatus parameters, 1 = 28" and d = .03", a graph of $J(\theta)$ is shown in Figure 2.7. Also shown is $\Delta\theta(\theta)$ which represents an upper limit on the angular resolution. While setting η independent of $\delta\theta$ is certainly invalid, the quantity $J(\theta)\sigma_{obs}(\theta)$ agrees with the small angle formula for $\sigma_{th}(\theta)$ well within the experimental error for θ down to $.5^{o}$.

2.9 Lab to Centre of Mass Transformation

Since theoretical results are always expressed in a Centre of mass co-ordinate system, it is necessary to transform results taken in the lab to the centre of mass frame. The exact transformation is given by Reddington, but since for the experiments reported in this work the cross beam velocity is never more than 1% of the main beam velocity, the approximate transformation for a stationary cross beam is given here.

The Newton diagram for the scattering process is shown in Figure 2.8 and the parameters defined. The centre of mass velocity is

$$Vcm = \frac{M_K V_K}{M_K + M_T}$$

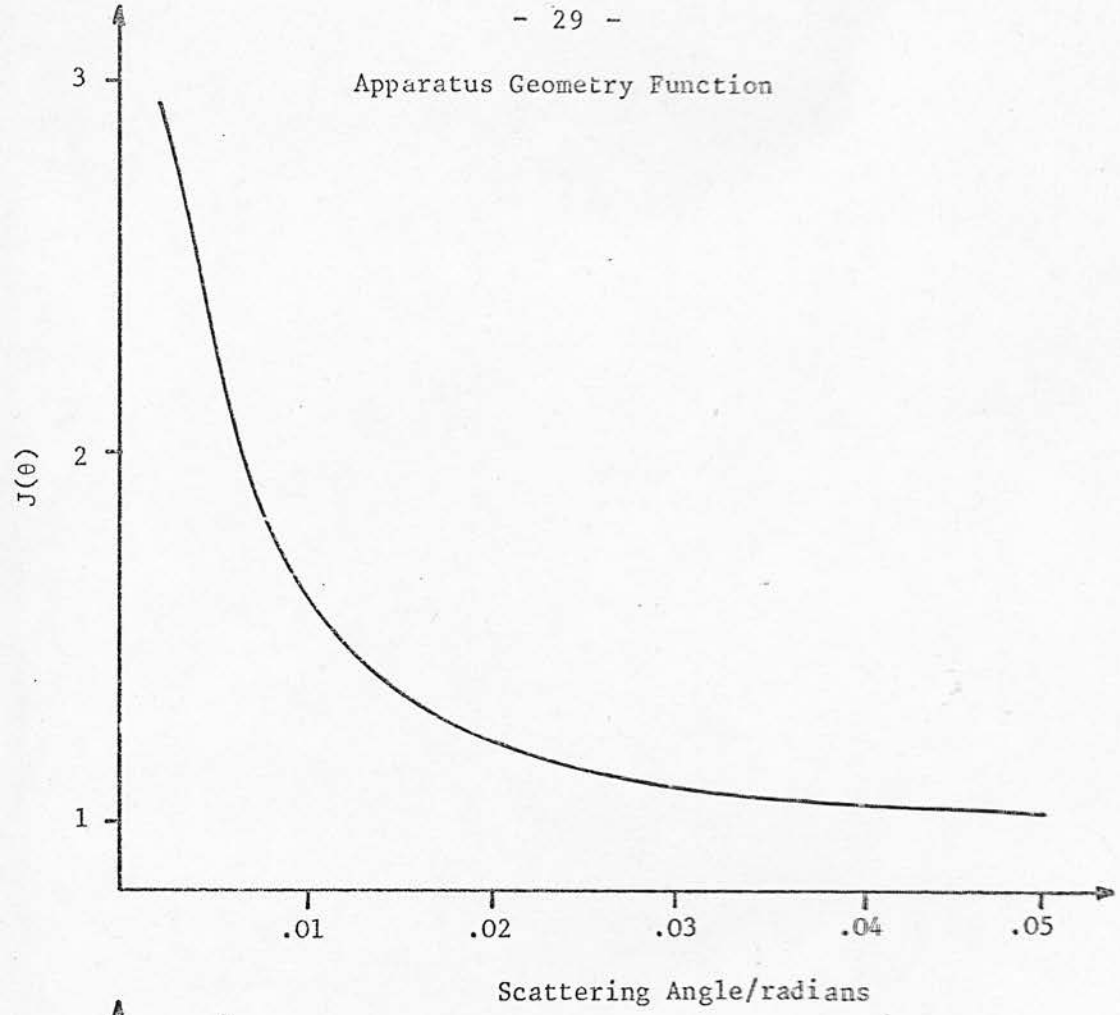
Apparatus Geometry Function
J(θ)
3
2
1
.01
.02
.03
.04
.05
Scattering Angle/radians

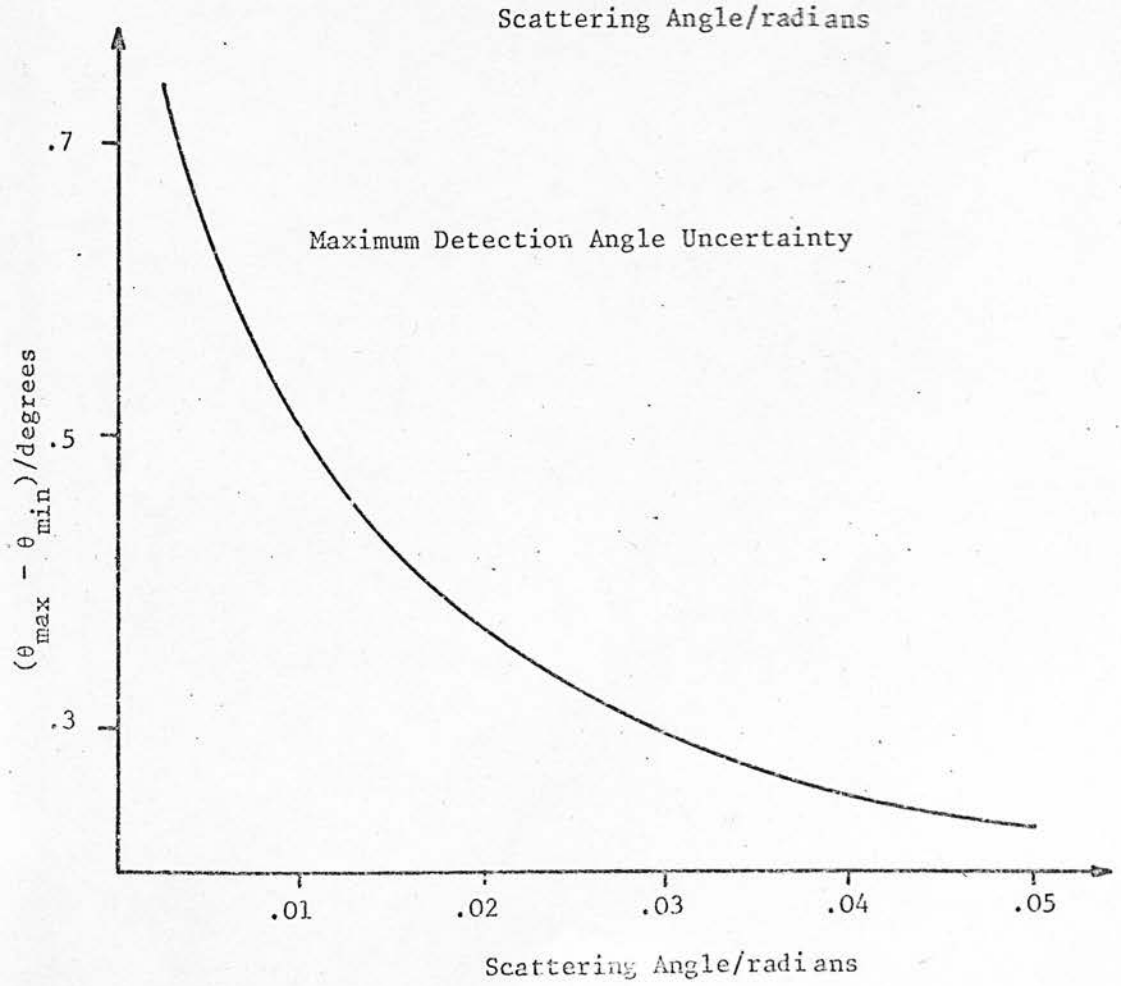
Maximum Detection Angle Uncertainty
(θmax - θmin)/degrees
.7
.5
.3
.01
.02
.03
.04
.05
Scattering Angle/radians

Newton diagram for elastic scattering

from stationary target

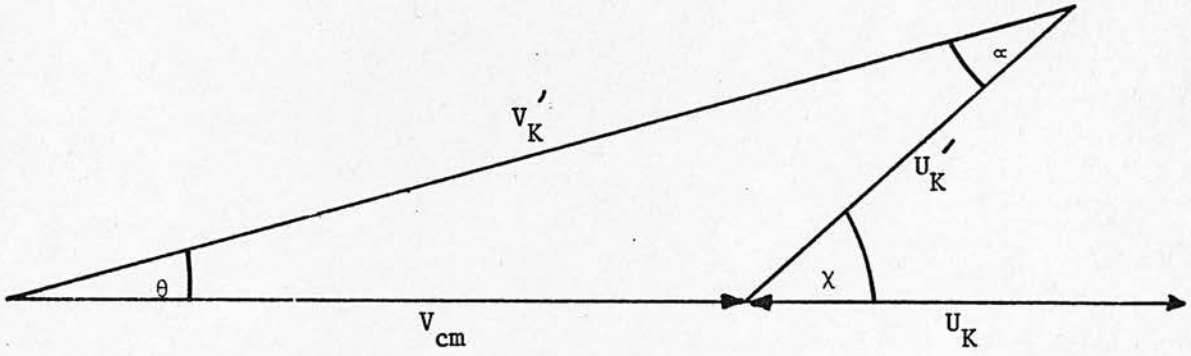

Newton diagram showing effect

of small energy loss

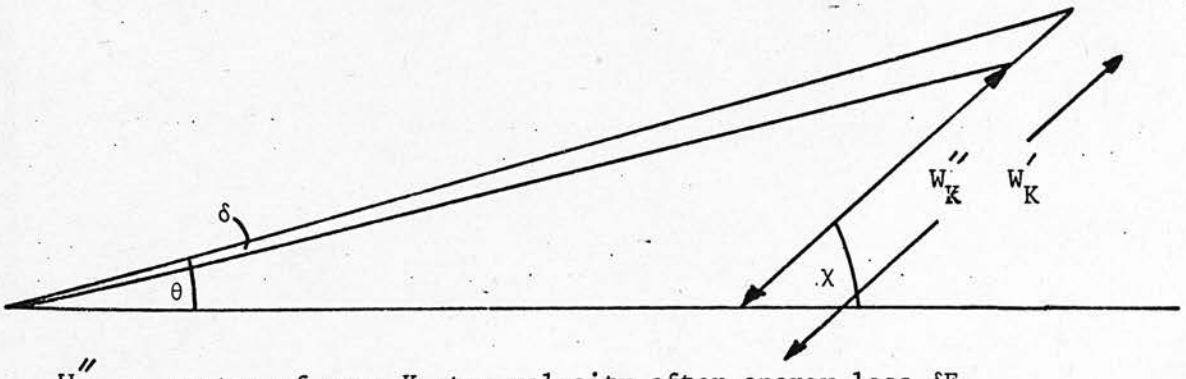

W_K'' = centre of mass K atom velocity after energy loss δE

FIGURE 2.8

and $U_K = V_K - V_{cm} = \frac{m_T V_K}{M_K+M_T}$

For an elastic collision,

$$U_K = U'_K$$

and, using the sine rule

$$\chi = \arcsin\left(\frac{M_K}{M_T}\sin\theta\right) + \theta$$

The collision energy in the centre of mass frame is related to that in the lab frame by

$$\xi_{cm} = \frac{M_T}{M_K+M_T}\,\xi_{LAB}$$

It is also necessary to correct the data for the different solid angles subtended by the detector in the LAB and COM frames. The area element, dA, normal to u'_k, subtends the solid angle element $dw = dA/u_k^{12}$ at the scattering centre. The normal to dA makes an angle $\propto$ with the velocity vector V'_k in the lab frame. The solid angle subtended by dA at the scattering centre in the lab frame is therefore $dw_L = dA\cos\propto/V_k^{12}$. The cross section in the COM is obtained by multiplying the LAB cross section by dw_L/dw where

$$dw_L/dw = \left(\frac{U'_K}{V'_K}\right)^2 \cos\propto$$

and

$$\cos\propto = (u_K^{12} + V_K^{12} - V_{cm})/2u'_K V'_K$$

2.10 Effect of Energy Loss on Lab to CM Transformation

Since no energy selection of the scattered potassium atoms is carried out, the effect of an inelastic channel is considered. The Newton diagram in the case of a small energy loss $\Delta\xi$ is shown in Figure 2.8. For the same centre of mass scattering angle, the laboratory angle is reduced from the elastic value by δ. The ratio of final velocities for elastic and inelastic collision is

$$\frac{w''_K}{w'_k} = \left(\frac{\xi-\Delta\xi}{\xi}\right)^{\frac{1}{2}}$$

and

$$x = w'_k - w'_k\left(\frac{\xi-\Delta\xi}{\xi}\right)^{\frac{1}{2}}$$

If $M_k = M_T$, $\chi = 2\theta$ and $w'_k = V_{cm}$

Then $$x = V_{cm}\left(1-\left(\frac{\xi-\Delta\xi}{\xi}\right)^{\frac{1}{2}}\right)$$

and $$y = x \sin\theta$$

Since δ is small,

$$\delta \simeq y/V'_k$$

and $$V'_k = V_{cm} \times \sin 2\theta/\sin\theta$$

Therefore $$\delta \simeq \left\{1-\left(\frac{\xi-\Delta\xi}{\xi}\right)^{\frac{1}{2}}\right\}\frac{\sin^2\theta}{\sin 2\theta}$$

The maximum value of θ is 5^o and since ξ is in the 100eV region, a reasonable maximum for $\Delta\xi/\xi$ is .1. Thus the maximum value of δ is

around .01°. We can therefore say that a calculated scattering pattern for any likely energy loss will not be shifted relative to the elastic scattering pattern by being observed in the apparatus.

CHAPTER 3

COMPUTER CONTROLLED DATA COLLECTION SYSTEM

Experimental results have been reported for the apparatus described in Chapter 2 in which a paper tape punch was used to collect the data (DUC 71). This method was felt to be inadequate however and the requirements of the data collection system were re-examined with a view to using an on-line computer.

3.1 Characteristics of the Experiment from the Point of View of Data Collection

The basic method of the experiments is to build up a picture of the differential scattering cross section by counting the number of scattered particles incident on the detection filament until an accurate value of the signal at that point is obtained, and repeating the process at different detection positions until the whole angular range is covered. Since a two channel counting scheme is operated the raw data consists of the cross beam on and cross beam off counts, the cross beam intensity, and to allow sampling flexibility, the current detector position. The time spent at any angle depends on the noise characteristics and the accurancy required, and in that time enough samples must be taken to form a reasonable estimate of the standard deviation. The signal size is limited principally by the main beam intensity which varies with beam energy due to the divergence of ion beams. The main beam also varies unpredictably between experiments due to changes in efficiency of the ioniser and lens system, slight misalignments etc, but a typical intensity is 10^{12} particles st^{-1} sec^{-1} - rather low for this type of experiment. The cross beam

intensity must be kept low enough to prevent double collisions in the intersection region. The background pressure in the scattering chamber is another constraint and the experiments were usually performed with an observed main beam attenuation of 10-20% corresponding to a cross beam density of approximately 5×10^{13} particles cm^{-3}. Thus the number of scattered particles is rather low and falls steeply with increased angle of observation ($\sigma \propto \sim \theta^{-2}$). The time required to achieve a specified ratio of signal to standard deviation increases with angle. For S/N ~ 10, sample times of a few seconds to about one minute are typically required, the requirement of having enough observations to estimate the standard deviation sets the data transfer rate at 2-3 per second.

To achieve the desired angular resolution, slit widths are chosen such that the beam divergence is ~ $.05^{o}$ (FWHH) and the detector filament subtends an angle of $.04^{o}$ at the scattering centre. The detector assembly can be located to a precision of $.002^{o}$ and observations are normally taken at $.01^{o}$ separations as reproducibility between adjacent observations is a better guide to signal quality than the counting standard deviations.

The low beam intensity and high angular precision required resulting in very low signals at the extremes of the angular range (~ 1 hz) with their inherent statistical fluctuations along with the inevitable background scattering (~ 4 hz) indicate a long counting time for the experiment and indeed the design lifetime of the main

beam ovens is 100 hrs. The cross beam, if delivered from an external gas line can be run indefinitely. Typically, experiments are terminated by some failure rather than depletion of ovens but experimental times of 60 - 80 hours have been achieved. Despite the long observation time available, there are three factors which make an efficient data collection system essential. Firstly, since a large number of components have to work correctly, a great deal of time and effort is required for a successful run. At present the average down time is 2 - 3 months. Secondly, since the angular range is small, a good range of main beam energies is required to explore the potential over a large region. The third and most important reason is instability in the main beam. As long as the beams are stable, signal to noise ratios may be improved indefinitely by increasing the counting time. In practice, instabilities arise for the following reasons: oven and ioniser temperatures may vary due to imperfections in the control circuits or mains voltage fluctuations, deposition of potassium may cause leakage between lens plates, charge may build up on non-conducting spots on the lens plates thus deflecting the beam, the pressure may vary etc. These instabilities may be prevented from perturbing the observed shape of the differential cross section by covering the angular range in some pseudo random manner. The instabilities are then folded into the data as noise which may make the resolution of small amplitude structure difficult. If the data collection efficiency is sufficient to cover the period of any structure in the cross section before the beam intensity has drifted significantly, changing the angle by regular steps is preferable.

Thus the data collection efficiency is important and must be maximised by minimising the dead time due to data transfers and shifting the detector position. The time spent at any angle must be optimised in terms of the signal to noise ratio at that point and allowance must be made for changing the angle sampling scheme according to the characteristics of individual experiments.

3.2 Data Handling and Feedback Requirements

The rate of data transfer implied by the above arguments is about 3 kbytes min^{-1}. This is an extremely large amount of data over the duration of an experiment and some reduction in volume is essential. At the same time, the limited core size and mathematical facilities available on a small computer plus the fact that data processing interferes with data collection, restrict the amount of processing that it is desirable to do on-line. Simple evaluation of mean and standard deviation of the signal as a function of detector position is adequate to reduce the volume of data to manageable proportions and provide the required feedback. Further processing may be done off-line on a large computer but the data must be identified with the values of the various apparatus and experimental parameters.

Feedback from the computer to the experiment can have two possible routes; automatic control of apparatus variables via stepper motor, relay or digital to analogue output, or feedback to the operator via a Teletype or visual display unit. Control of the

detector position is the principal candidate for automation. This would allow efficient coverage of any scanning sequence plus periodic monitoring of the main beam intensity. It would also be easy to vary the sampling time according to signal quality. The various steering and focussing lens potentials ought to remain constant throughout an experiment but in practice a certain amount of returning is sometimes necessary. The possibility of automatic control of these was considered but it was thought preferable to work on improving the stability of the hardware first.

Feedback to the operator can take two forms. Warnings can be given of various failures that may occur to allow corrective action to be taken with minimum loss of experimental time and to avoid corruption of the data. In this way the hardware itself can be checked by including checking patterns in the binary code by which the data is transferred and by checking the performance of the detector positioning mechanism. The cross beam monitor signal and periodic checks of the main beam can be used to give warnings of serious drifts in beam intensity. Since experience shows that failures can be rather frequent, it is obviously desirable that these checks be made in real time. The other form of feedback to the operator is simply the ability to look at the data collected in a meaningful form. Initially this will help in setting the various experimental variables to optimise the beam intensity, stability, attenuation and signal to noise ratio. Thereafter, the ability to

look at the data while the experiment is in progress will help in making scientific decisions such as which energy and angle range to concentrate on, as well as satisfying the impatience and curiosity of the experimenter.

3.3 The Type of System Required

It is necessary to decide exactly what type of computer system will best meet the requirements outlined above. The large amount of checking, control, analysis and feedback plus the necessity of working on fairly large amounts of data suggest that the core space requirements will be considerable. In view of the complexity of the system, the ability to program in a high level language is also desirable. Back up storage sufficient to hold complete cross sections at various energies is also necessary if trends are to be observed in real time. Other hardware features required are a stepper motor drive unit, a Teletype and/or V.D.U. for communication with the operator and an output device for communication with a large computer. These factors point to a relatively large sophisticated system but the low data transfer rate and small amount of c.p.u. time required relative to the duration of the experiment make it wasteful to have such a system dedicated to the experiment. The best solution is to use a machine that is multiprogrammed so that the facilities can be shared with other experimenters. A multiprogrammed computer system was planned for on-line handling of experiments in the Edinburgh University Physics Department and since the facilities met our requirements, arrangements were made to interface the experiment to it.

The machine is a Digital Equipment Corporation PDP-11/45 with 32 kilowords of core memory. The hardware facilities include a 1M disc back up store, a 1M drum used to expand the effective amount of core, a magnetic tape unit and line printer. The locally written operating system handles all devices, buffering input and output where necessary and the paging system removes any effective limitation on program size. The disc provides ample back up storage space and data is conveniently transferred to a large computer by magnetic tape.

3.4 Description of Data Collection Hardware

A block diagram of the data collection hardware is shown in Figure 3.1. The slotted disc used to modulate the cross beam chops a light beam in phase with it. This signal is picked up by a photocell and used to gate the two channel detection system. Four pulse width delays are used to produce the two gating signal whose widths and delays can be varied to produce the optimum contrast between in phase and out of phase count rate and to allow for flight times. The modulation cycles are counted by a Watesta batching counter which on reaching a preset number, gates off the scalers and initiates a data transfer. At this point the modulation trains are switched to eliminate any bias to either in or out of phase signal. The scalers count the detector pulses and their output is fed to a multiplexer along with a modeflag which points to the in phase scaler, a three bit flag set manually (used to control software options), the output from the detector position encoder, the cross beam monitor and various

FIGURE 3.1

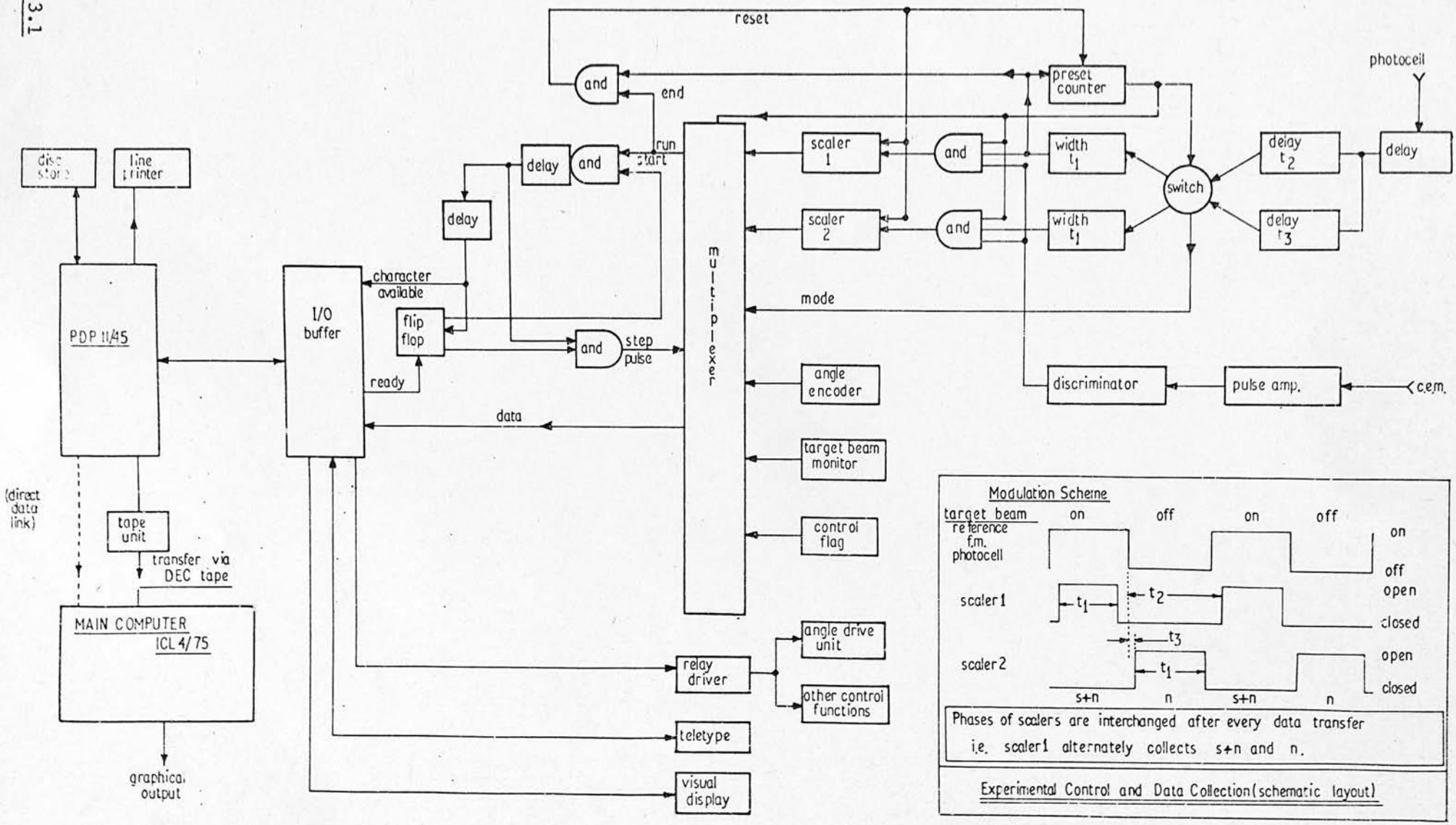

Experimental Control and Data Collection (schematic layout)

checking codes. When the modulation counter reaches its set number, its output level changes, putting the multiplexer into its run state, which then converts the input data into sixteen eight bit characters. The format of this 'sentence' is shown in Figure 3.2.

The 'ready' pulse from the computer usually arrives before the onset of 'run' and is stored in a flip-flop, but may arrive after. In any case, the coincidence of 'run' level and 'ready' pulse causes a step pulse to the multiplexer which puts its first character onto the eight parallel data lines and after a 10μsec delay, a 'character available' pulse is sent to the computer, and the flip-flop is reset. On receipt of the first 'character available' the operating system is interrupted and the first character read into a core location under program control Its arrival initiates another 'ready' which repeats the cycle until sixteen characters have been sent, when the multiplexer drops out of run. The trailing edge of the run level is used to reset the scalers and the batching counter, but the reset pulse is synchronised with the start of the modulation cycle to eliminate any bias against the scaler which would happen to be gated open otherwise. The system described above, in which computer and interface 'shake hands' over every character, eliminates timing problems, ensures that no data goes astray, and takes less than .1msec per complete sentence. The system also consists of two analogue input channels, with AD conversion under program control, a stepper motor drive unit driven under program control and a relay

Data Sentence Format

0 1 2 3	4 5 6 7
Start Code	Scaler A(BCD) 10^{0}
10^{1}	10^{2}
10^{3}	10^{4}
10^{5}	10^{6}
Detector position/inches (Inverted BCD) 10^{-3}	10^{-2}
10^{-1}	10^{0}
Mode Manual Flag	Scaler B (BCD)
10^{1}	10^{2}
10^{3}	10^{4}
10^{5}	10^{6}
Checkbits 0,4 6,4 4,0 6,0	Fixed Code
Cross Beam Monitor (Inverted Binary) 2^{0}	2^{7}
2^{8} 2^{11}	End Code

FIGURE 3.2

driver. There is two way communication between operator and computer via a Teletype in the lab, and a 512 point VDU is available for examining the data.

3.5 Data Collection Software : General Considerations

The features required of the system are reliability, simplicity and efficiency of operation and protection of the data under all circumstances. It is especially important that software crashes are kept to a minimum to avoid the loss of valuable experimental time. The effect of all possible combinations of input both from the apparatus and the operator must be considered and tested, and since the experiment is designed to run for up to 100 hours, the effect of operator errors and hardware failures must also be forseen and allowed for as far as possible. In addition all illegal input must be detected immediately and not allowed to corrupt the experimental observations.

The operation of the data collection system must be simple enough not to distract the operator from the main task of getting the apparatus to perform as well as possible and must not require detailed knowledge of the system itself. A simple set of instructions sufficient to operate the system in all normal situations and in the event of all forseeable failures, must be supplied. The system must also make running the experiment easier from the operator's point of view by accepting some responsibility in deciding when intervention is required so that feedback is useful. It is also important that as many routine

tasks as possible are automated to free the operator and reduce the probability of error.

For small computer systems generally, the pressure on central processor unit (c.p.u.) time is less than that on available core. In the system used about 24k is available for user programs and the amount of virtual memory on the drum is effectively unlimited. Drum transfers are relatively slow however (average ~ .1sec) and it is desirable for the system as a whole to reduce the number and duration of these by keeping core requirements to a minimum. Clarity of programming and good documentation are also necessary to reduce the effort in modification and debugging.

3.6 Data Collection and Examination Program

Since multiprogramming is available, any number of programs may be run simultaneously to perform the required functions. For greatest economy of core usage, the time intervals of the various operations must be considered. These are: data acquisition - .5 - .3 secs, data analysis - 5 - 10 secs, detector repositioning 5 - 60 secs, checking for beam drift ~ 1 hour. Since all the code in any program must be in core at one time, requirements could be minimised by having each function performed by a separate program. To date this complication has not been necessary. It is also possible to use the multiprogramming facility to save time by allowing data acquisition to proceed simultaneously with some other operation. The

time taken is negligible for the first four operations but can be considerable for data examination. For this reason and since the data collection procedure is not dependent on the ability to look at the data being collected, all the data acquisition, checking and analysis operations were grouped into one program with data examination in another.

3.7 Data Collection Program

The basic step in the operation is to read the data from the interfaces as shown in Figure 3.2 into sixteen core locations (an array). The first and last of these are checked for the four bit start and end codes respectively. If either is absent, extra characters are read into the bottom of the array until the check is successful. The sentence of sixteen characters is then assumed to be correctly positioned and the hardware in phase with the software. The following checks are made at a frequency set by the operator. The parity of each of the four major components is checked, the four bit binary coded decimal digits are checked to ensure they are less than 10 and the two most significant digits of the counters are checked against zero as the full capacity is never used. A check is also made to ensure that the value of the mode bit is alternating between consecutive sentences. Error messages are given to the operator after every ten failures. The cross beam count, angle and contents of scalers A and B are then decoded along with the manual flag. At this point three modes of operation are available for checking the hardware,

tuning up the apparatus and actually collecting data. In tune up or data collect the cross beam count is put in an array and the contents of scalers A and B into a signal and a signal plus noise array according to the value of the mode.

In data collection, the arrays are processed every time sixteen sentences are added. Working arrays are first produced by averaging consecutive elements to eliminate counter bias. The mean and standard deviation of signal, signal normalised by cross beam intensity, background count rate and cross beam intensity are calculated. As occasional noise spikes are observed in the counters, care is taken not to allow these to bias the signal as follows: On first pass through the mean and standard deviation routine the ten percent most deviant observations are set aside and the mean and standard deviation of the remainder calculated. On the second pass any observations more than two standard deviations from the mean are discarded and a new mean and standard deviation calculated. At any angle, more batches of sixteen observations are included until a preset ratio of signal to standard deviation is achieved, up to a limit which prevents delaying the experiment too long in regions where the signal is very poor. When either of these criteria is satisfied the processed data is added to the disc file and the angle selection and drive routine is activated. In a typical experiment observations are taken at $.01^{o}$ separations up to $\sim 4^{o}$ from the main beam centre. Two sampling schemes are available for achieving this and are selected by the operator

according to the characteristics of the experiment. The detector may simply be stepped out .01° at a time which is the most efficient in driving time. To prevent beam drifts distorting the envelope a sampling scheme in which the observations within the width of the angular resolution are taken over the duration of the whole experiment is available. The detector is driven from the beam centre to the extreme of the range in 25 steps and back again. This is repeated until the entire grid is covered. To avoid introducing any spurious perodicity into the observations, the length of each step is varied in a pseudo random manner. The sequence is generated by combining two 25 element arrays and normalising to the angle range to be covered, which is variable. The program can be made to start at any point in the sequence.

When the new detector position has been selected, the shift required is calculated and converted to the number of steps required by the motor. This goes to a register used by the stepper motor drive unit and the supervisor is interrupted. The drive unit sends out a train of steps at a frequency set by a hardware clock to the apparatus interface, decrementing the register as it does so. The train ceases when the contents of the register reach zero and the program is re-started. Thus all data collection is suspended while the detector is in motion. The new detector position is then read and compared with the calculated one. To allow for small discrepancies due to backlash or 'sticktion' in the lead screw, a correction may then be applied unless the error is greater than .04° in which case some failure of

the position encoding or drive mechanism is assumed and a warning given to the operator.

When the observation at one angle is completed, the processed data is added to the disc file. The data recorded at any angle is; the detector position, the time on the computer's internal clock, the current on the ion dump plates and the mean, standard deviation and number of observations contributing to the signal, signal normalised by cross beam intensity, background count rate and cross beam intensity. The file is organised in 'blocks' of sixteen writes and each write is identified by a line number and block number. The sixteenth line in each block contains parameters defining the configuration of the experiment.

The response of the channeltron shows strong deviations from linearity at very high count rates. This is due to the dead time immediately following a pulse caused by depletion of electrons on the surface. This effect was found to be significant for count rates of 10^5 sec^{-1} - below the normal main beam intensity. To allow accurate measurements of the main beam and attenuation, the count rate is reduced by switching the filament bias from +150 volts to a voltage variable between 0 and -100 volts. This voltage is set such that the count rate at the main beam centre is about 7×10^4 sec^{-1} and the switching is done automatically whenever the detector is within $.06^o$ of the beam centre. The count rates within this range are corrected by the ratio of count rates for the two voltages

measured at an angle where the distortion is unimportant.

Four quantities are measured as a check on the stability of the beams. These are the cross beam intensity, read every data transfer, the ion current on the post charge exchange chamber dump plates which is input via an analogue to digital converter and read every time the disc writing routine is called, and the main beam intensity and attenuation measured by automatic driving of the detector to the main beam centre at intervals set by the operator. The experiment is started with both beams at optimum settings, so drifts tend to be downwards. Although this can be corrected by normalisation, lower beam intensity results in a lower signal to noise ratio and beyond a certain level can usually be attributed to a significant deviation from its optimum setting of some apparatus variable. To relieve the operator of the responsibility for checking all variables throughout the experiment, the four measured parameters are checked for drifts and appropriate warnings given. The level at which operator intervention is effective is difficult to set in advance but by trial and error the following settings were chosen. The ion current and cross beam intensity are checked for drifts of 10 and 5 percent respectively and appropriate warnings given to the operator. Similar warnings are given of 5% drifts in main beam intensity or attenuation between subsequent observations and in addition data collection is suspended for drifts of over 10% thus making operator action necessary.

At every change in main beam energy or cross beam material or in the event of any failure, 'tuning up' of the apparatus is necessary. The main beam is maximised and the cross beam intensity optimised with respect to the ratio of scattered signal to noise caused by background scattering. To assist in this process, a 'tune up' mode was incorporated in the data collection program. The data is processed as for data collection but selected parameters are printed at the lab Teletype and no writing to disc is done. When the detector is at the main beam centre, the main beam intensity, cross beam intensity and percentage attenuation are printed, at other angles the scattered signal, ratio of signal to standard deviation and background count rate are printed.

The three modes of operation, ie collect data, tune up and check only, are controlled by the three bit pattern in the sentence which is set manually by the operator.

The manual flag also serves to stop the data collection completely and to control the reading of input data. Since the system requires two programs to be running simultaneously, it is convenient if only one of them reads data from the Teletype. This was chosen to be the data inspection program as it requires more frequent input. The data is read into a common area of core and taken from there by the data collection program when the appropriate flag is set. The data is of two sorts; parameters which control the operation of the program are the frequency of checking, frequency of main beam

monitoring, limits on angular range, the required signal to noise ratio, the maximum number of observations at any angle and two parameters which allow the pseudo random angle sequence to be started at any point. The parameters which identify the experimental system and configuration are an experiment number, the date, the main beam, cross beam and detector heights and widths, the main beam energy and atomic weight, the cross beam nozzle temperature and molecular weight and the position of the main beam centre. These parameters are added to the disc file after every fifteen data writes. If any are changed, lines of zeros are inserted into the disc file to separate the data taken with different configurations. The operation of the manual flag is shown in Figure 3.3.

A simplified flow diagram for the data collection program is given in Figure 3.4 and a diagram of the modular organisation showing the function of the principal routines in Figure 3.5. A complete listing is given in the Appendix.

3.8 Data Inspection Program

This program's function is to provide the operator with information on the progress of the experiment by displaying selected values from the data accumulating in the disc file either on the Teletype or on the V.D.U. in the lab. The options available are - histograms of scattered signal versus detector position, main beam or cross beam intensity against time and a report on the most recent values of main beam, cross beam and attenuation. In addition the program is used to pass data to the data collection program.

Function of Manual Control Flags

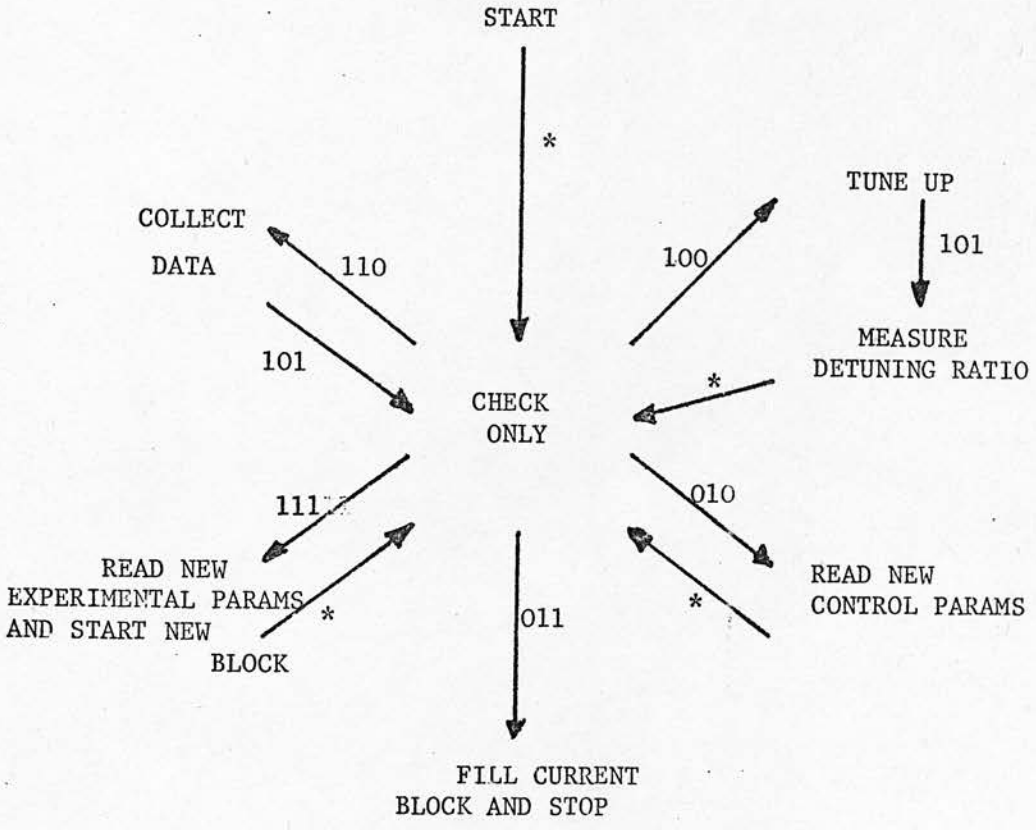

* - Automatic transitions

FIGURE 3.3

Flowchart for data collection Program

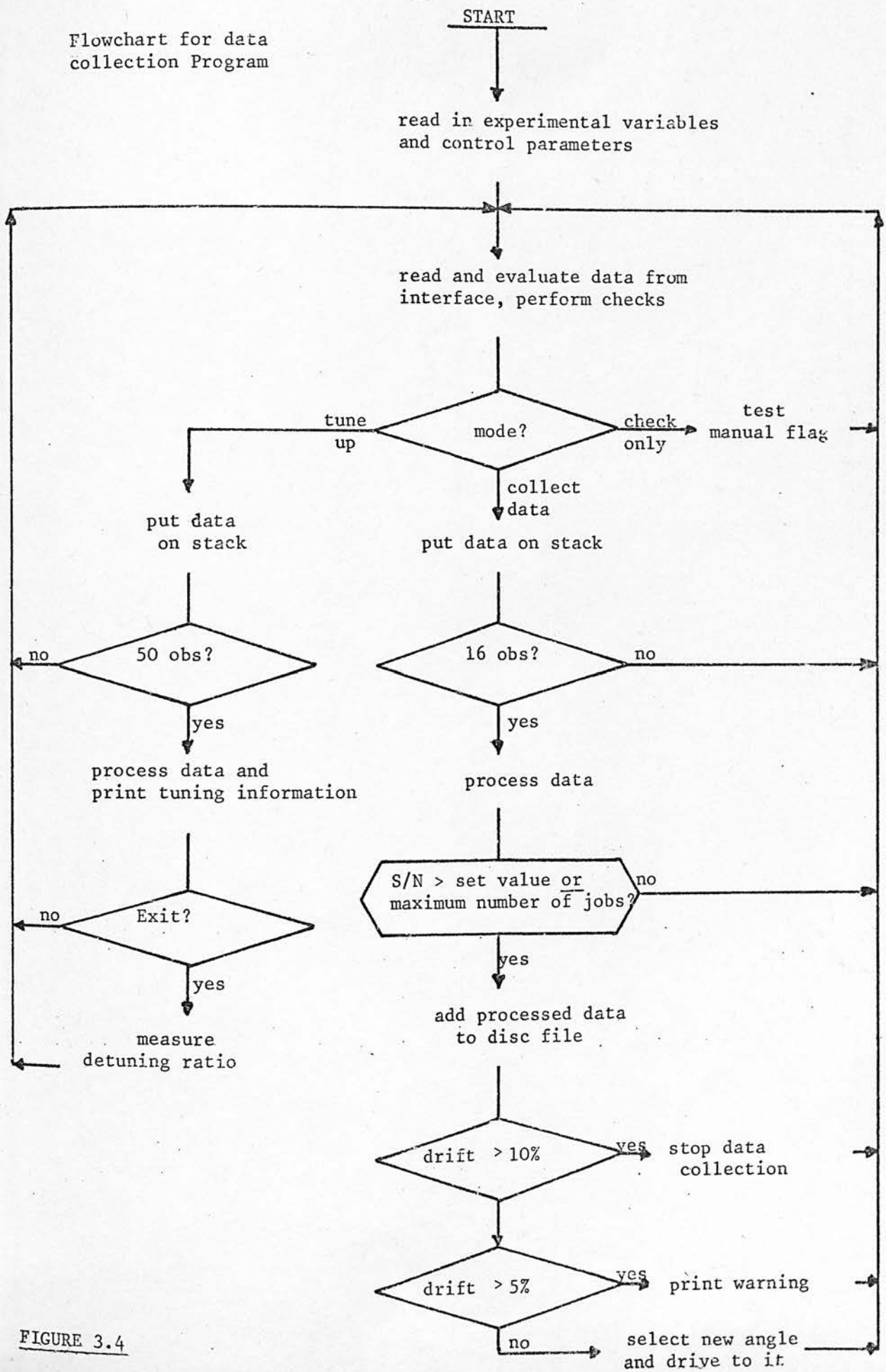

FIGURE 3.4

Modular Structure of Data Collection Program

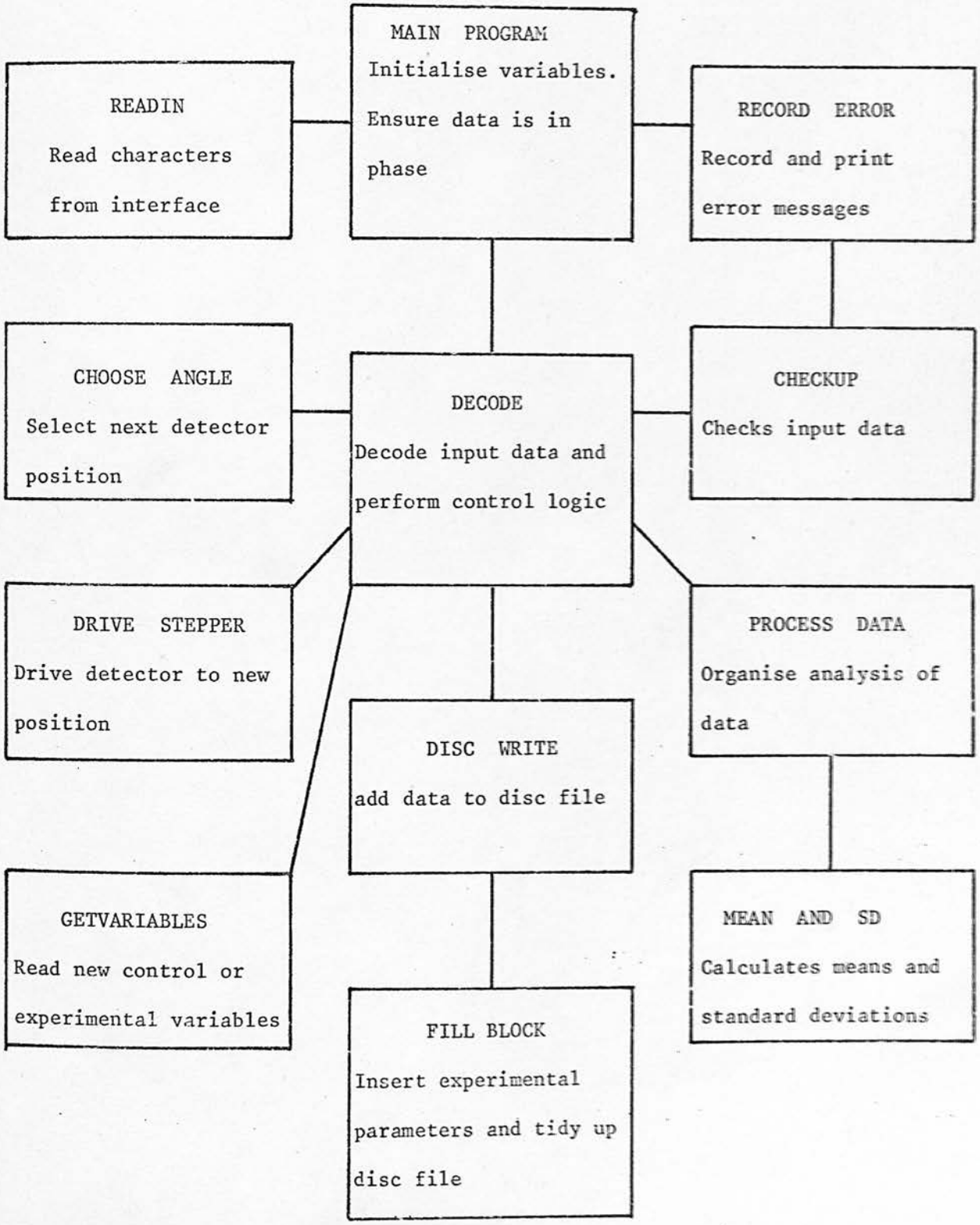

FIGURE 3.5

3.9 Testing Software

Both at the development stage and in subsequent trouble-shooting, it was found useful to have programs available to define the exact nature and source of faults which arose. The operation of these testing programs will be described briefly.

To test the data collection hardware, two programs were written. To locate faults in the multiplexer and check for noise on the data transmission lines, a special plug was built to replace the normal input. The plug could be switched such that all 128 bits of input are either set or not, resulting in a sentence of all ones or all zeros being read at the computer. A program was written which accepted such a sentence and printed the number of deviations for each bit per 1000 sentences. Failures in the multiplexer were located exactly by this method and the effect of noise was undetectable. Another program was written which simply echoed the normal input data on the Teletype both in raw and decoded form. The contents of all three counters and the angle encoder are displayed so the transmission and decoding can be checked by direct comparison. The mode, manual flag, checking bits and start and end code can also be checked directly.

Special programs were also written to test the operation of the other pieces of hardware, the stepper motor driving the detector, the relay switching the voltage at the detector filament, and the analogue input channel. In each case the operation was controlled by input from the Teletype and the effect could be observed directly.

Finally, the operation of the entire system and performance of the analysis procedure is checked by running the data collection program with dummy input data.

3.10 Performance of the System

After the initial development phase, software crashes and failures in the data collection hardware never terminated an experiment and on no occasion was data found to be invalid due to some error after it had been collected. Occasional failures of the computer itself or the operating system occurred, but these were not frequent and were generally a result of further development rather than a fundamental weakness. Direct comparison of data collected on paper tape and with manual positioning of the detector against that collected by the computer system is rather unfair as considerable improvements in beam intensity and stability have been achieved concurrently with its implementation. However the time taken to cover the angle range has been reduced from 12 to ~ 2 hours with considerable improvements in signal to noise ratio and reproducibility between adjacent observations. The experimental time wasted due to running with some fault in the system has been considerably reduced by the real time checking and the feedback has allowed the operator to be much more effective in optimising and stabilising the beams.

3.11 Off-line Data Processing

The data collected on-line is transferred to a large computer by magnetic tape. There, further analysis is performed and the data prepared for output as shown in Figure 3.6. This procedure will now be described briefly.

The angular range covered in the experiment extends from one side of the main beam to the wide angle limit on the other side. To convert the measured detector linear displacement to angle of scattering, the position of the main beam centre is first found by taking the mean of position weighted by background (cross beam off) count rate in the region of the maximum. The LAB scattering angle is then calculated from the formula

$$\theta_i = |\arctan((P_i - \text{centre})/D)|$$

where P_i is the detector position at the ith observation and D is scattering centre to detector distance. The signal is then normalised to the main beam intensity using linear interpolation between subsequent main beam observations. The data is then sorted into angle order. In the region of the main beam, the scattered signal cannot be measured exactly because of the attenuation of the main beam. Conversely, the attenuation is not determined exactly because of material scattered into the beam. The attenuation is estimated as 1.5 times the observed attenuation and the scattered signal is corrected by this amount. This procedure prevents the appearance of unphysical negative signals at small angles. Since

Off-Line Data Analysis Summary

START

Read in and check data

* Apply cross beam normalisation

* Apply main beam normalisation

Convert detector position to scattering angle

Sort data into angle order

Scale by angle squared

Apply exponential smoothing and report quality of data

Repeat smoothing with rejection of deviant observations

* Convert angles to Centre of Mass

* Plot raw data

Plot smoothed data

STOP

* - optional

FIGURE 3.6

the differential cross section is known to fall off approximately as θ^{-2}, the scattered signal is scaled by θ^2 for display purposes. This also prevents the angular variation appearing as noise in the smoothing process. The cross beam measurements are now used to normalise the data. It has been found that due to noise in the cross beam monitor, the averaged cross beam signal produces better results than the instantaneous value. The quality of the experimental data is then evaluated using the procedure of exponential smoothing in which the signal is replaced by the mean of the adjacent signals weighed by an exponential function of their angular separation. The standard deviation is similarly defined and the exponential window is of width approximately equal to the resolving power of the apparatus. Defining a weighting function d_{ij}

$$d_{ij} = \exp\{(\frac{\theta_i - \theta_j}{z})^2/_2\}$$

where z is the half width of the window, the smoothed signal is given by

$$s^1_j = \sum_{j=i-n}^{i+n} d_{ij}\, s_i \;/\; \sum_{j=i-n}^{i+n} d_{ij}$$

where n is large enough that $d_{in} \simeq 0$. The variance is then given by

$$\mathrm{var}(s^1_i) = (\sum_{i-n}^{i+n} d_{ij} s^2_j - (s^1_i)^2 \sum_{i-n}^{i+n} d_{ij})/(\sum_{i-n}^{i+n} d_{ij} - 1)$$

and the ninetyfive percent confidence limit is the value of s^1_i is

$$c_i = 1.96(\mathrm{var}(s_i^1)/\sum_{i-n}^{i+n} d_{ij})^{\frac{1}{2}}$$

The quality of the data is then defined as

$$q = \Sigma s_i^1/c_i$$

This quantity is used as a check on the relative efficiency of the normalisation procedures. The procedure as described is correct for observations distributed normally about the differential cross section. In the experiment however, systematic deviations occasionally occur. These are dealt with by repeating the smoothing process, rejecting all observations more than 2 x c_i from s_i^1. The smoothed, scaled signal is then plotted against angle with error bars of length $2c_i$.

CHAPTER 4

RESULTS AND DISCUSSION

4.1 Systems Studied

Differential cross sections have been measured for the collision systems K/CH_3I, K/SF_6, K/A and K/N_2 at the LAB energies shown in the table in Figure 4.1. As each measurement consists of around 500 observations over the LAB angular range of about 4 degrees and the apparatus resolving power is .1 to .2 degrees depending on angle, a considerable degree of checking of the reproducibility of the results is contained in one measurement. Nevertheless, in most cases, the entire procedure was repeated, duplicated measurements being indicated in the table.

In all cases the data has been analysed by the procedure outlined in Chapter 3 and graphs of the results are given in the figures indicated in the Table. The data is plotted in the LAB frame and the error bars represent 95% certainty in the position of the line. The effect of the smoothing procedure is illustrated in Figure 4.13 which shows the smoothed and unsmoothed data for one of the K/SF_6 runs.

The system K/CH_3I has been much studied at thermal energies (BER 73) where it is the classic example of the rebound mechanism for chemical reaction. There have also been many Monte Carlo trajectory studies, eg (LAB 73) and although the reaction cross section has a maximum at a collision energy of .18eV and is not expected to be significant in the present experiments, it was hoped that the presence of an ionic surface would result in structure through the effects discussed later in this chapter. Such structure in the differential cross section would allow information to be obtained about the potential

Differential Cross Sections Measured

System	LAB Collision Energy / eV	
$K + CH_3I$	100 (2)	Fig 4.2
"	200 (2)	Fig 4.3
"	300 (2)	"
"	250 (2)	Fig 4.4
"	350	Fig 4.5
"	470	"
K + A	400 (2)	Fig 4.6
"	300 (2)	"
$K + SF_6$	400 (2)	Fig 4.7
"	300 (2)	"
"	100	Fig 4.8
$K + N_2$	100	"
"	150 (2)	Fig 4.9
"	200 (2)	"
"	250 (2)	Fig 4.10
"	300 (2)	"
"	350 (2)	Fig 4.11
"	400 (2)	"
"	450 (2)	Fig 4.12
"	500 (2)	"

FIGURE 4.1

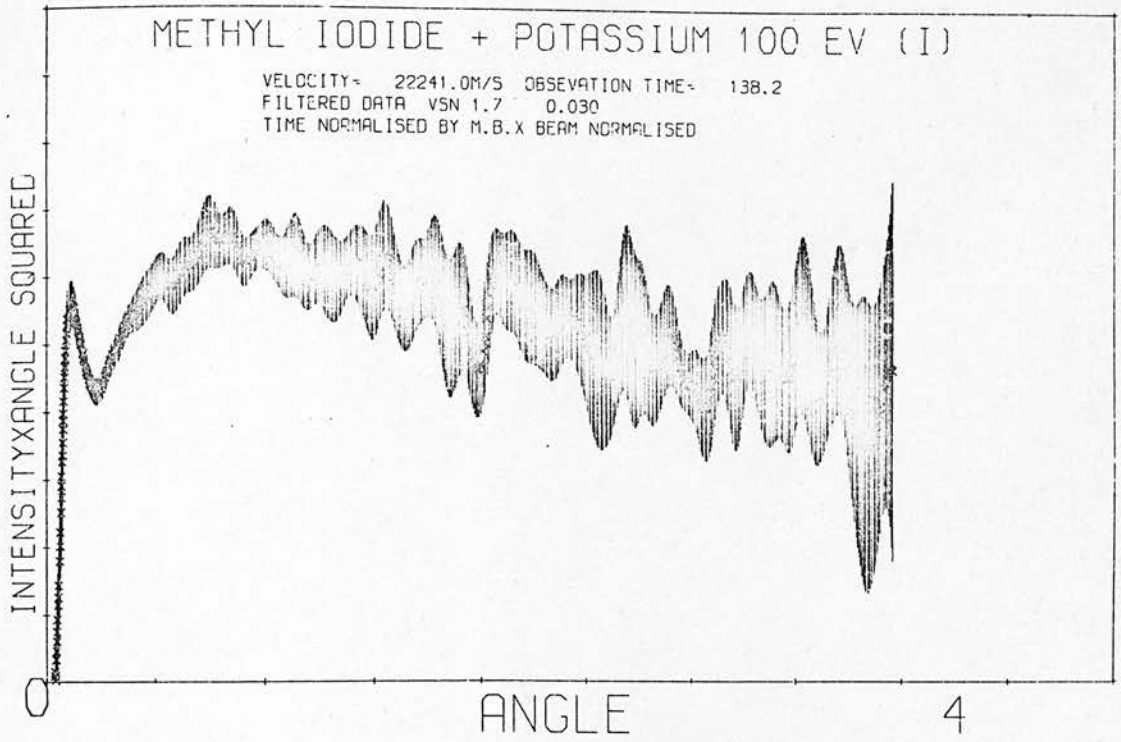
METHYL IODIDE + POTASSIUM 100 EV (I)
VELOCITY= 22241.0M/S OBSEVATION TIME= 138.2
FILTERED DATA VSN 1.7 0.030
TIME NORMALISED BY M.B.X BEAM NORMALISED
INTENSITYXANGLE SQUARED
0
ANGLE
4

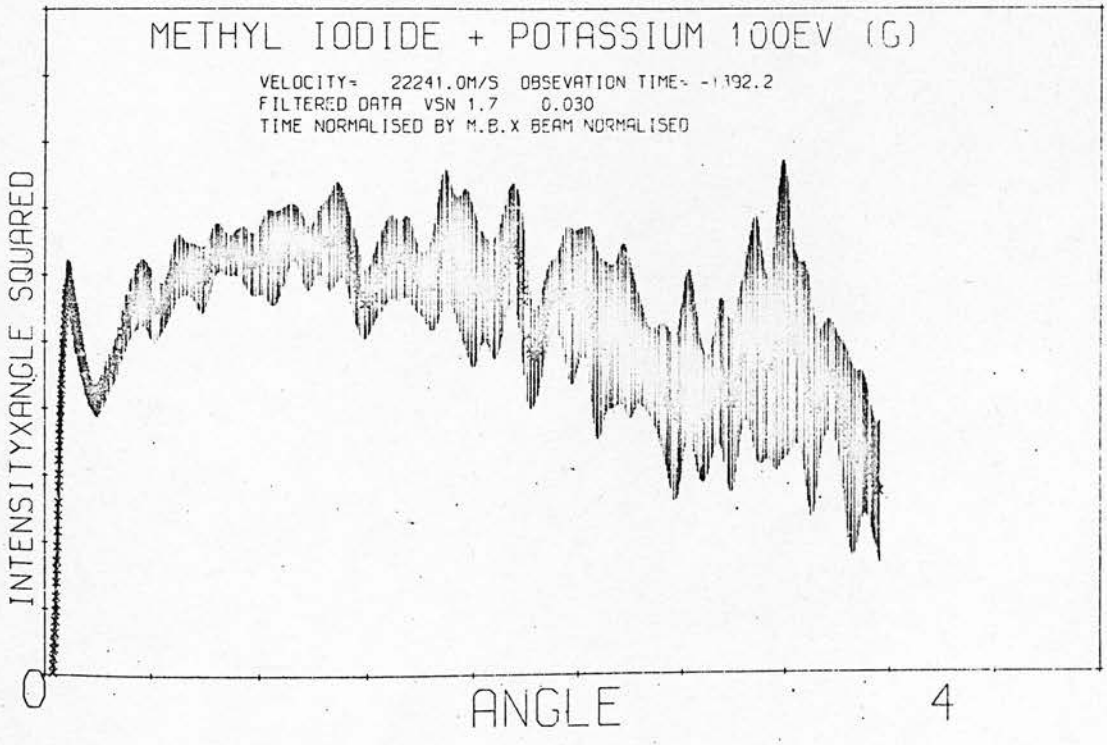
METHYL IODIDE + POTASSIUM 100EV (G)
VELOCITY= 22241.0M/S OBSEVATION TIME= 1192.2
FILTERED DATA VSN 1.7 0.030
TIME NORMALISED BY M.B.X BEAM NORMALISED
INTENSITYXANGLE SQUARED
0
ANGLE
4

FIGURE 4.2

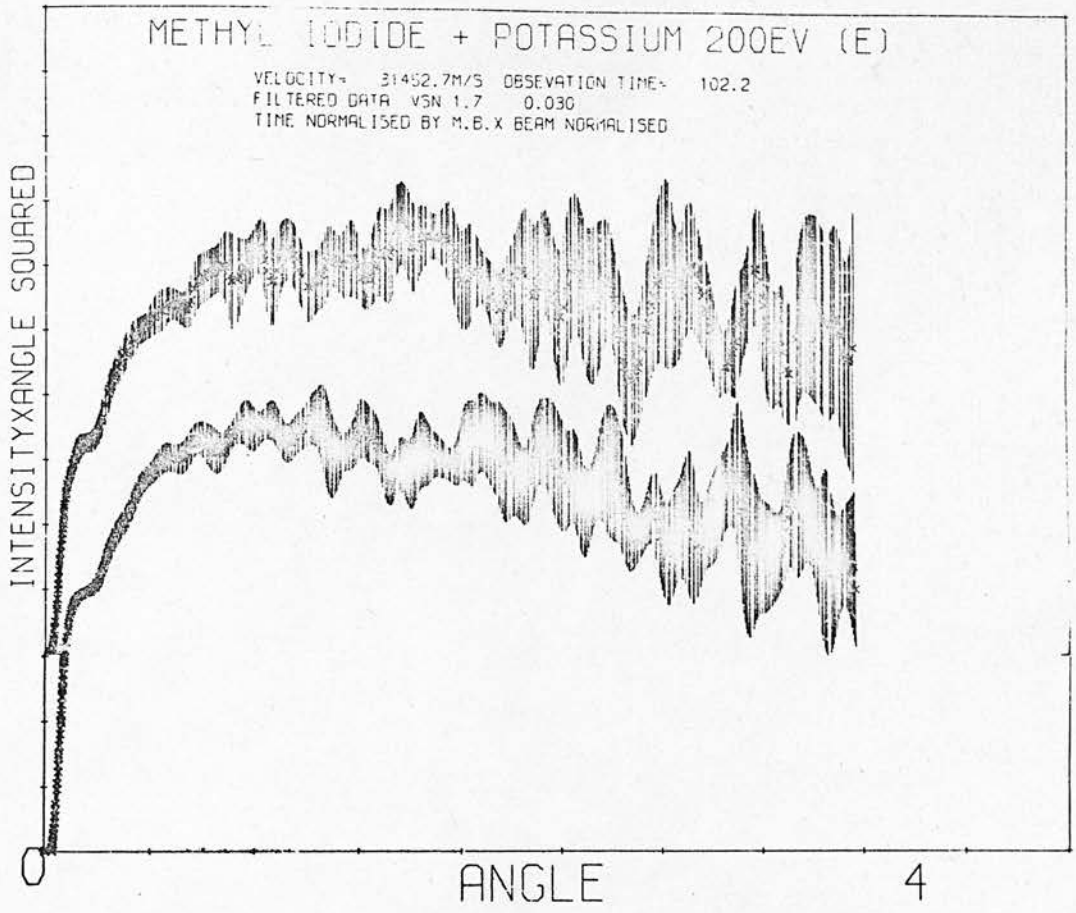
METHYL IODIDE + POTASSIUM 200EV (E)
VELOCITY= 31452.7M/S OBSEVATION TIME= 102.2
FILTERED DATA VSN 1.7 0.030
TIME NORMALISED BY M.B.X BEAM NORMALISED
INTENSITYXANGLE SQUARED
0
ANGLE
4

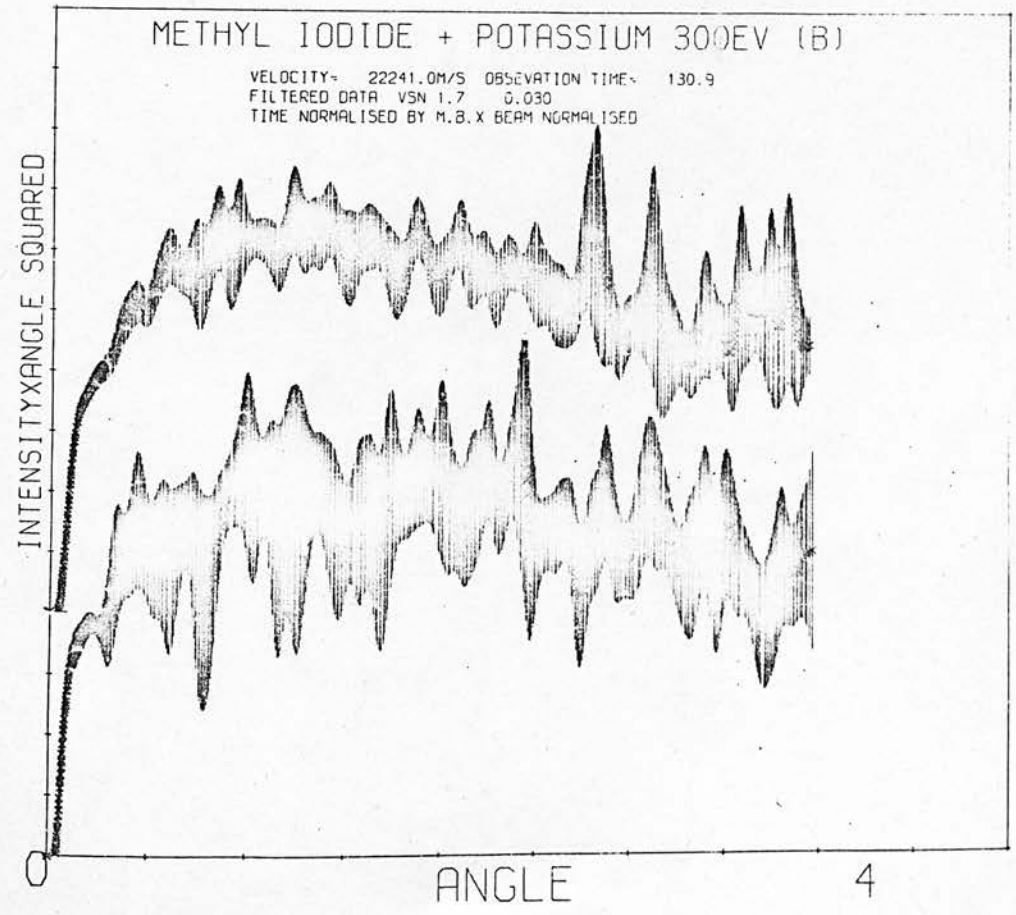
METHYL IODIDE + POTASSIUM 300EV (B)
VELOCITY= 22241.0M/S OBSEVATION TIME= 130.9
FILTERED DATA VSN 1.7 0.030
TIME NORMALISED BY M.B.X BEAM NORMALISED
INTENSITYXANGLE SQUARED
0
ANGLE
4

FIGURE 4.3

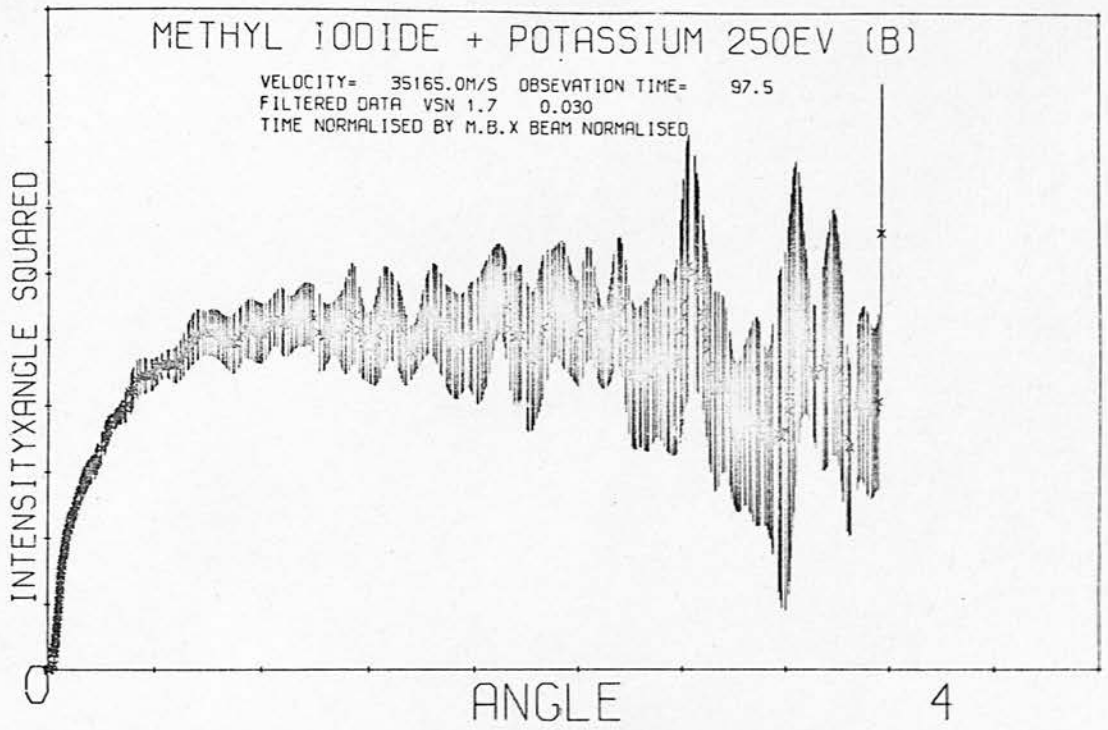
METHYL IODIDE + POTASSIUM 250EV (B)
VELOCITY= 35165.0M/S OBSEVATION TIME= 97.5
FILTERED DATA VSN 1.7 0.030
TIME NORMALISED BY M.B.X BEAM NORMALISED
INTENSITYXANGLE SQUARED
0
ANGLE
4

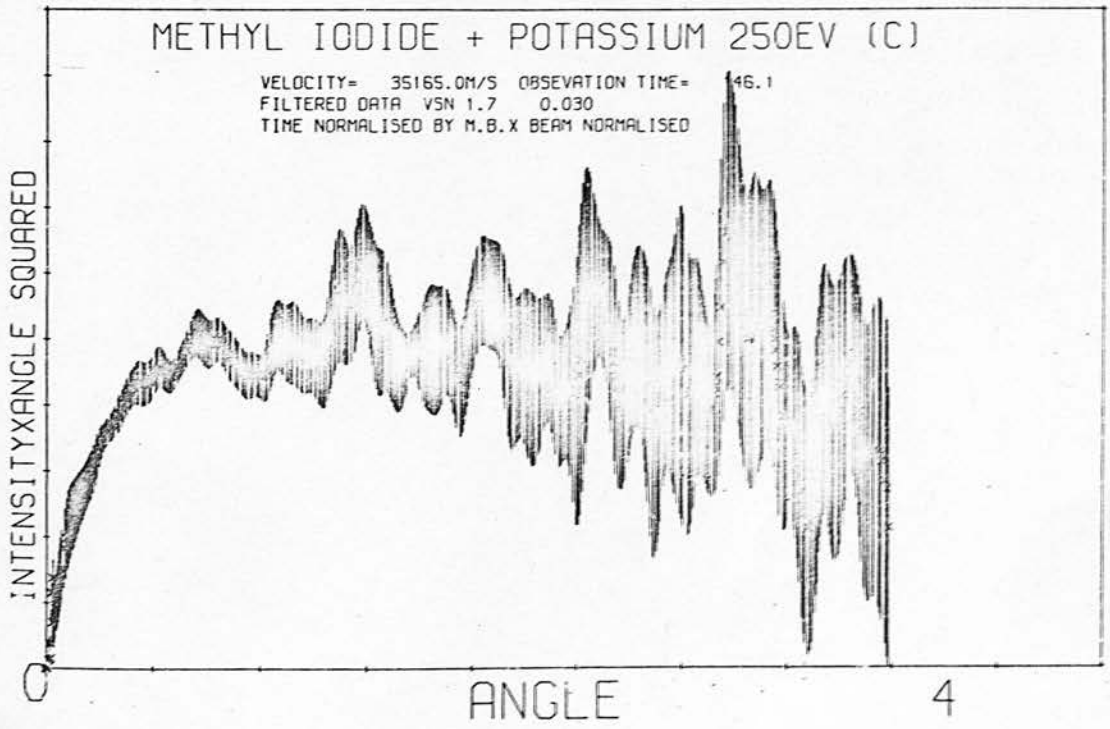
METHYL IODIDE + POTASSIUM 250EV (C)
VELOCITY= 35165.0M/S OBSEVATION TIME= 46.1
FILTERED DATA VSN 1.7 0.030
TIME NORMALISED BY M.B.X BEAM NORMALISED
INTENSITYXANGLE SQUARED
0
ANGLE
4

FIGURE 4.4

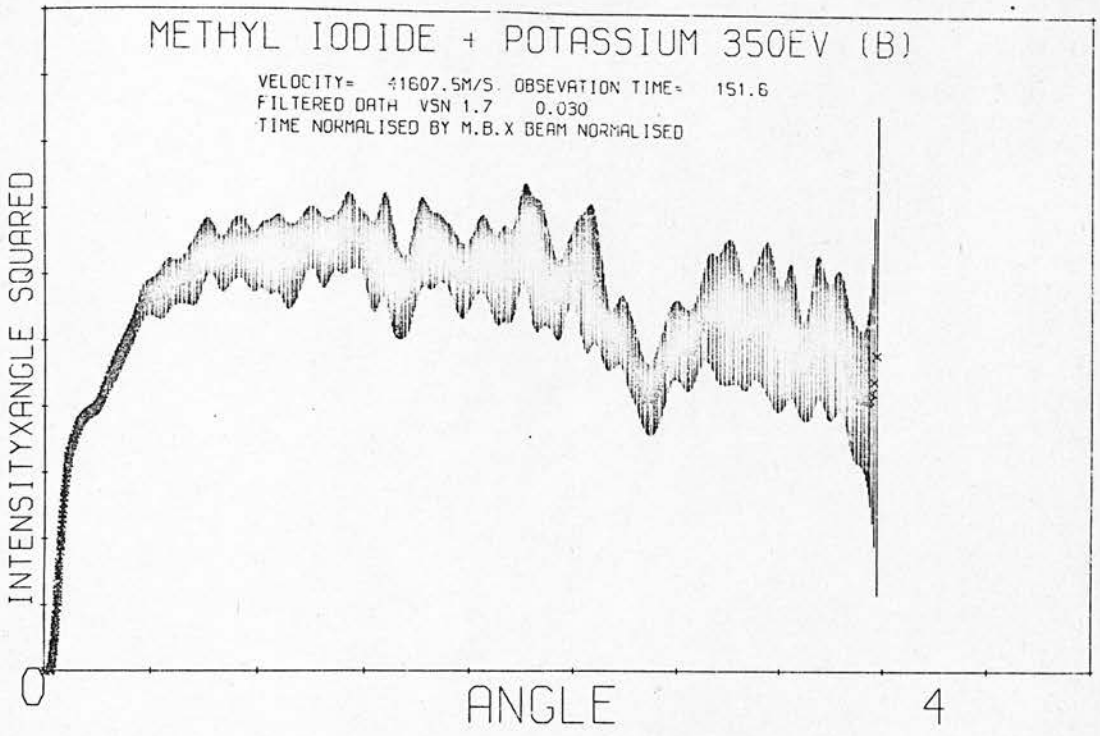
METHYL IODIDE + POTASSIUM 350EV (B)
VELOCITY= 41607.5M/S OBSEVATION TIME= 151.6
FILTERED DATH VSN 1.7 0.030
TIME NORMALISED BY M.B.X BEAM NORMALISED
INTENSITYXANGLE SQUARED
0
ANGLE
4

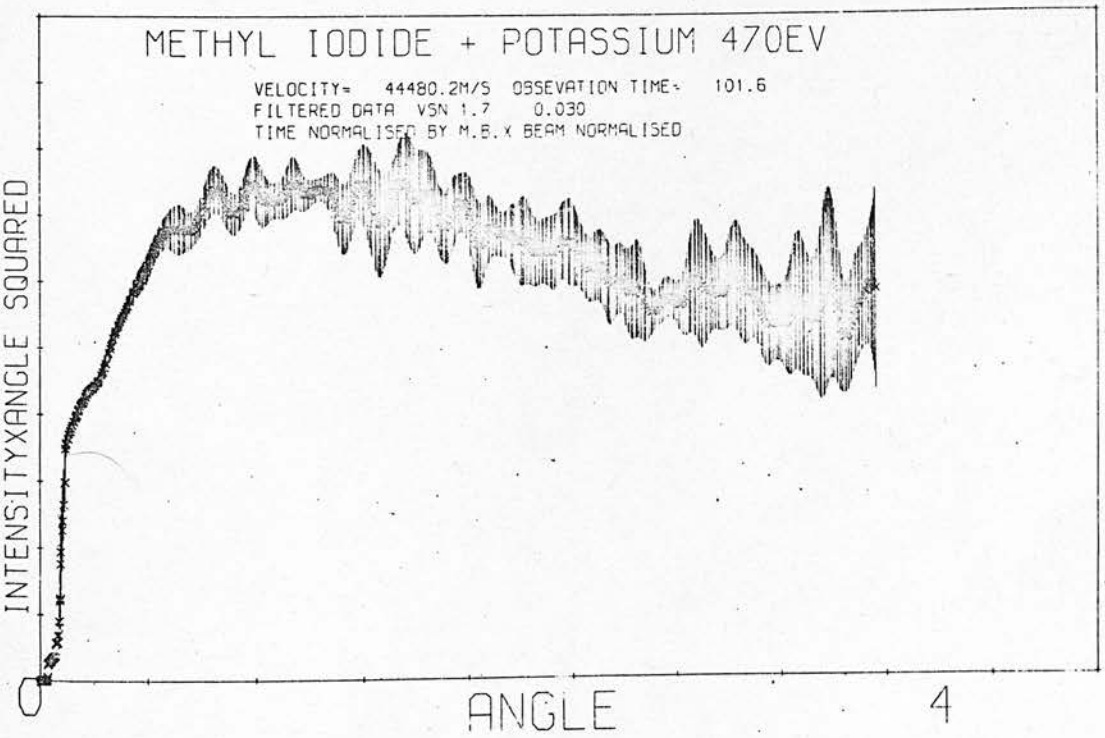
METHYL IODIDE + POTASSIUM 470EV
VELOCITY= 44480.2M/S OBSEVATION TIME= 101.6
FILTERED DATA VSN 1.7 0.030
TIME NORMALISED BY M.B.X BEAM NORMALISED
INTENSITYXANGLE SQUARED
0
ANGLE
4

FIGURE 4.5

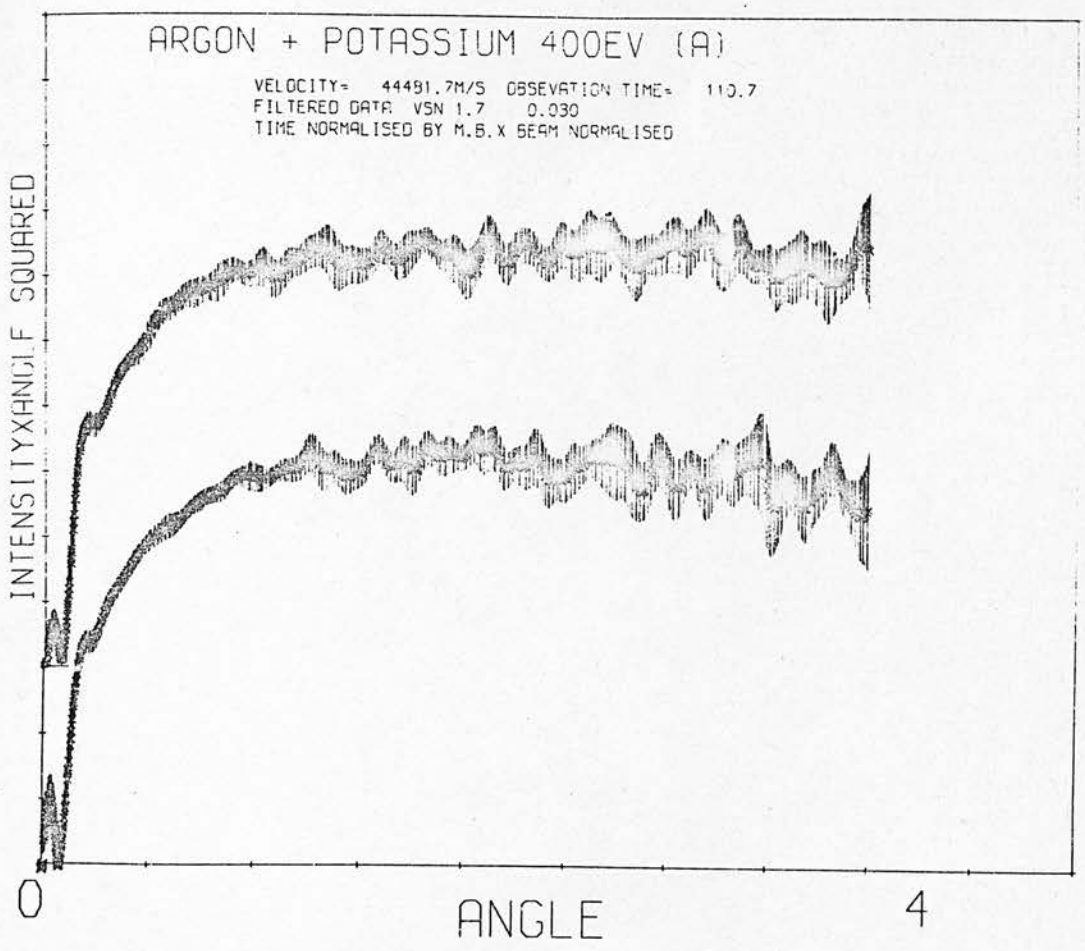
ARGON + POTASSIUM 400EV (A)
VELOCITY= 44491.7M/S OBSEVATION TIME= 110.7
FILTERED DATA VSN 1.7 0.030
TIME NORMALISED BY M.B.X BEAM NORMALISED
INTENSITYXANGLE SQUARED
0
ANGLE
4

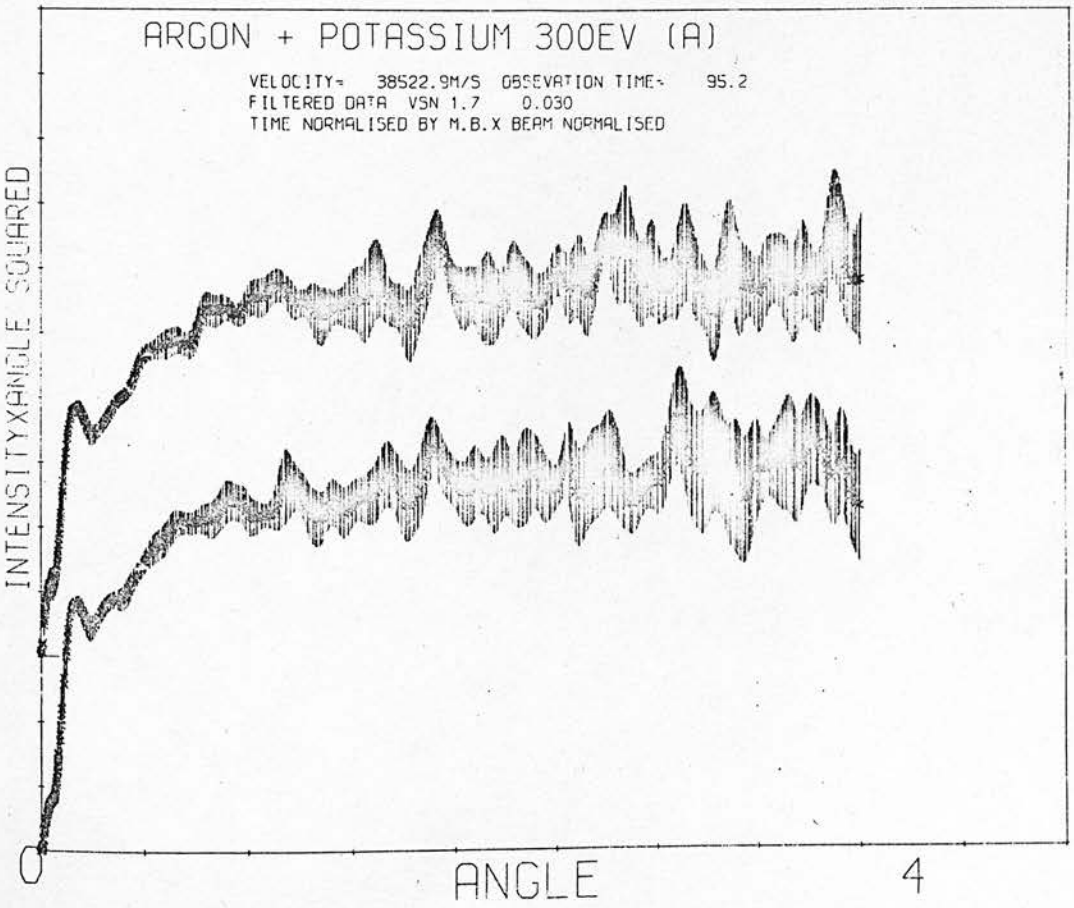
ARGON + POTASSIUM 300EV (A)
VELOCITY= 38522.9M/S OBSEVATION TIME= 95.2
FILTERED DATA VSN 1.7 0.030
TIME NORMALISED BY M.B.X BEAM NORMALISED
INTENSITYXANGLE SQUARED
0
ANGLE
4

FIGURE 4.6

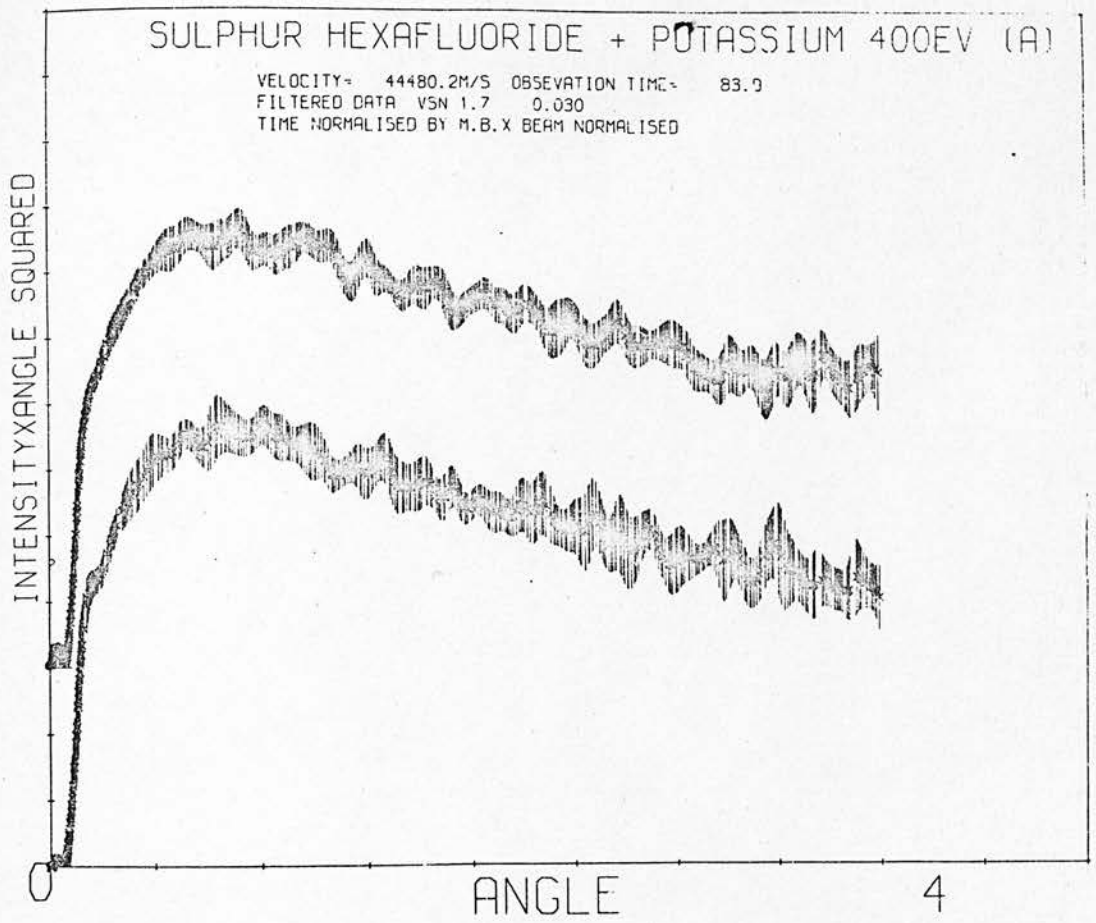
SULPHUR HEXAFLUORIDE + POTASSIUM 400EV (A)
VELOCITY= 44480.2M/S OBSEVATION TIME= 83.9
FILTERED DATA VSN 1.7 0.030
TIME NORMALISED BY M.B.X BEAM NORMALISED
INTENSITYXANGLE SQUARED
0
ANGLE
4

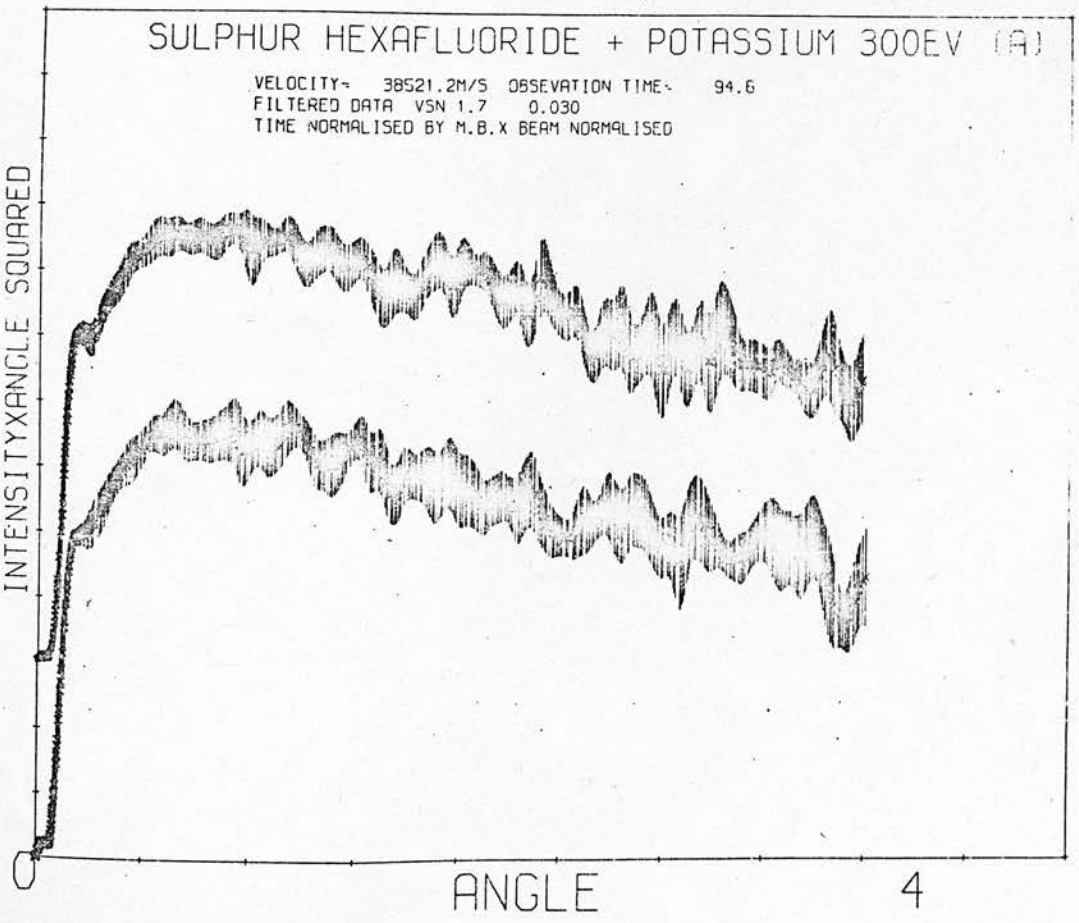
SULPHUR HEXAFLUORIDE + POTASSIUM 300EV (A)
VELOCITY= 38521.2M/S OBSEVATION TIME= 94.6
FILTERED DATA VSN 1.7 0.030
TIME NORMALISED BY M.B.X BEAM NORMALISED
INTENSITYXANGLE SQUARED
0
ANGLE
4

FIGURE 4.7

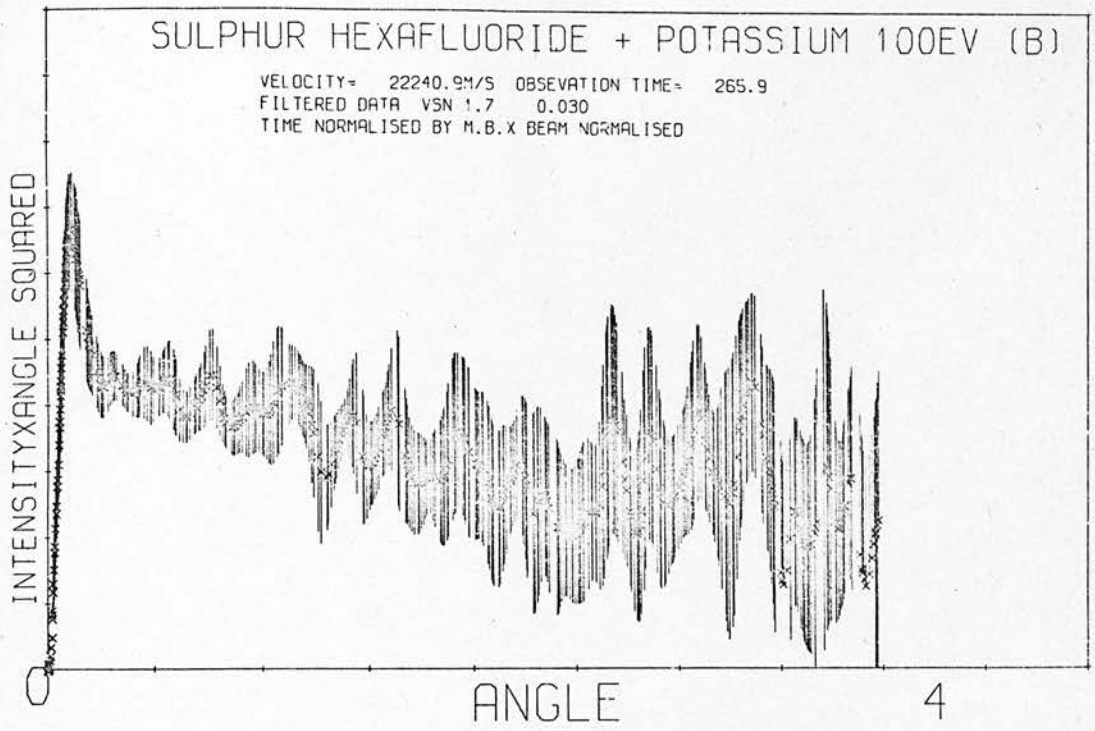
SULPHUR HEXAFLUORIDE + POTASSIUM 100EV (B)
VELOCITY= 22240.9M/S OBSEVATION TIME= 265.9
FILTERED DATA VSN 1.7 0.030
TIME NORMALISED BY M.B.X BEAM NORMALISED
INTENSITYXANGLE SQUARED
0
ANGLE
4

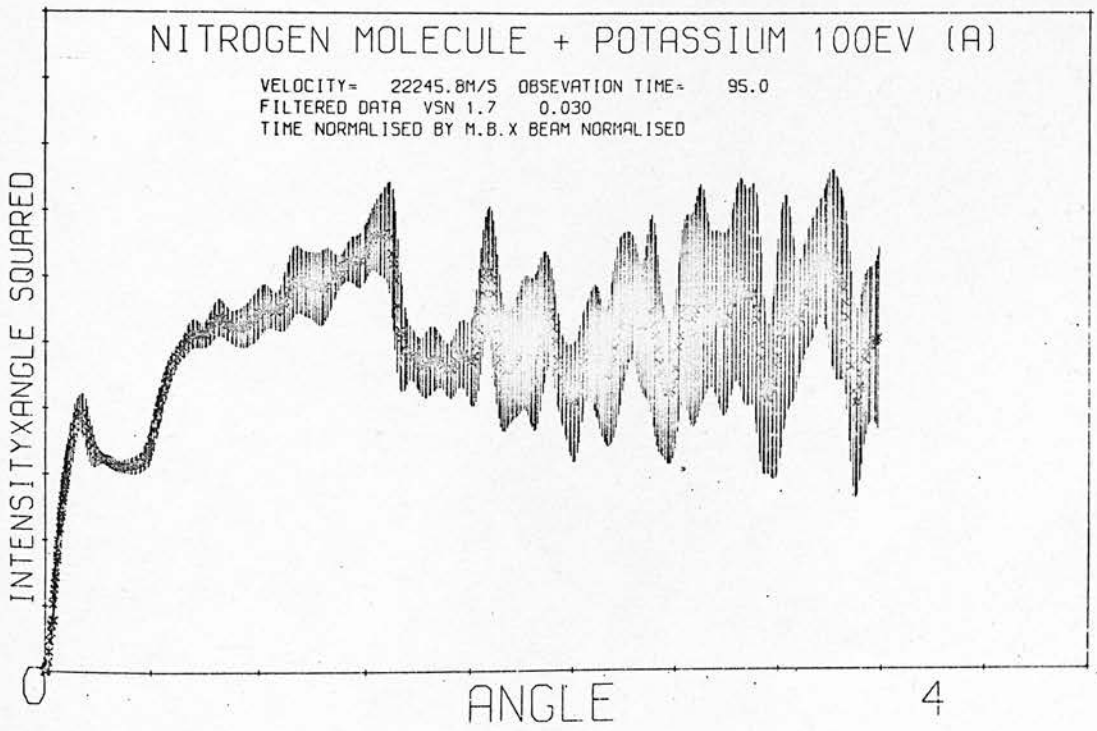
NITROGEN MOLECULE + POTASSIUM 100EV (A)
VELOCITY= 22245.8M/S OBSEVATION TIME= 95.0
FILTERED DATA VSN 1.7 0.030
TIME NORMALISED BY M.B.X BEAM NORMALISED
INTENSITYXANGLE SQUARED
0
ANGLE
4

FIGURE 4.8

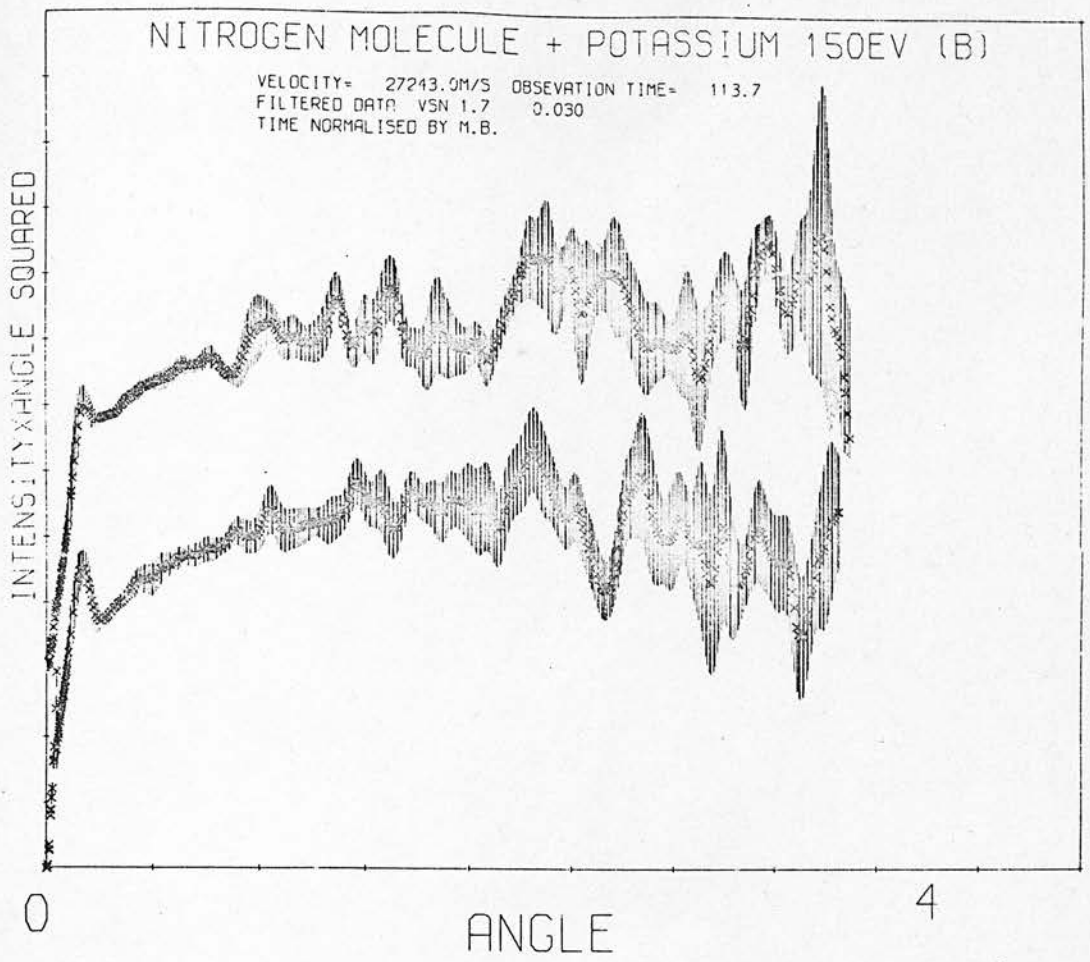
NITROGEN MOLECULE + POTASSIUM 150EV (B)
VELOCITY= 27243.9M/S OBSEVATION TIME= 113.7
FILTERED DATA VSN 1.7 0.030
TIME NORMALISED BY M.B.
INTENSITYXANGLE SQUARED
0
ANGLE
4

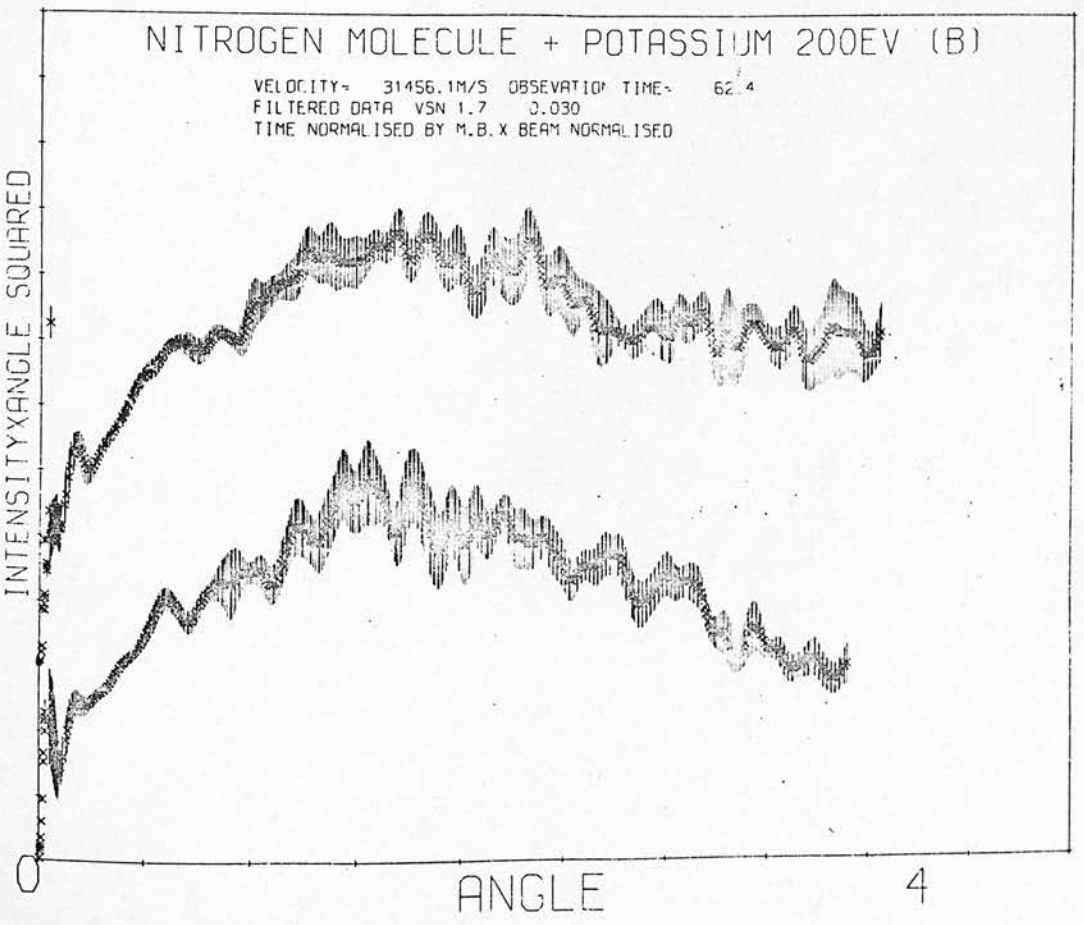
NITROGEN MOLECULE + POTASSIUM 200EV (B)
VELOCITY= 31456.1M/S OBSEVATION TIME= 62.4
FILTERED DATA VSN 1.7 0.030
TIME NORMALISED BY M.B.X BEAM NORMALISED
INTENSITYXANGLE SQUARED
0
ANGLE
4

FIGURE 4.9

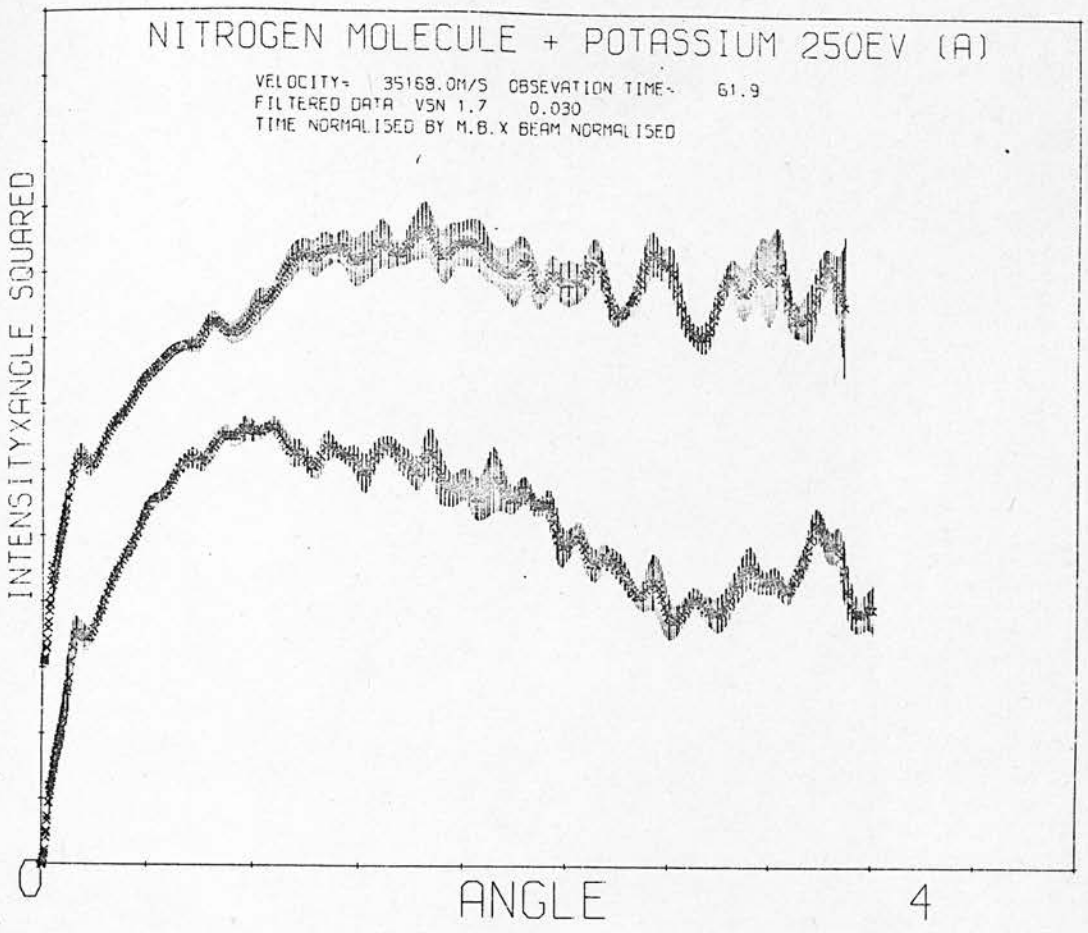
NITROGEN MOLECULE + POTASSIUM 250EV (A)
VELOCITY= 35168.0M/S OBSEVATION TIME= 61.9
FILTERED DATA VSN 1.7 0.030
TIME NORMALISED BY M.B.X BEAM NORMALISED
INTENSITYXANGLE SQUARED
0
ANGLE
4

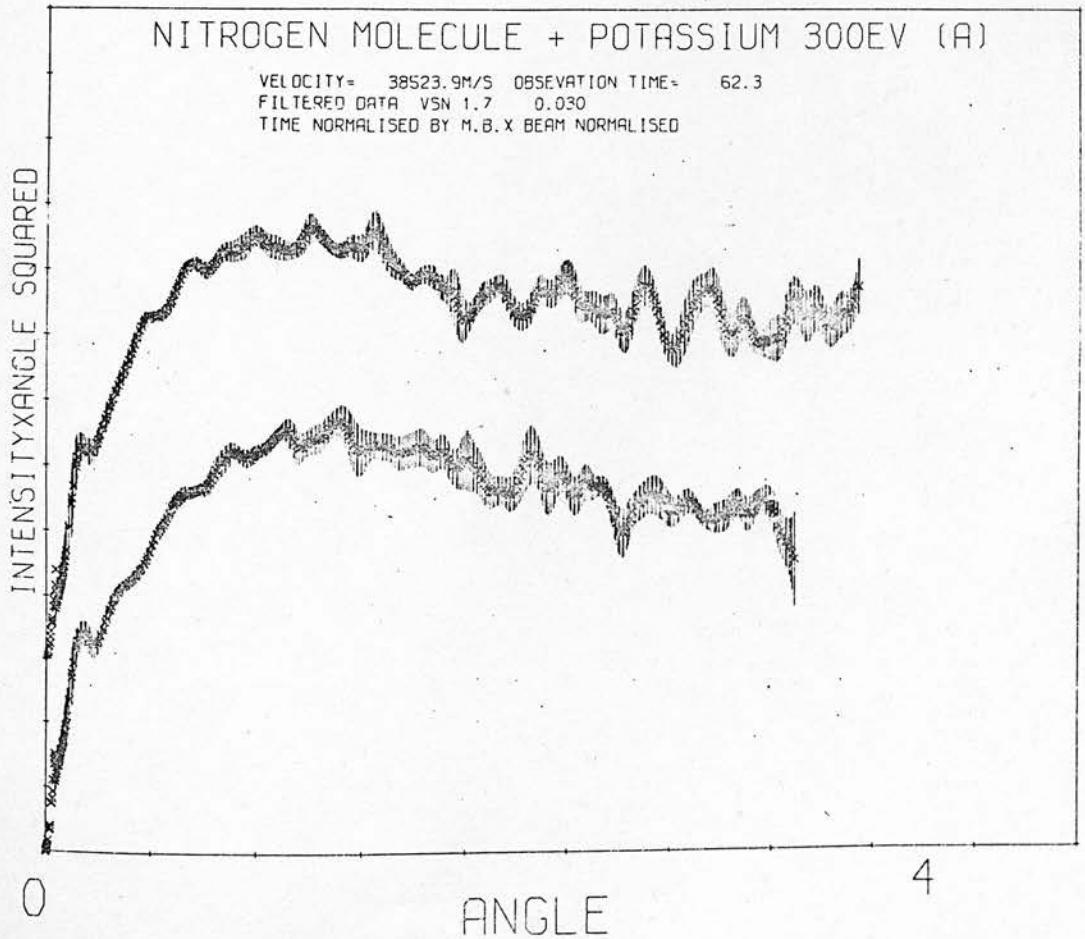
NITROGEN MOLECULE + POTASSIUM 300EV (A)
VELOCITY= 38523.9M/S OBSEVATION TIME= 62.3
FILTERED DATA VSN 1.7 0.030
TIME NORMALISED BY M.B.X BEAM NORMALISED
INTENSITYXANGLE SQUARED
0
ANGLE
4

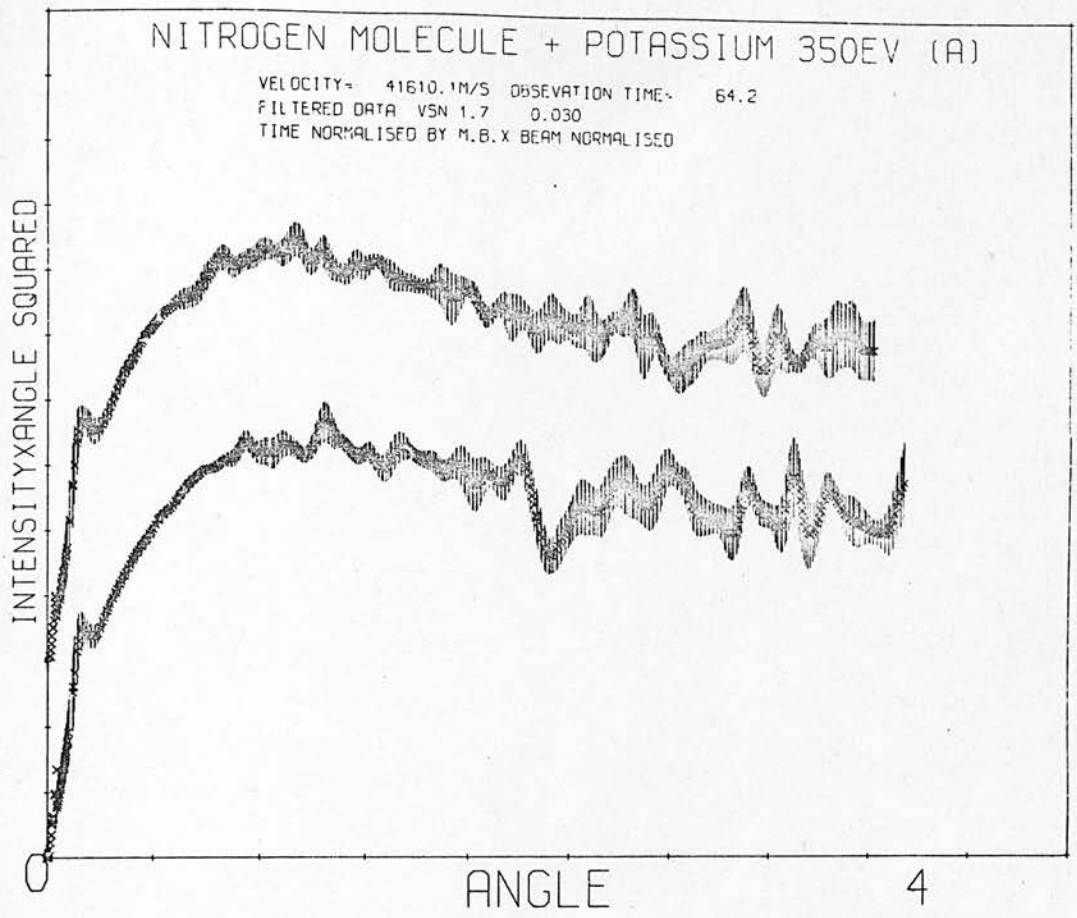
NITROGEN MOLECULE + POTASSIUM 350EV (A)
VELOCITY= 41610.1M/S OBSEVATION TIME= 64.2
FILTERED DATA VSN 1.7 0.030
TIME NORMALISED BY M.B.X BEAM NORMALISED
INTENSITYXANGLE SQUARED
0
ANGLE
4

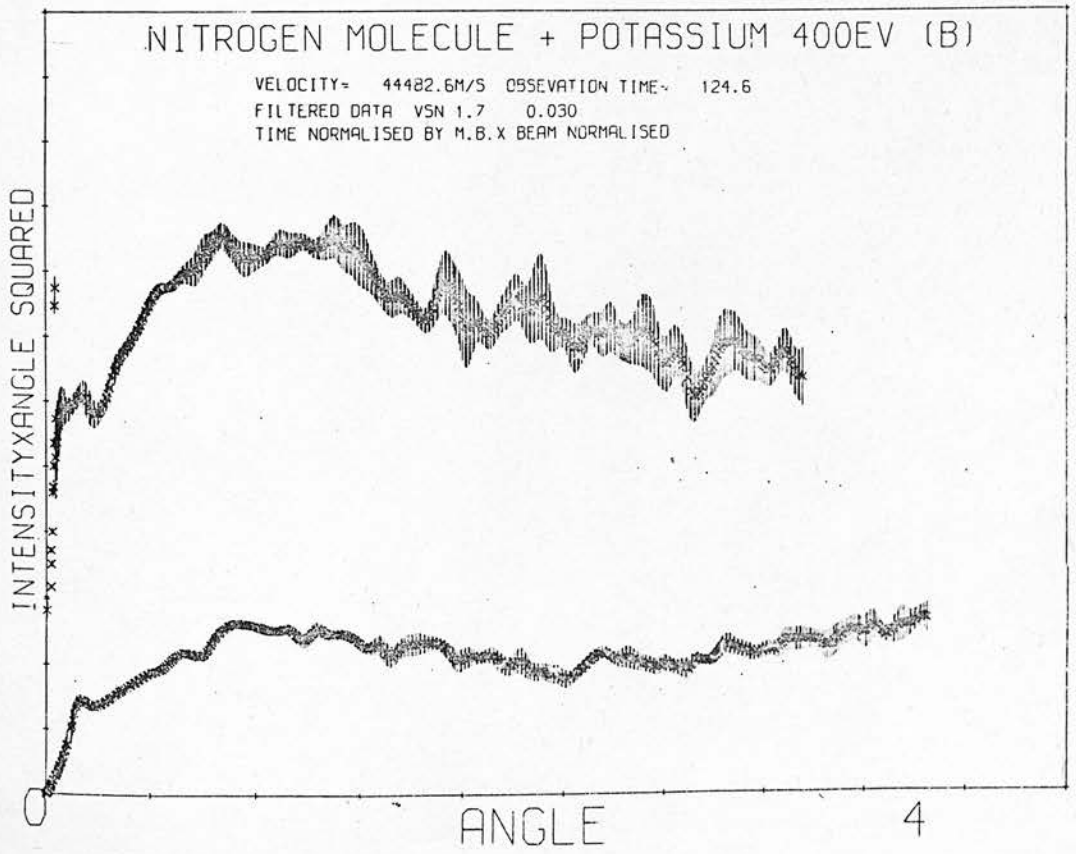
NITROGEN MOLECULE + POTASSIUM 400EV (B)
VELOCITY= 44482.6M/S OBSEVATION TIME= 124.6
FILTERED DATA VSN 1.7 0.030
TIME NORMALISED BY M.B.X BEAM NORMALISED
INTENSITYXANGLE SQUARED
0
ANGLE
4

FIGURE 4.11

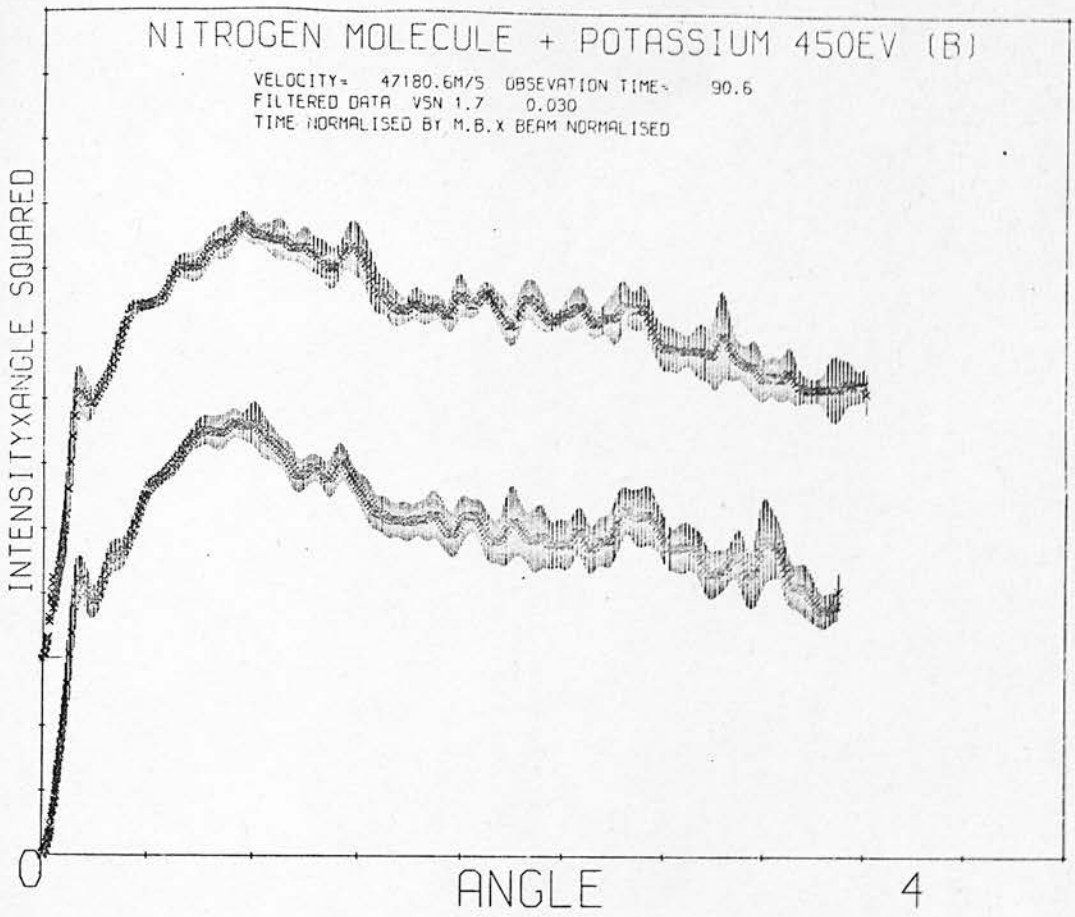
NITROGEN MOLECULE + POTASSIUM 450EV (B)
VELOCITY= 47180.6M/S OBSEVATION TIME= 90.6
FILTERED DATA VSN 1.7 0.030
TIME NORMALISED BY M.B.X BEAM NORMALISED
INTENSITYXANGLE SQUARED
0
ANGLE
4

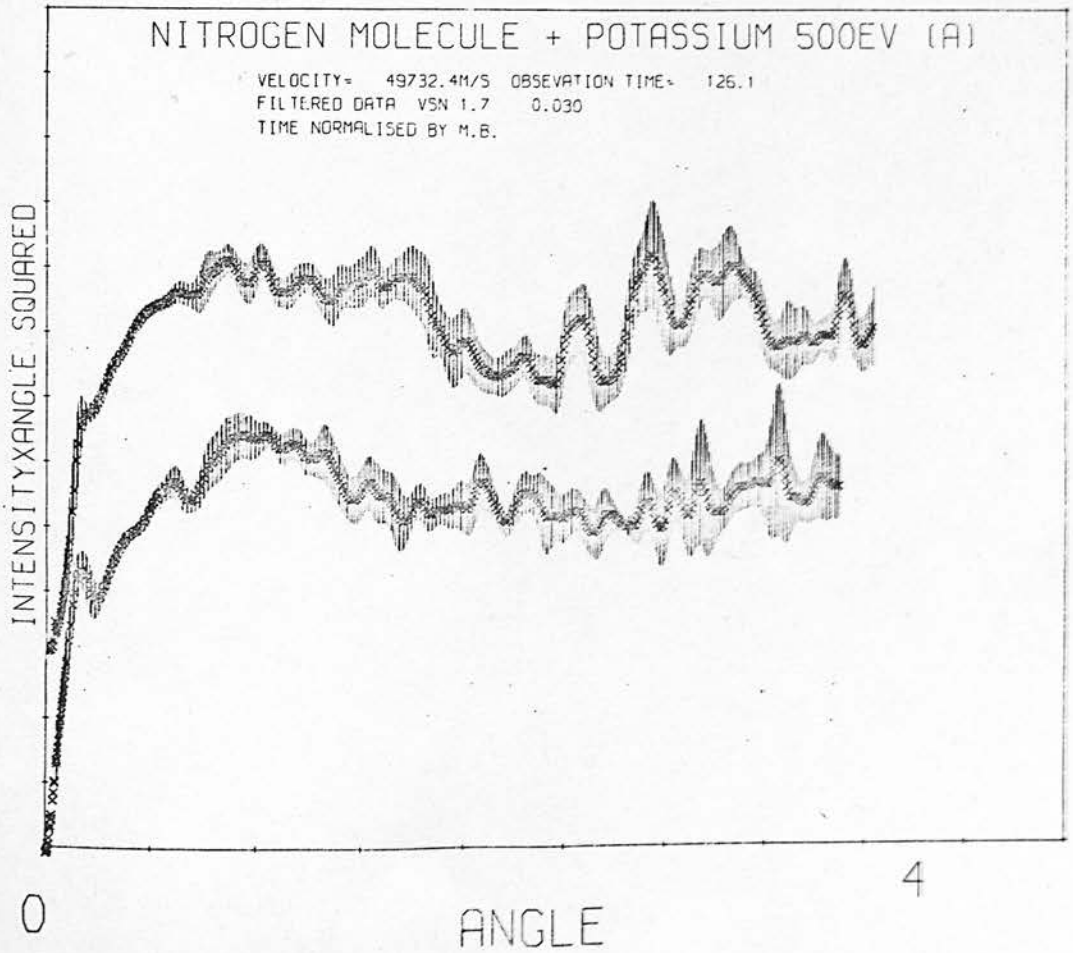
NITROGEN MOLECULE + POTASSIUM 500EV (A)
VELOCITY= 49732.4M/S OBSEVATION TIME= 126.1
FILTERED DATA VSN 1.7 0.030
TIME NORMALISED BY M.B.
INTENSITYXANGLE SQUARED
0
ANGLE
4

FIGURE 4.12

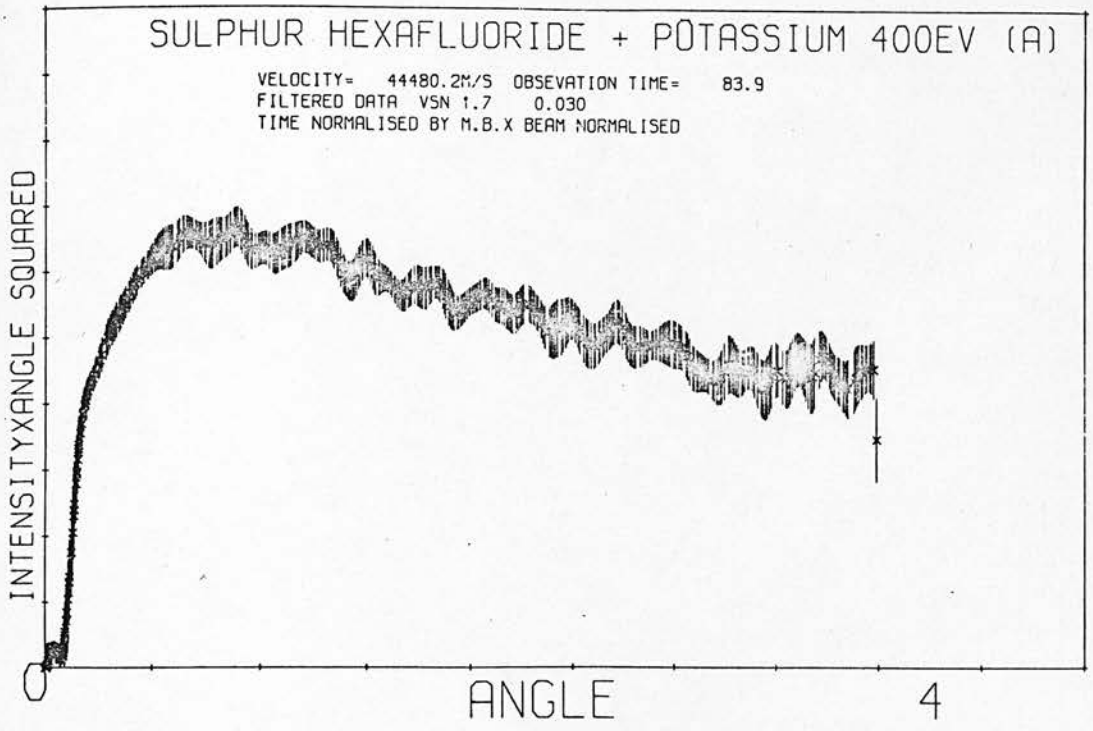
SULPHUR HEXAFLUORIDE + POTASSIUM 400EV (A)
VELOCITY= 44480.2M/S OBSEVATION TIME= 83.9
FILTERED DATA VSN 1.7 0.030
TIME NORMALISED BY M.B.X BEAM NORMALISED
INTENSITYXANGLE SQUARED
ANGLE
4

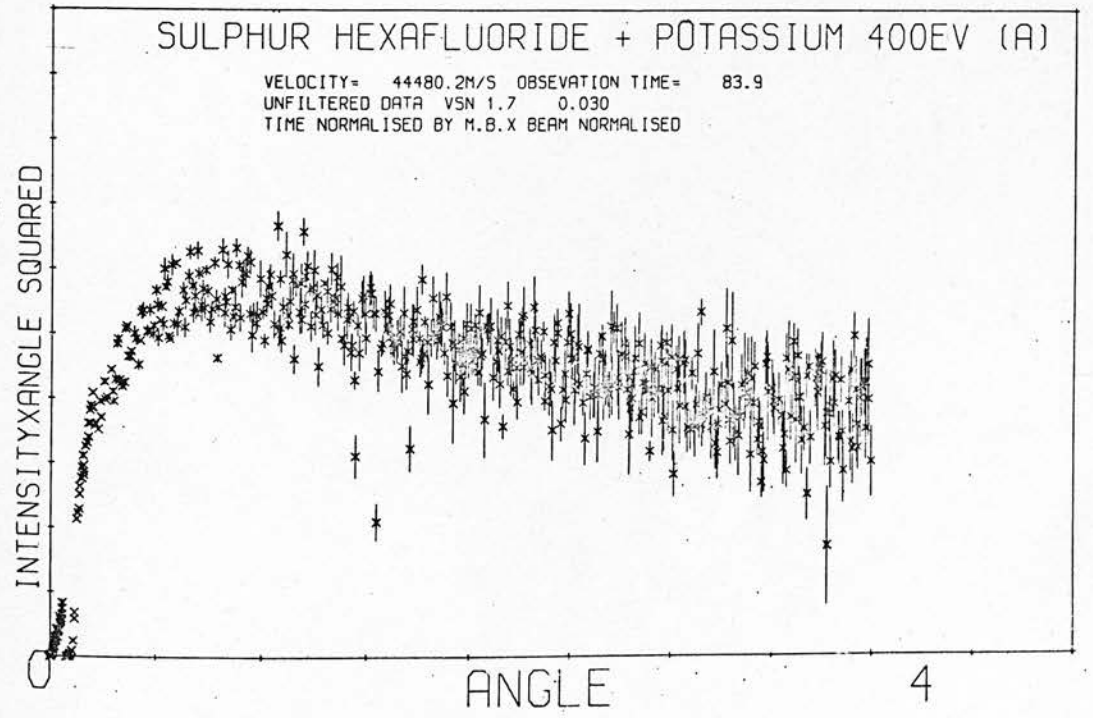
SULPHUR HEXAFLUORIDE + POTASSIUM 400EV (A)
VELOCITY= 44480.2M/S OBSEVATION TIME= 83.9
UNFILTERED DATA VSN 1.7 0.030
TIME NORMALISED BY M.B.X BEAM NORMALISED
INTENSITYXANGLE SQUARED
ANGLE
4

FIGURE 4.13

surfaces. In addition, some experimental results had already been obtained with the present apparatus (RED 73) which appeared to show oscillatory structure. This turned out not to be reproducible and is thought to have been artificially produced by the analysis procedure.

Although various bumps appear in the cross sections, these are not reproduced between different measurements and do not move in any systematic way with energy. Structure has not therefore been resolved in the experiments. A possible cause for this is the anisotropy of methyl iodide as collision time is short compared with the rotational period. Experiments were therefore performed on the spherically symmetric systems argon and sulphur hexafluoride. The quadrupole mass filter was removed at this stage and the reduced noise due to increased beam intensity may be observed.

Finally a series of measurements was taken on the collision system potassium/nitrogen. It is known from collision induced fluorescence (KEM 70) and time of flight (GER 73) experiments that there is a fairly large cross section for production of excited potassium on collision with N_2 in the 100 - 500eV energy region. Again, the presence of a second potential surface was expected to produce structure in the elastic differential cross section through the effects described later in this chapter. The energy range was covered rather finely in order to pin down effects occurring at the threshold for production of the various excited states. In these experiments the pseudo random method of covering the angular range was abandoned allowing perturbations of the overall shape of the envelope in the hope of achieving better resolution of high frequency structure.

In no instance are reproducible features or structure to be seen. The shape of the envelope was therefore analysed to give some information on the dependence of the potential or internuclear separation, r.

4.2 Estimation of r dependence of potentials

If the potential in the range explored by the experiment can be represented by the form

$$V(r) = \frac{K}{r^s}$$

the classical expression for the small angle differential cross section is

$$\sigma(x) = s^{-1}\{s\pi^{\frac{1}{2}}\frac{\Gamma(\frac{s+1}{2})K}{\Gamma(\frac{s}{2})E}\}^{2/s}\chi^{-(2+2/s)}$$

Thus, a plot of log $(\chi^2\sigma_{ex}(\chi))$ vs. log (χ) should be a straight line with gradient $g = \frac{-2}{s}$ if the above assumption is valid. The value of K could then be obtained from the intercept if the absolute differential cross section was measured, which is not the case in the present experiments. The observed cross sections were corrected for beam drifts and apparatus angular resolution, then coverted to the centre of mass coordinate system as described in Chapter 2. Plots of log $(\chi^2\sigma_{ex}(\chi))$ vs. log (χ) are shown in Figure 4.14 for the potassium/argon data of Figure 4.7 and in Figure 4.15 for the potassium/sulphur hexafluoride data of Figure 4.6. The small angle data is uncertain due to the effect of the main beam wings, and since the apparatus

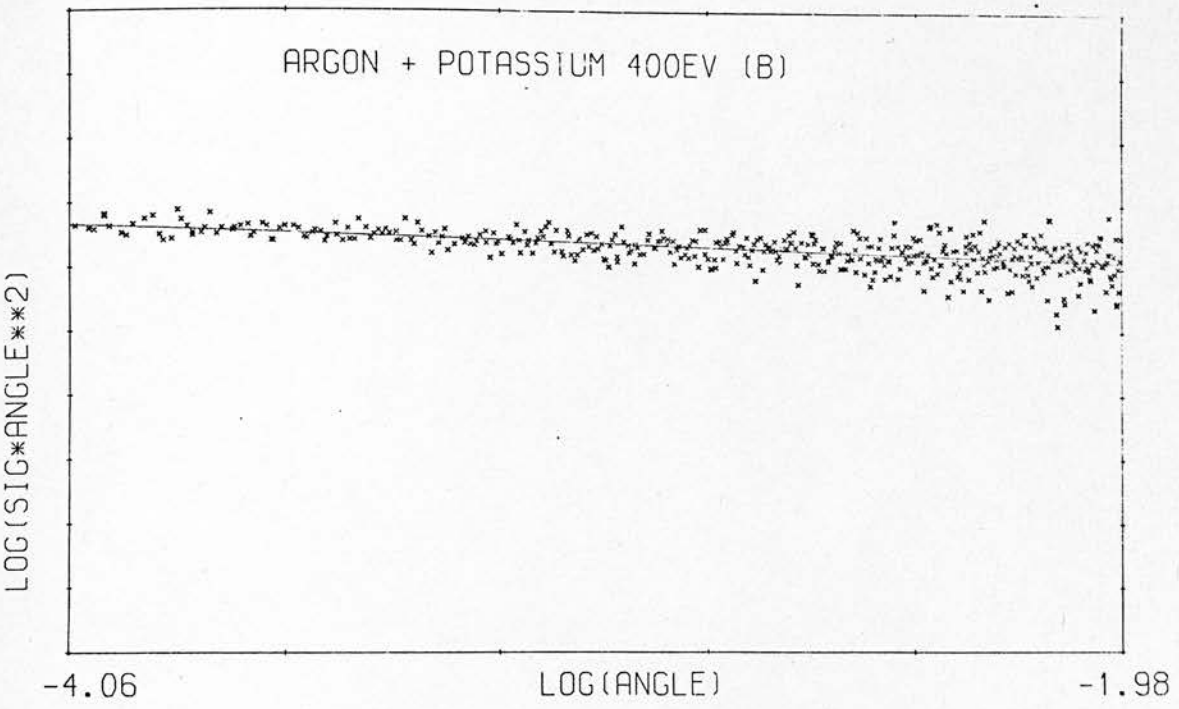
ARGON + POTASSIUM 400EV (B)
LOG(SIG*ANGLE**2)
-4.06
LOG(ANGLE)
-1.98

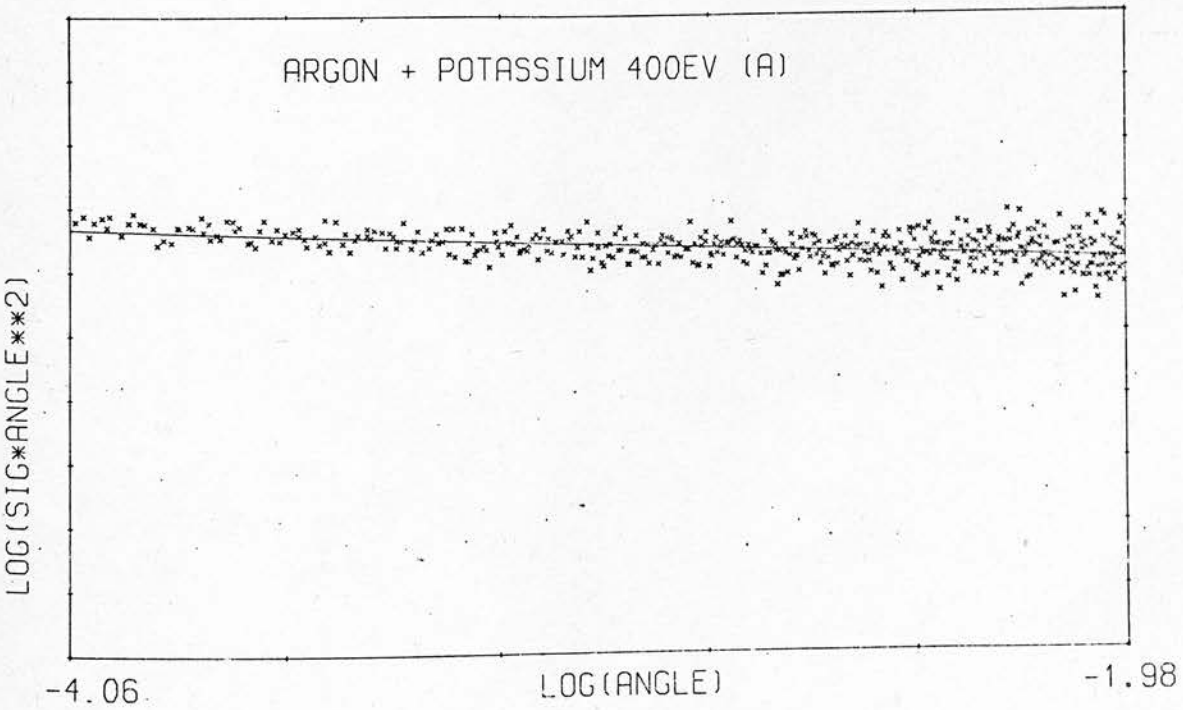
ARGON + POTASSIUM 400EV (A)
LOG(SIG*ANGLE**2)
-4.06
LOG(ANGLE)
-1.98

FIGURE 4.14

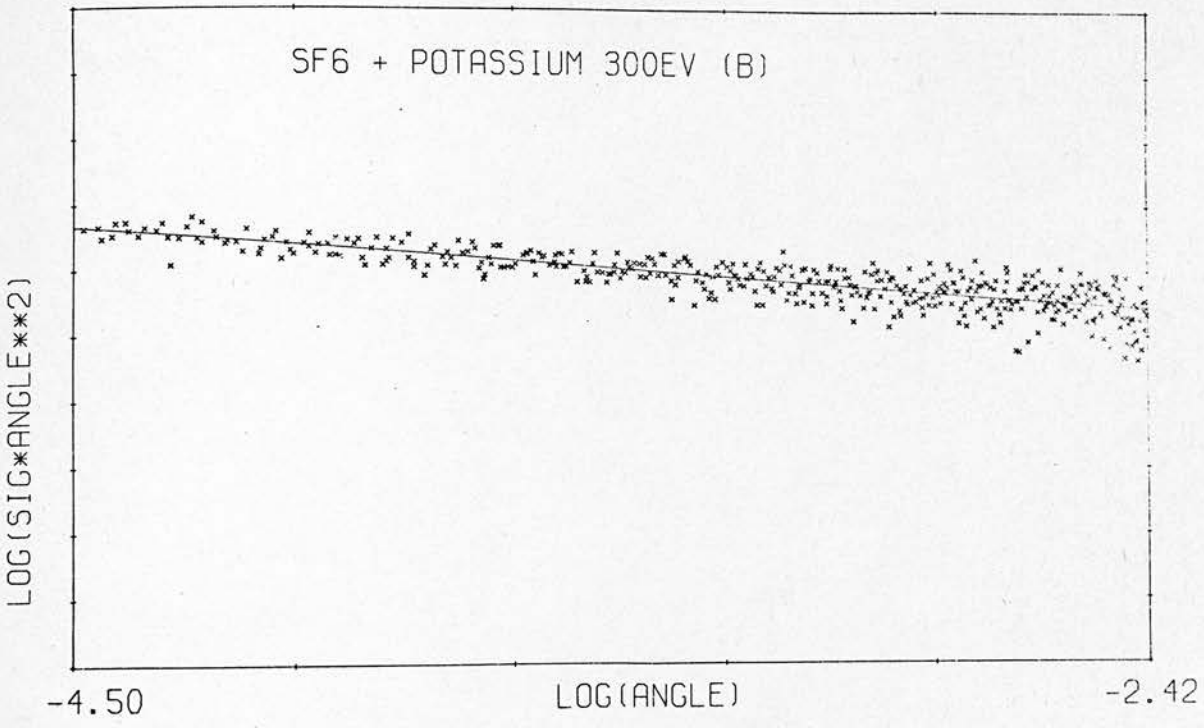
SF6 + POTASSIUM 300EV (B)
LOG(SIG*ANGLE**2)
-4.50
LOG(ANGLE)
-2.42

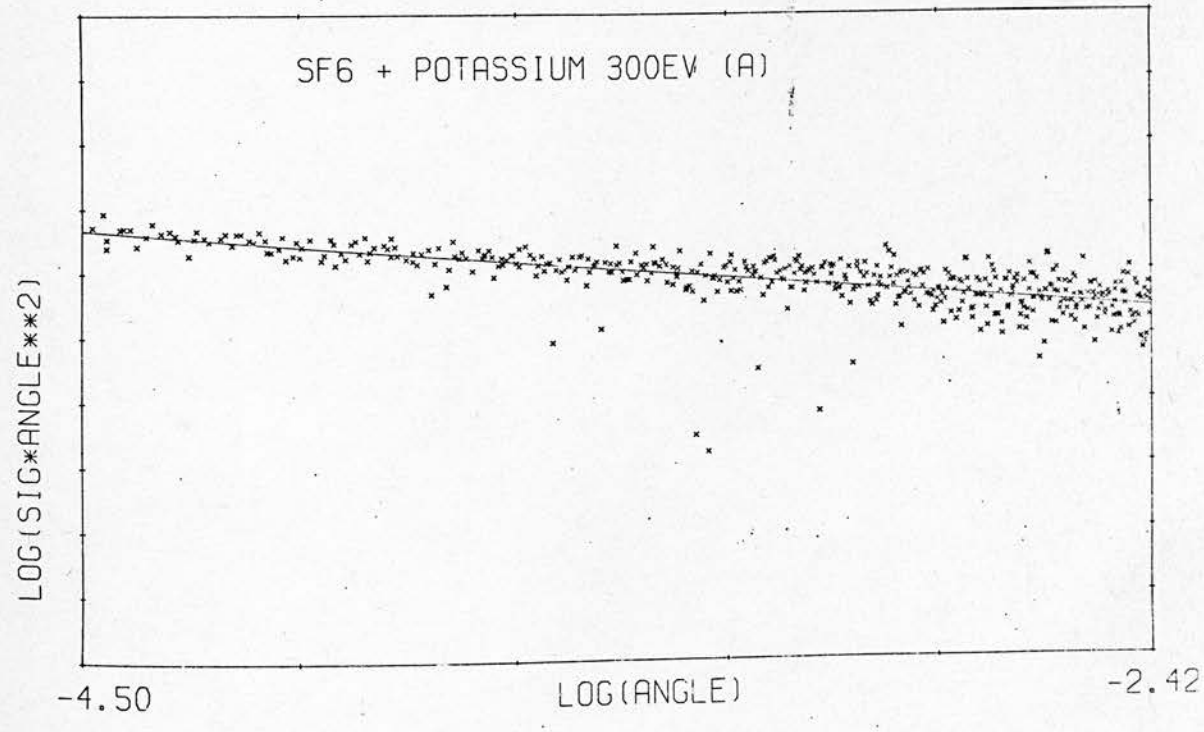
SF6 + POTASSIUM 300EV (A)
LOG(SIG*ANGLE**2)
-4.50
LOG(ANGLE)
-2.42

FIGURE 4.15

resolution correction becomes large, it was felt unwise to place too much reliance on the data in this region. In all cases therefore the data at angles less than 0.5^{o} in the LAB was rejected. The graphs appeared to be well described by a straight line and the best estimate of the gradient was obtained by minimisation of squared deviations. The gradients and corresponding values for s are given in Figure 4.16.

The error limits in s correspond to the 95% confidence limits quoted for g. In both systems the results for s agree within experimental error for the different runs and energies. The range in V(r) over which these results are valid is given by the classical expression for the value of V(R) at the turning point r_o

$$V(r_o) = \frac{E_{cm}\chi_{cm}}{C_s} , \quad C_s = \frac{\sqrt{\pi}\ \Gamma\left(\frac{s+1}{2}\right)}{\Gamma\left(\frac{s}{2}\right)}$$

Applying this relation to the extreme values of the observed energy and angle gives the results:

Potassium/Argon

$$V(R) = \frac{K_A}{r^s} , \quad s = 15 \pm 3 , \quad 5.9 > V(R)/eV > .7$$

Potassium/Sulphur Hexafluoride

$$V(R) = \frac{K_{SF_6}}{r^s} , \quad s = 4.7 \pm .2 , \quad 10.6 > V(R)/eV > .3$$

The same procedure was applied to the systems K/N_2 and K/CH_3I, but with much poorer agreement between experiments. No systematic variation with energy or angle was discernable and the poor quality of

Experimental Power Dependences for the K + A and $K + SF_6$ Potential Functions

System	CM Energy / eV	Gradient	s
K + A	202	-.13 ± .02	15 ± 2
"	"	-.13 ± .02	15 ± 2
"	152	-.10 ± .03	20 ± 6
"	"	-.14 ± .06	15 ± 7
$K + SF_6$	316	-.43 ± .02	4.6 ± .2
"	"	-.43 ± .02	4.7 ± .3
"	237	-.43 ± .04	4.7 ± .4
"	"	-.42 ± .03	4.7 ± .3
"	79	-.34 ± .09	5.9 ± 1.6

FIGURE 4.16

the results was attributed in the case of methyl iodide to the low beam intensity resulting from the presence of the quadrupole mass filter and in the case of nitrogen to the abandonment of the random scanning procedure. The values were simply averaged to give the results quoted below:

Potassium/Nitrogen

$$V(R) = \frac{K_{N_2}}{r^s} \quad , \quad s = 7 \pm 1 \quad , \quad 11 > V(R)/eV > .4$$

Potassium/Methyl Iodide

$$V(R) = \frac{K_{CH_3I}}{r^s} \quad , \quad s = 8 \pm 3 \quad , \quad 10 > V(R)/eV > .5$$

4.3 Calculation of Differential Cross Section

The structure which is expected to appear in differential cross sections in the energy and angular range covered by the experiments is now considered in more detail. Semi classical methods are used as the criterion for the semi classical approximation, that the wavelength is much less than the range of the potential, is well satisfied. Thus the scattered particle is taken to follow a classical path and have a phase shift, η, related to the classical action integral,

$$\eta(b) = k\{\int_{r_o}^{\infty}(1-\frac{V(r)}{E}-\frac{b^2}{r^2})^{\frac{1}{2}}dr - \int_{b}^{\infty}(1-\frac{b^2}{r^2})^{\frac{1}{2}}dr \qquad (4.1)$$

where b is the impact parameter, r_o the distance of closest approach and E the collision energy. To devise an approximation to this integral valid for small angle scattering, a straight line trajectory with constant velocity, v, was assumed and the integral was transformed to the time domain. The trajectory is given by

$$r^2 = b^2 + v^2 t^2$$

with $v = \frac{\sqrt{2E}}{\mu}$ and $r_o = b$ where μ is the reduced mass of the system. Then

$$\eta(b) = k \int_o^\infty \{(1 - \frac{V(t)}{E} \times \frac{v^2t^2+b^2}{v^2t^2})^{\frac{1}{2}} \frac{v^2t^2}{v^2t^2+b^2} - \frac{v^2t^2}{v^2t^2+b^2}\}dt \quad (4.2)$$

where t = 0 at r = b. Since V(t)<<E for small angles of scattering, the first term may be expanded in powers of V/E and terms of order $(V/E)^2$ neglected. The approximation for the phase shift is then

$$\eta(b) = -\frac{1}{\hbar} \int_o^\infty V(t)dt \quad (4.3)$$

For the potential of the form

$$V(r) = K/r^s, \quad (4.4)$$

the integral may be evaluated analytically by the recurrence relation

$$\int_o^{t^1} \frac{Kdt}{(b^2+v^2t^2)^{s/2}} = \frac{Kt^1}{(s-2)b^2(b^2+v^2t^2)^{s/2-1}} + \frac{(s-3)}{(s-2)b^2} \int_o^{t^1} \frac{Kdt}{(b^2+v^2t^2)^{s/2-1}}$$

For $t^1 \to \infty$, all terms disappear but the last which is for even, integral s:

$$\frac{(s-3)(s-5)....3 \times 1}{(s-2)(s-4)....4 \times 2} \frac{1}{b^{s-2}} \int_0^\infty \frac{Kdt}{v^2(\frac{b^2}{v^2} + t^2)}$$

Using the definition of the gamma functions

$$\Gamma(n) = (n-1)\Gamma(n-1) \quad \text{and} \quad \Gamma(\tfrac{1}{2}) = \sqrt{\pi}$$

and evaluating the integral,

$$\eta(b) = -\frac{1}{h} \frac{\sqrt{\pi}\Gamma(\frac{s+1}{2})}{(s-1)\Gamma(\frac{s}{2})} v \frac{K}{b^{s-1}} \tag{4.6}$$

The semi classical phase shift is related to the deflection function ($\chi(b)$) by the equation

$$\frac{d\eta}{dl} = \frac{\chi}{2} \quad \text{where } l = \mu v b/h \tag{4.7}$$

The result for χ calculated from the expression 4.6 is

$$\chi = \frac{\sqrt{\pi}\ \Gamma\ (\frac{s+1}{2})}{\Gamma(s/2)E} \times \frac{K_s}{b^s} \tag{4.8}$$

which is identical to the result of Kennard (KEN 38) produced with similar approximations for the integral over dR. The advantage of the method given above is that contributions to the phase shift for sections of the trajectory are easily obtained by inserting the appropriate limits. This is useful when crossings between two different potentials are considered.

The differential cross section is related to the deflection function by

$$\sigma(\chi) = \frac{b}{\left|\frac{d\chi}{db}\right| \sin \chi} \tag{4.9}$$

Inserting the result obtained above and setting $\sin\chi = \chi$ gives the following result for the small angle differential cross section

$$\sigma(\chi) = \frac{1}{s}\{s\sqrt{\pi}\,\frac{\Gamma(\frac{s+1}{2})}{\Gamma(\frac{s}{2}+1)E}K_1\frac{2}{s}\,\chi\}^{-(2+\frac{2}{s})} \tag{4.10}$$

The result (4.10) fails when more than one region of a deflection function contributes to the scattering at any angle due to quantum interference effects. The quantum mechanical cross section must then be used, ie

$$\sigma_q(\chi) = |f(\chi)|^2$$

$$f(\chi) = \frac{1}{2ik}\sum_{\ell=0}^{\infty}(2\ell+1)(\ell^{2i\eta_\ell}-1)\,P_\ell(\cos\chi) \tag{4.11}$$

Ford and Wheeler (FOR 59) have shown that where semiclassical approximations are valid this summation may be replaced by an integral which can be evaluated by the method of stationary phase. In particular if there are two regions of stationary phase χ_0 and χ_1 with corresponding classical differential cross sections σ_0 and σ_1 then σ_q is given by the relation

$$\sigma_q(\chi) = \sigma_0 + \sigma_1 + 2\sqrt{\sigma_1\sigma_0}\cos(\beta_1 - \beta_0) \tag{4.12}$$

The interference structure is governed by the quantity

$$\beta_1 - \beta_0 = 2\eta_1 - \ell_1\chi - 2\eta_0 + \ell_0\chi \tag{4.13}$$

From equations (4.6) and (4.8), it follows that

$$\ell\chi/2\eta = -2(s-1) \tag{4.14}$$

and since s is expected to be about 12 for repulsive potentials, the phase shifts can be omitted from expression (4.13) to give

$$\beta_1 - \beta_o \simeq (\ell_o - \ell_1) \tag{4.15}$$

If two potential surfaces V_o and V_1 with $V_1 > V_o$ as $r \to \infty$, cross at r_c, then for trajectories beginning and ending on V_o, two phase shifts can be defined, η_{00} and η_{10}. These can be calculated semi-classically by assuming the trajectory to traverse either V_1 or V_o between crossings and the subscripts refer to the surfaces before and after the second crossing respectively. The result (4.12) derived by Ford and Wheeler for the case of interference between two branches of one deflection function can be applied to interference between the two deflection functions χ_{oo} and χ_{o1} related to η_{oo} and η_{o1} by eqn. (4.7). if the probability of crossing is P, the resulting deflection functions will give the following classical cross sections,

$$\sigma_{oo} = (1-P)^2 b / \left|\frac{d\chi_{oo}}{db}\right| \sin\chi_{oo} \tag{4.16}$$

$$\sigma_{10} = P^2 b / \left|\frac{d\chi_{10}}{db}\right| \sin\chi_{10} \tag{4.17}$$

The cross sections may be rewritten

$$\sigma_{oo} = (1-P)^2 \, C_{oo}(\chi)$$

$$\sigma_{10} = P^2 C_{10}(\chi)$$

For V_o similar to V_1, $C_{10} \approx C_{oo}$ and from eqn (4.12) the relative amplitude of the structure will be given by

$$2\sqrt{\sigma_{oo}\sigma_{10}} = 2\sigma(1-P) \qquad (4.18)$$

For the structure resulting from a crossing of two surfaces, the limits of amplitude and frequency of structure which could be resolved by the apparatus can be related to the probability of crossing, P_c, and the separation between the two deflection functions Δb respectively. If ε is a measure of the scatter in the estimate of σ, the amplitude of the structure will be resolved if

$$\frac{\varepsilon}{\sigma} < P_c(1-P_c)$$

Equating ε to the standard deviation over the smoothing window, a typical value of $\frac{\varepsilon}{\sigma}$ is .1 and the constraint on P_c is

$$.1 < P_c < .9$$

If $\Delta\theta$ is the smallest separation between peaks which can be resolved, the separation between two deflection functions, Δb, which will result in visible structure is limited by

$$\Delta b < \frac{h}{\Delta\theta\sqrt{2\mu E}}$$

For K/N_2 at the lowest energy covered, the upper limit on Δb is 2Å.

4.4 Effect of crossing on repulsive wall

To give a numerical illustration of the results quoted in 4.3 calculations were performed using a potential model for the potassium nitrogen system. V_0 was taken to correspond to the ground states and V_1 to the ground state of nitrogen and the first excited state of potassium. The energy difference at infinite separation is therefore 1.61eV corresponding to the process

$$K(3s) \rightarrow K(4p)$$

The remaining potential parameters were fixed arbitrarily except that the crossing distance r_c was chosen to be accessible within the energy and impact parameter range covered by the experiment. The potentials are

$$V_0 = C_0/r^{10} \qquad V_1 = C_1/r^8 + 1.61 \qquad (4.19)$$

$$C_0 = 3000\text{eV } \text{A}^{10} \qquad C_1 = 430\text{eV}\text{A}^8$$

These potentials are shown in Figure 4.17. The phase shifts for trajectories exiting on V_o are

$$\eta_{oo} = -\frac{1}{h}\int_o^\infty V_o dt \qquad (4.20)$$

$$\eta_{10} = -\frac{1}{h}\{\int_o^{t_c} V_1 dt + \int_{t_c}^\infty V_o dT\} \qquad (4.21)$$

Estimated Intermolecular Potential for $K + N_2$

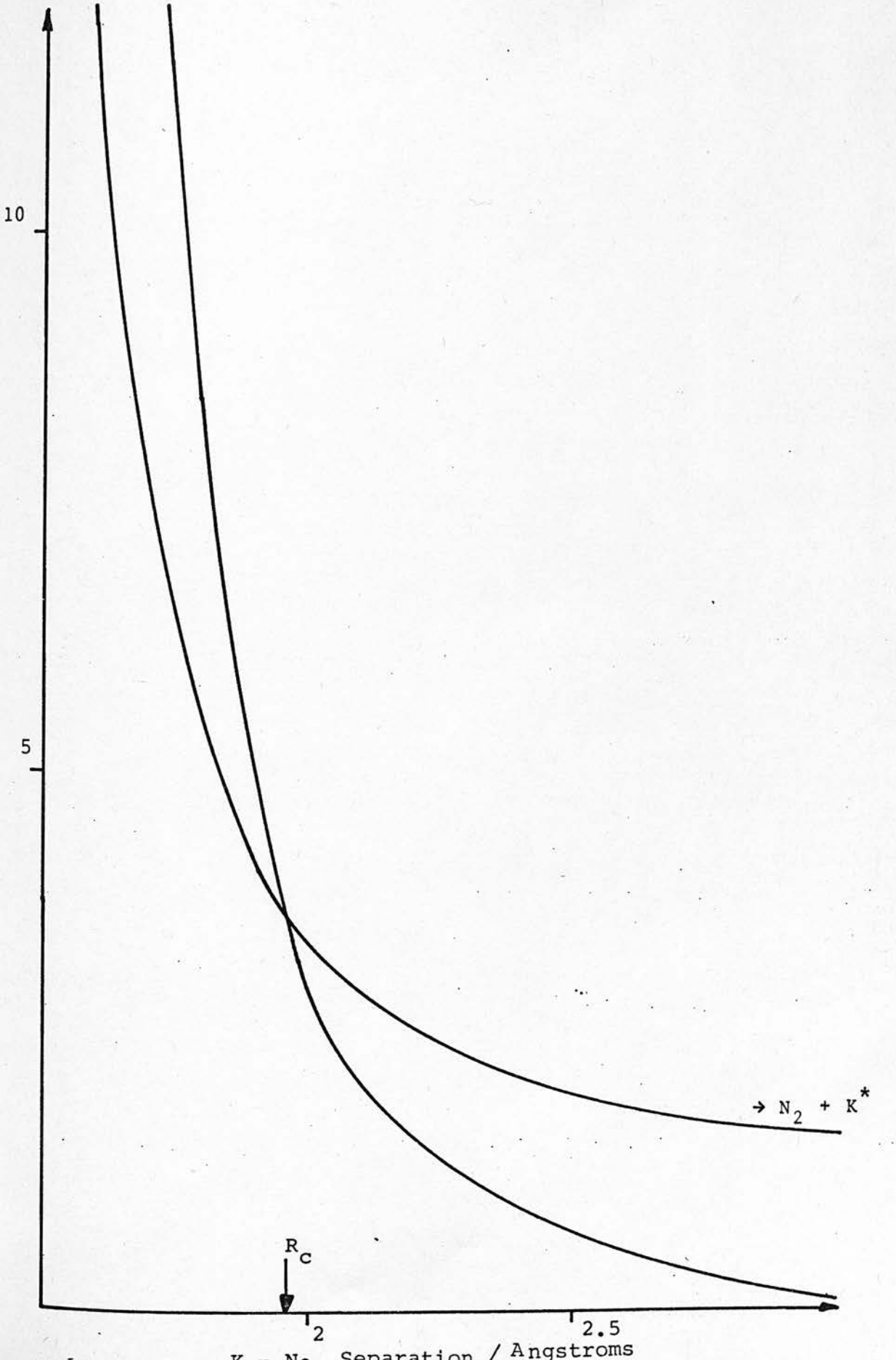

FIGURE 4.17

These integrals were evaluated analytically and the results are shown in Figure 4.18. For exit on V_1, the phase shifts are obtained by averaging over the whole trajectory.

$$\eta_{10} = -\frac{1}{2h}\{\int_{-\infty}^{t_c} V_o dt + \int_{t_c}^{\infty} V_1 dt\} \tag{4.22}$$

$$\eta_{11} = -\frac{1}{2h}\{\int_{-\infty}^{-t_c} V_o dt + \int_{t_c}^{\infty} V_1 dt\} \tag{4.23}$$

These are shown in Figure 4.19. t_c is the time from turning point to crossing point.

$$t_c = \frac{1}{v}\sqrt{r_c^2 - b^2} \tag{4.24}$$

The deflection functions for exit on V_o are shown in Figure 4.20 and for exit on V_1 in Figure 4.21. These were produced by numerical differentiation of the phase shifts. The minima caused by the abrupt change in gradient at r_c are clearly shown. The cross sections σ_{el} and σ_{ex} corresponding to exit on V_o and V_1 respectively are shown in Figure 4.22

$$\sigma_{el} = \sigma_{oo} + \sigma_{10} + 2\sqrt{\sigma_{oo}\sigma_{10}}\cos((\ell_{oo}-\ell_{10})\chi) \tag{4.25}$$

and

$$\sigma_{ex} = \sigma_{01} + \sigma_{11} + 2\sqrt{\sigma_{01}\sigma_{11}}\cos((\ell_{01}-\ell_{11})\chi) \tag{4.26}$$

where σ_{oo} are classical cross sections corresponding to the individual deflection functions. σ_{el} and σ_{ex} have arbitrarily been assigned equal amplitudes in order to show the period and phase relationships.

$K + N_2$ Phase Shift Curves (exit in ground state)

Collision Energy = 200eV

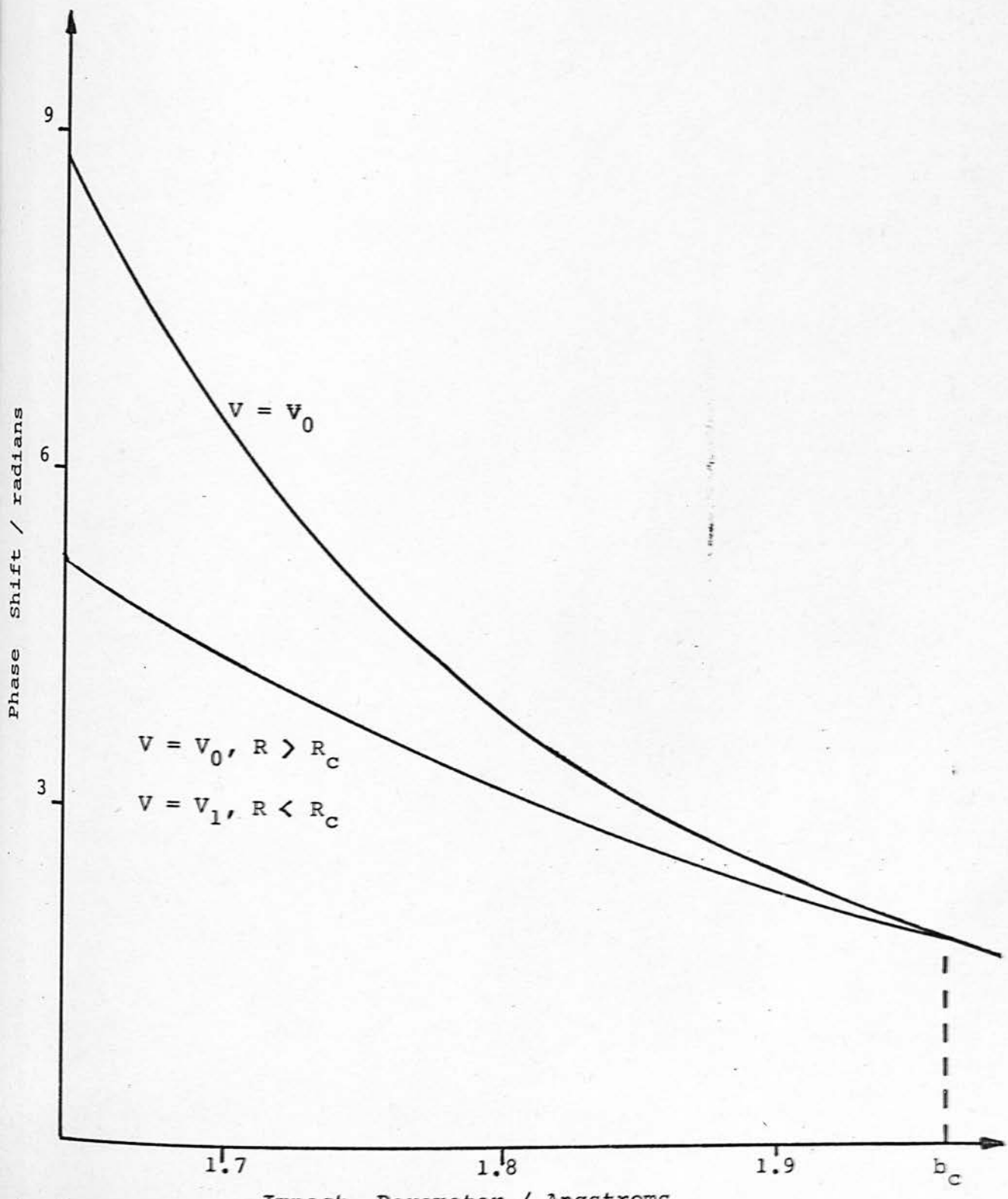

FIGURE 4.18

$K + N_2$ Phase Shift Curves (exit in excited state)

Collision Energy = 200eV

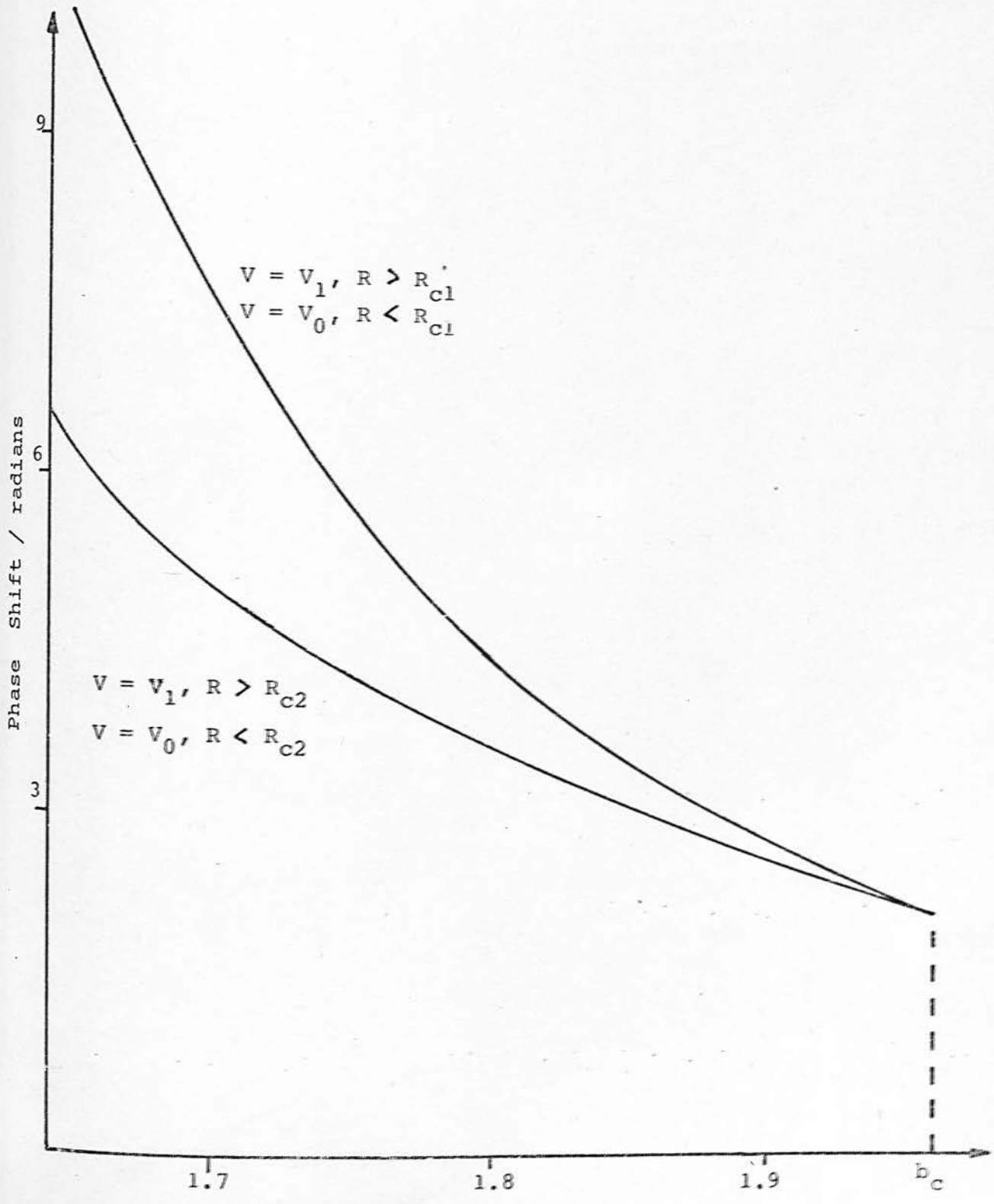

FIGURE 4.19

$K + N_2$ Deflection Function

Collision Energy = 200eV

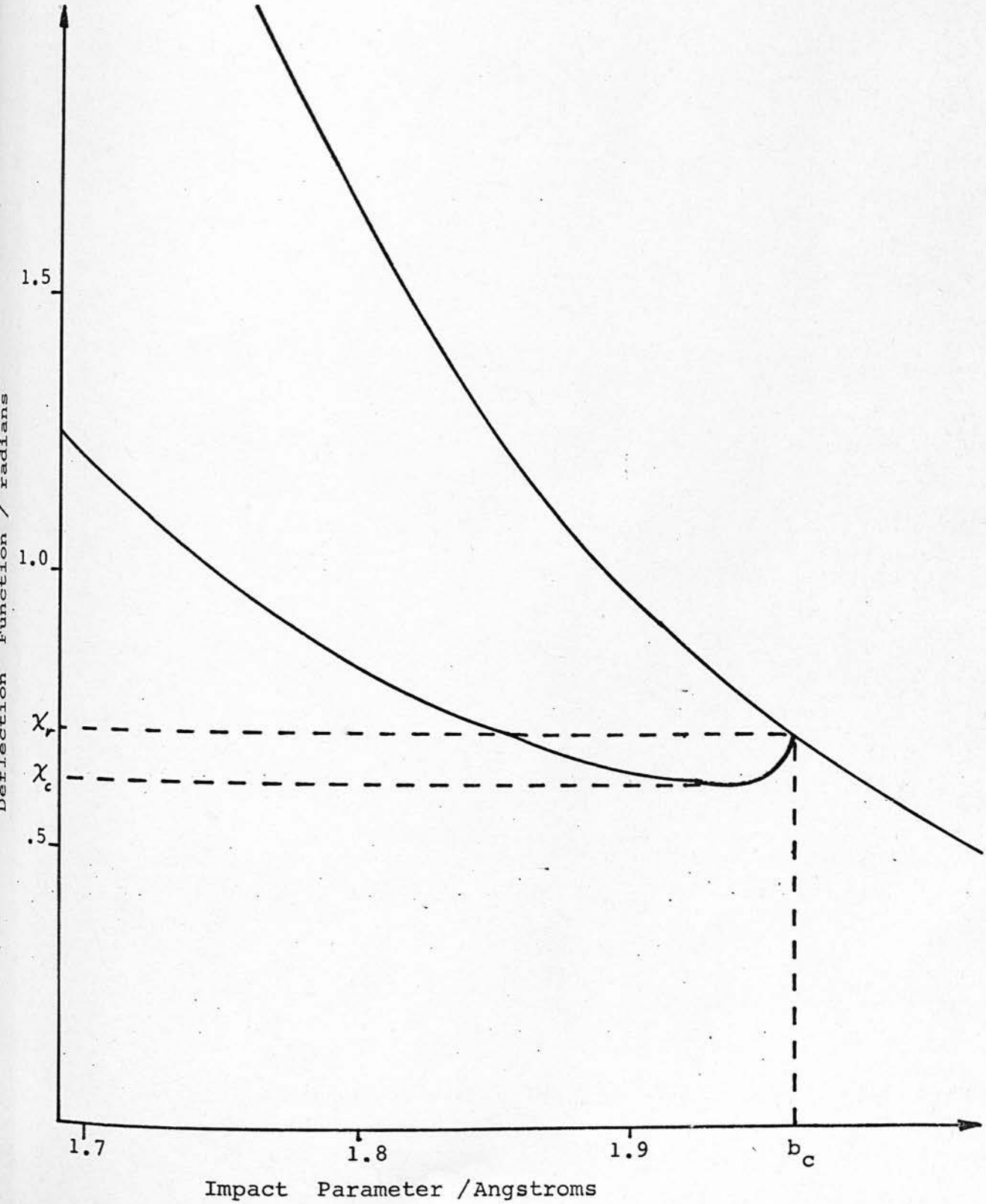

FIGURE 4.20

$K + N_2$ Deflection Function (exit in excited state)

Collision Energy = 200eV

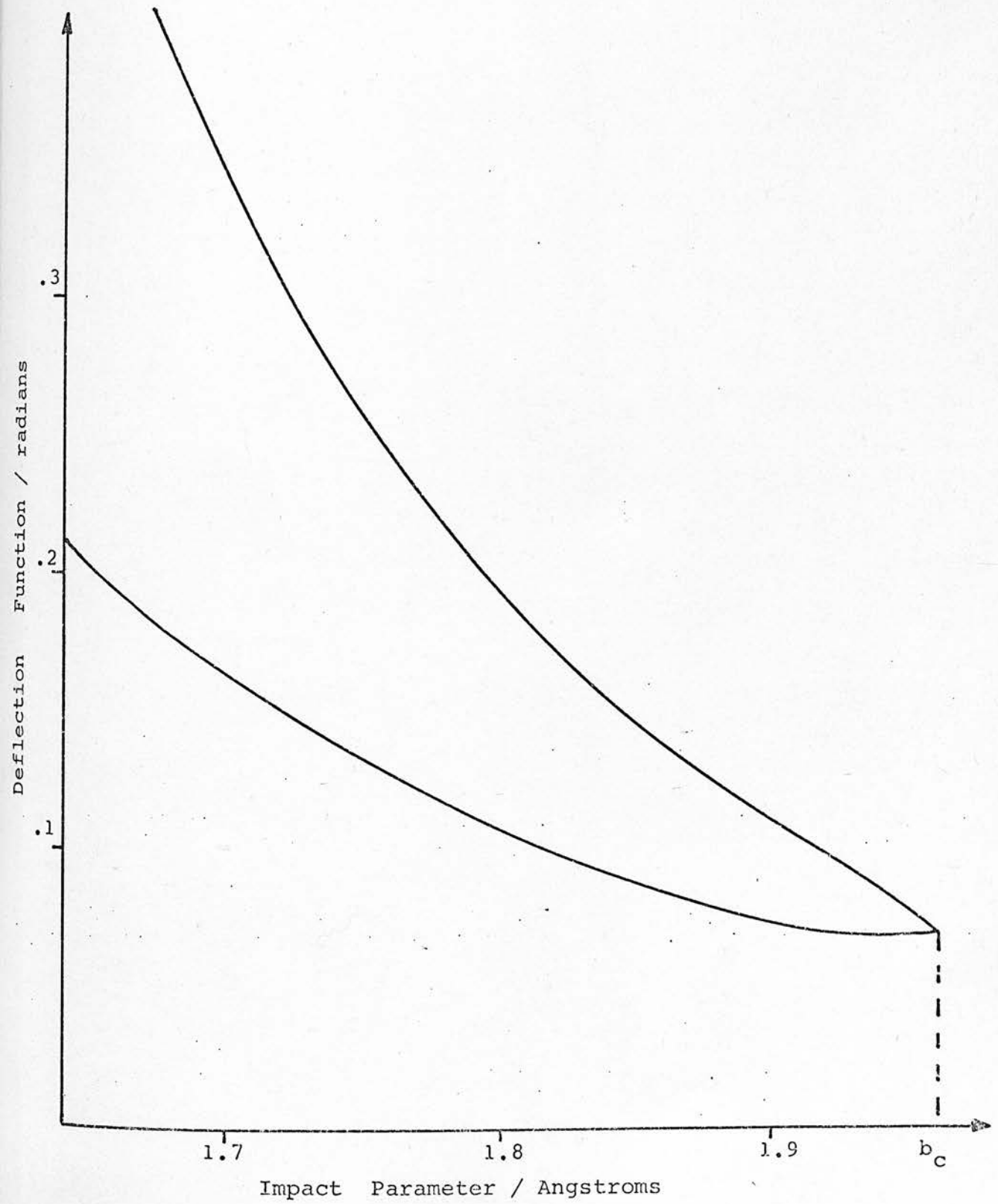

FIGURE 4.21

$K + N_2$ Differential Cross Sections

Collision Energy = 200eV

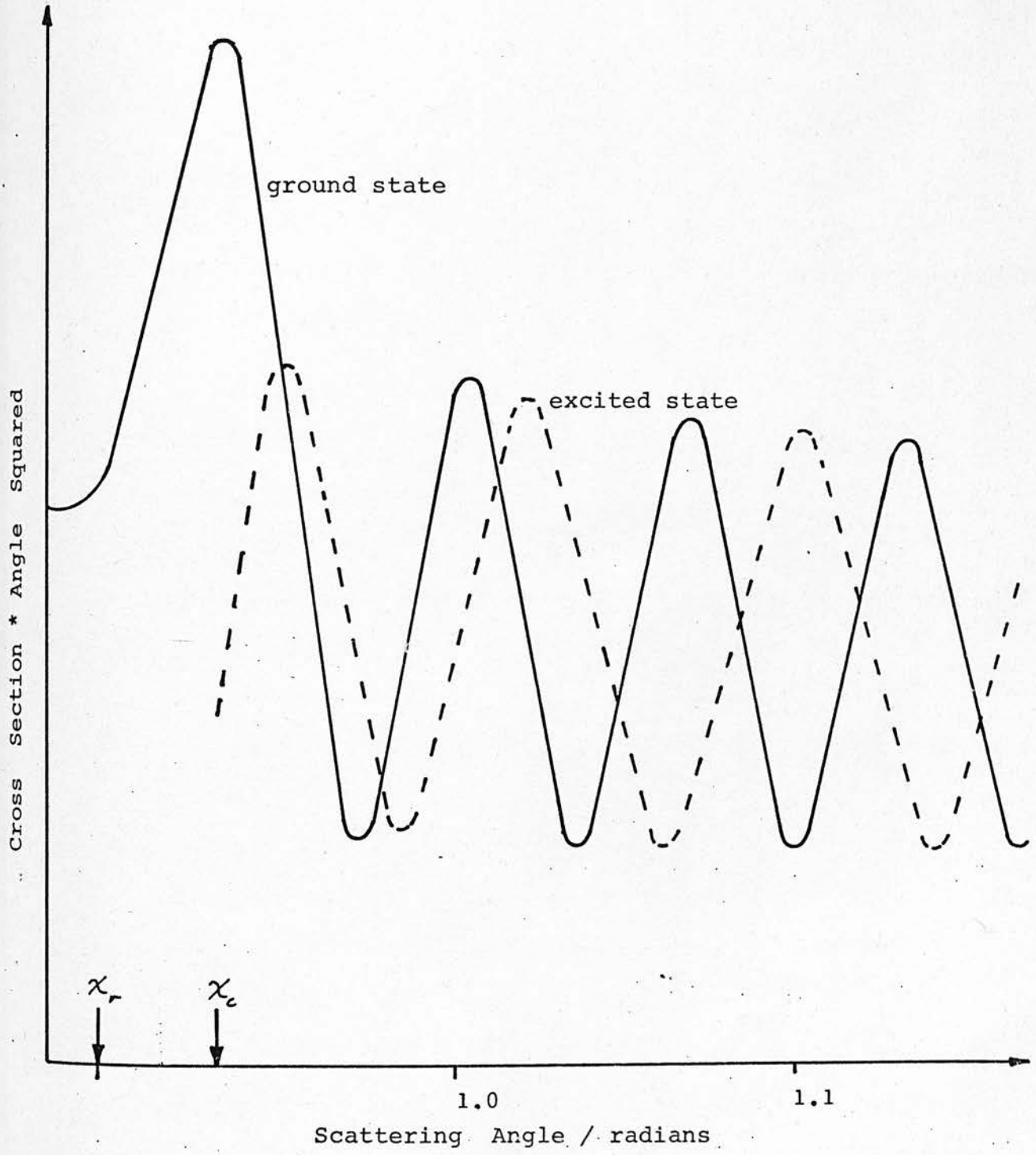

FIGURE 4.22

The individual periods given by

$$\frac{2\pi}{\ell_1 - \ell_0} \tag{4.27}$$

are around 1^o, well within the resolving power of the apparatus. In practice the sum of the two cross sections will be observed, these have differing periods so the 'beat' pattern should be clearly visible assuming nearly equal amplitude in both channels.

The above analysis is invalid in the region of χ where three regions of stationary phase contribute. This situation could be analysed by the method of Miller (MIL 68) who has given a uniform approximation for the cross section where up to three regions of stationary phase contribute, which may coalesce. However in considering σ_{el}, the major effect is expected to be the pseudo rainbow caused by the minimum in χ_{10}. Rainbow effects are well described by the Airy function which is an approximation to the integral expression for the differential cross section where two regions of stationary phase coalesce at a minimum in the deflection function. The result is derived from a parabolic approximation to the deflection function in the region of the minimum. For the situation illustrated in Figure 4.20, this is only valid for $\chi < \chi_c$, the rainbow structure will be terminated abruptly at this angle. The deflection function of Figure 4.20 is also unusual in that any supernumerary bows would appear at angles greater than χ_r (in the LAB) which is the inverse of the usual case. The differential cross section around χ_r is

$$\sigma(\chi) = \frac{2\pi b}{k \sin\chi} \left| \left(\frac{d^2\chi}{d\ell^2}\right)_{\ell_r} \right|^{-2/s} \{Ai(x)\}^2 \qquad (4.28)$$

where $$x = \left| \left(\frac{d^2\chi}{d\ell^2}\right)_{\ell_r} \right|^{-1/3} (\chi_r - \chi)$$

and Ai(x), the Airy function is most conveniently calculated from Bessel functions.

$$Ai(x) = \frac{1}{3}\sqrt{x}\{I_{-\frac{1}{3}}(z) - I_{\frac{1}{3}}(z)\}$$

$$Ai(-x) = \frac{1}{3}\sqrt{x}\{J_{\frac{1}{3}}(z) - J_{-\frac{1}{3}}(z)\}$$

$$z = \frac{2}{3} \times 3/2$$

The first maximum of this function appears at x = -1.02. For the deflection function of Figure 4.19, $\left(\frac{d^2\chi}{d\ell^2}\right)_{\ell_r} = 3.2 \times 10^{-6}$ and the value of x at χ_c where the rainbow pattern is truncated is -.67. The 'well' is therefore too shallow to support even the first rainbow maximum and there will be no supernumary bows. The cross section as calculated from eqn. (4.28) is shown in Figure 4.22 in the range $\chi_r < \chi < \chi_c$.

The analysis given above assumes a spherically symmetric potential. Although this may be a good approximation for distant collisions, anisotropy in the potential can be expected to be significant for close encounters. At such high collision energies there will be no rotational averaging of the potential either. The interference

pattern will be different for different orientations but an idea of whether the result will be significant smearing out of structure can be obtained from an estimate of how χ_c varies with orientation. χ_c is proportional to $V(r_o)$ and the simplest assumption would be that $V(r_o)$ is independent of orientation. However assuming $V(r_o)$ does change, the change in χ_c is given by

$$\frac{\Delta\chi_c}{\chi_c} = \frac{\Delta V(r_c)}{V(r_c)}$$

Significant smearing out of the structure can be expected if $\Delta\chi_c \sim$ $\frac{1}{2}$ period of oscillations. For the data of Figure 4.22 this gives $\frac{\Delta\chi_c}{\chi_c} \simeq .2$ and it seems unlikely that the relative values of ground and excited state potentials will depend strongly enough on orientation to change $V(r_c)$ by this amount.

4.5 Effect of Crossing to an Ionic Surface

To calculate the effect of a curve crossing where one of the surfaces is ionic, the above calculations were repeated for the system K/SF_6 with a crossing to the ionic surface K^+/SF_6^-. The covalent potential for K/SF_6 has been measured by molecular beam experiments at thermal energies (AIR 67). The deduced potential parameters are

$$\varepsilon = .31 \pm .03 \quad \text{Kcal mole}^{-1}$$

$$r_m = 6.3 \pm .08 \quad \text{Å}$$

Choosing a Lennard Jones form, the attractive term may be ignored in the superthermal region and the potential approximated by

$$V_c = K_c/R^{12} \qquad K_c = 51 \times 10^6 \text{ eV } \overset{o}{A}{}^{12} \tag{4.29}$$

The energy at infinite separation of the system K^+, SF_6^- is

$$V_I(\infty) = \text{I.P.}(K) - \text{E.A.}(SF_6) \tag{4.30}$$

The ionisation potential of potassium is 4.339eV and the most recent estimate of the electron affinity of SF_6 0.54eV (COM 73). The attraction between two ions is coulombic so the long range branch of the potential is

$$-\frac{e^2}{4\pi\varepsilon_o R} \quad , \quad \frac{e^2}{4\pi\varepsilon_o} = 14.4\text{eV}\overset{o}{A} \tag{4.31}$$

Considering the system at small separations to be $K^+F^-(SF_5)$, the well depth might be expected to be equal to that of KF, ie 5eV at a separation R equal to the equilibrium separation of KF plus the SF bond length in SF_6, ie $r = 4.1\overset{o}{A}$. Such a high degree of polarisation seems unlikely however, and in the absence of any other information, the ionic well depth was taken to be 3.8eV with an inverse 12th repulsive term.

$$V_I = K_I/R^{12} - 14.4/R+3.8, \quad K_I = 1066 \times 10^3 \tag{4.32}$$

These potentials are shown in Figure 4.23. The phase shifts for exit in the neutral channel are given by

$K + SF_6$ Estimated Intermolecular Potential

$$\eta_o = -\frac{1}{h}\int_0^\infty V_c\,dt \tag{4.33}$$

$$\eta_1 = -\frac{1}{h}\left\{\int_0^{t_c} V_I\,dt + \int_{t_c}^\infty V_c\,dt\right\} \tag{4.34}$$

The deflection functions produced by differentiation of η_1 and η_o are shown in Figures 4.24 and 4.25 for two collision energies. The ionic rainbow is undetectably close to the main beam at 400eV but appears at $.5^o$ at 100eV. The period of the structure is $.14^o$ (LAB) at 400eV which is close to the limit of resolving power of the apparatus. At 100eV the period is $.28^o$ and should be resolvable. These conclusions are dependent on the value chosen for the ionic well depth, ε. Choosing ε to be closer to the value for KF which is an upper limit, would result in the structure having a longer period.

In the light of the experimental data and the above calculations the main conclusions will be presented for the four collision systems investigated along with suggestions for further work.

4.6 Potassium/Argon

The collision induced fluorescence results of (AND 69) indicate that the curve crossing responsible is about 50eV up the repulsive wall. This is well beyond the region probed by the experiment, so no structure was expected. The results may be taken as a test for hiccups in the experimental or analysis procedures. However the result s = 15 obtained from the envelope is interesting in that it

$K + SF_6$ Deflection Function

Collision Energy = 100eV

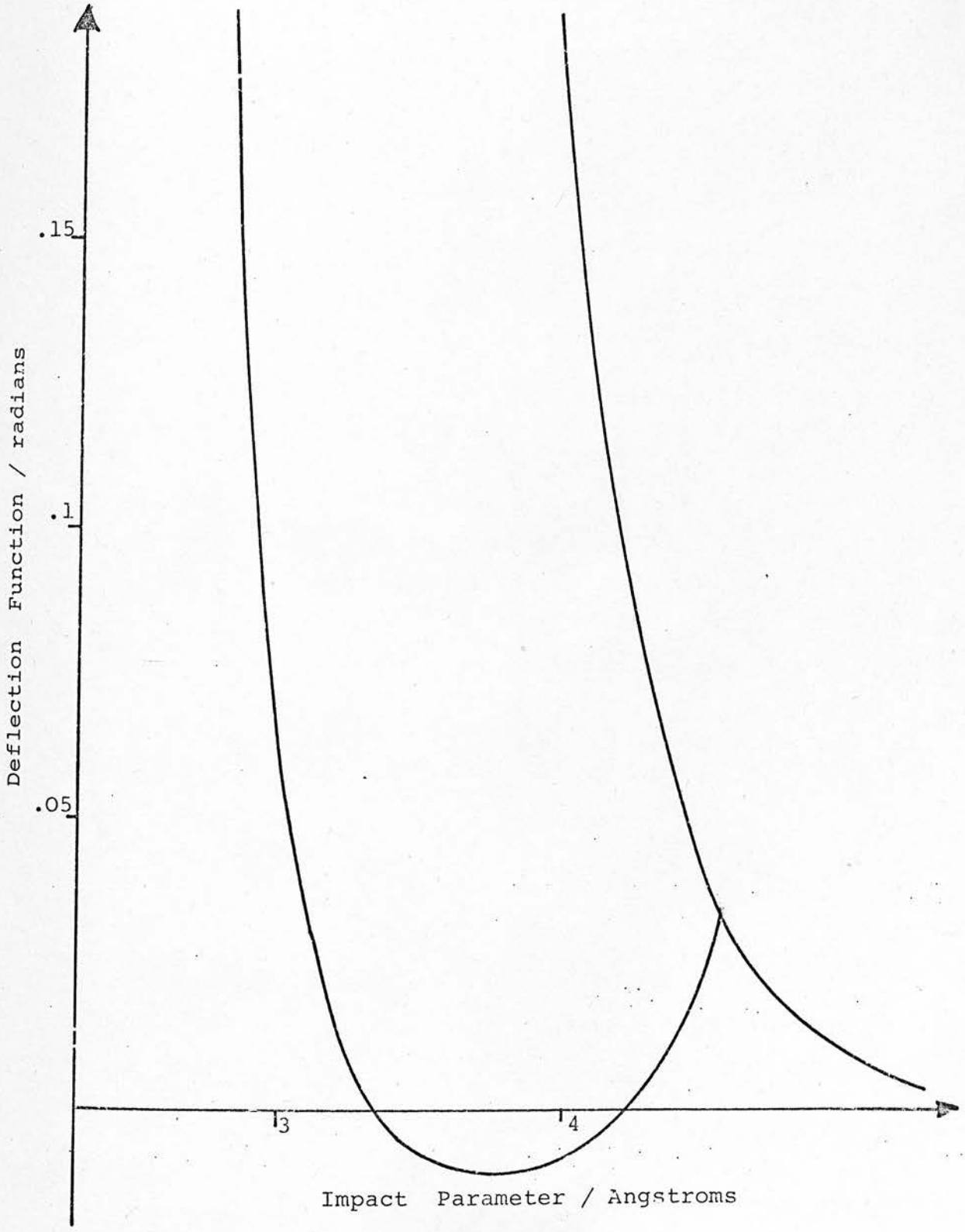

FIGURE 4.24

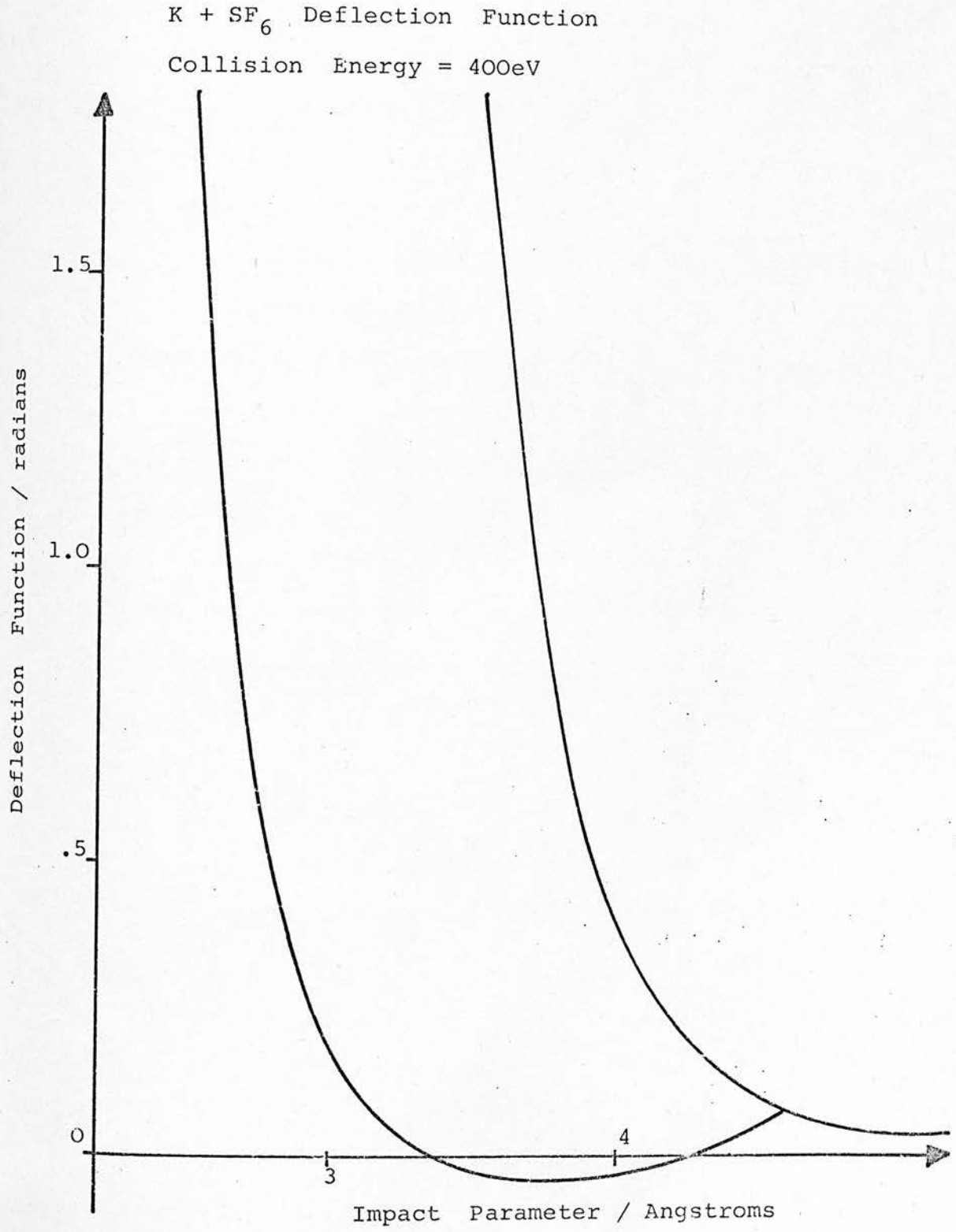
K + SF6 Deflection Function
Collision Energy = 400eV
Deflection Function / radians
1.5
1.0
.5
0
3
4
Impact Parameter / Angstroms

FIGURE 4.25

differs significantly from the results of (MAL 70) and (POL 70) who give s = 7.25 and s = 7 respectively (although their values for K_7 differ by a factor of four). An inverse seventh power repulsion is much softer than the potentials obtained for the rare gas/rare gas systems (AMD 66). This difference is attributed by Malerich & Cross to the fact that the outer shell of potassium has only one electron in it The range in V over which the results of (MAL 70) apply only extends up to .48eV however. Extrapolation of that potential into the regions explored by the present experiments takes the internuclear separation below the sum of the atomic radius of argon and the ionic radius of potassium where one would not expect the above explanation to be valid. It is not surprising therefore that present experiments predict a much steeper repulsion. The magnitude of the potential may be fixed by joining it to that obtained by Malerich and Cross. This was done at the smallest value of V reached in the present experiments, the difference in gradient being ignored. The potential obtained by this method is

$$V(R) = 1.03 \times 10^6/R^{15} \quad eV(R \text{ in } \overset{o}{A})$$

which is shown along with that of Malerich and Cross in Figure 4.26. Work is evidently required to explore the intermediate region 0.48 - .73 eV.

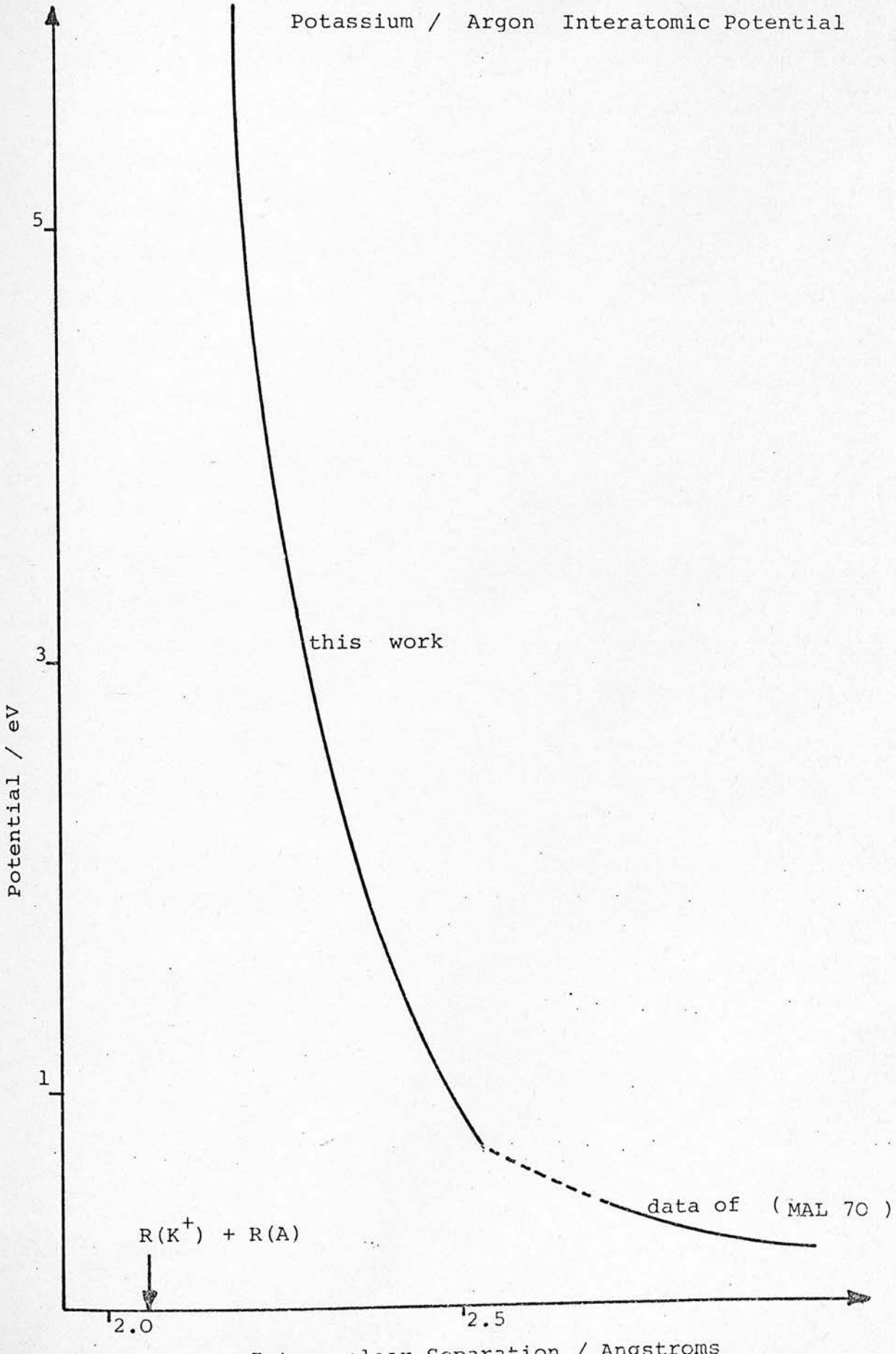
Potassium / Argon Interatomic Potential
5
3
1
Potential / eV
this work
data of (MAL 70)
R(K+) + R(A)
2.0
2.5
Angstroms

4.7 Potassium/Sulphur Hexafluoride

The most striking feature of this data is the anomalously low value for s, the power in the repulsive term in the potential. The value obtained is very low compared to the rare gas/rare gas results and is especially surprising in view of the fact that large K/F repulsion must be encountered even at relatively large K/S separations. The results reported in (AMD 66) for atom molecule systems show very steep repulsion indeed.

The effect of a crossing to an ionic potential surface was considered. Even if the ionic potential has a deep well and is used exclusively, the effect of the repulsive wall is dominant in the range of energy and angle covered. The degree to which a second term in the potential could produce an anomalous result for s depends on the amount of curvature in the log - log plot which could be hidden by the scatter in the data. If the potential is

$$V = \frac{K_s}{r^s} - \frac{K_{s1}}{r^{s1}} \tag{4.31}$$

the differential cross section may be written

$$\chi^2\sigma(\chi) = C_s\chi^{-2/s} + C_{s1}\chi^{-2/s}$$

The gradient of the log - log plot is then

$$\frac{d}{d\ell n\chi} = \frac{-2/sC_s\chi^{-2/s} - 2/s^1C_{s1}\chi^{-2/s^1}}{C_s\chi^{-2/s} + C_{s1}\chi^{-2/s^1}} \tag{4.31}$$

The confidence limits on the gradient were used to estimate the line of maximum curvature which could pass undetected in the experimental plot. By equating this to a McLaurin expansion of equation (4.32), (with $s^1 = s/2$), the maximum contribution from the second term is estimated to be $C_{s1} = C_s/30$ and the only effect is to change the estimate of s from 4.7 to 5.0. The effect of an ionic attractive branch does not therefore materially affect the conclusions about the form of the repulsive potential.

The anomaly was therefore explained in terms of an opacity function, ie the probability as a function of impact parameter that potassium atoms are removed from the scattering pattern in such a way as to make the differential cross section appear to result from a potential $V_{app} = K_{s1}/r^{s^1}$ with $s^1 = 4.7$ when the actual elastic potential is $V_{el} = K_s/r^s$ where s has a more normal value.

The result for P(b) is

$$P(b) = 1 - (b/b_c)^{-2+2s/s^1}$$

where b_c is some large impact parameter beyond which no removal takes place. This function is shown in Figure 4.27 for $S^1 = 4.7$ and $s = 12$. b_c was taken to be 4.6Å (the largest impact parameter sampled if V_n is taken to be that obtained from the experiments of (AIR 67) Also shown is the typical form of the Landau Zener excitation probability with a crossing at b_c. The function P(b) is only determined experimentally over the range $4.6 > b/Å > 3.0$ so the disagreement may not be as great as appears at first sight. The most probable process which could result in removal of potassium

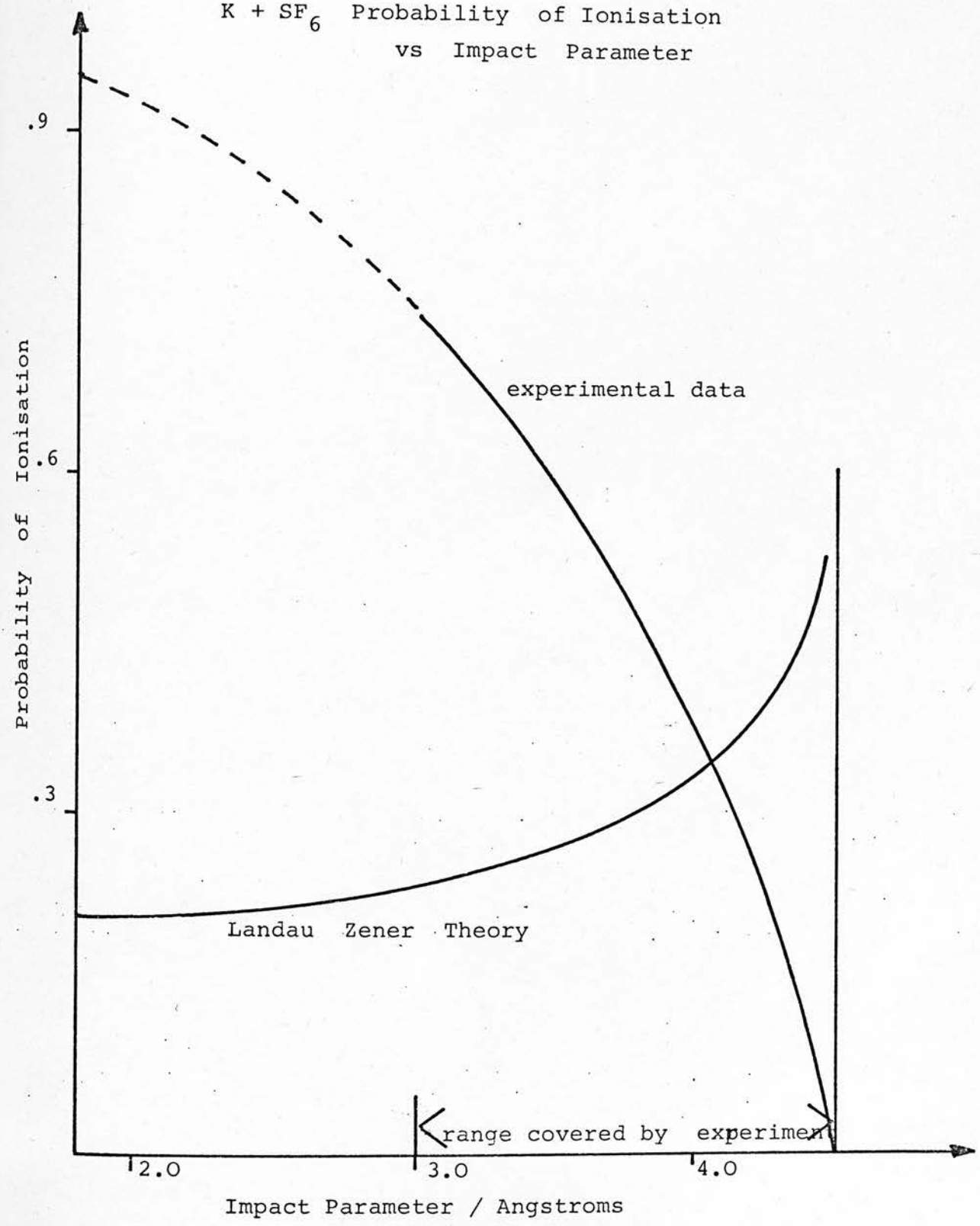
K + SF6 Probability of Ionisation
vs Impact Parameter
.9
.6
.3
Probability of Ionisation
experimental data
Landau Zener Theory
range covered by experiment
2.0
3.0
4.0
Impact Parameter / Angstroms

atoms is ionisation. As shown in Chapter 2, an energy loss of a few eV has negligible effect on the angle of scattering and chemical reaction is considered unlikely at such high energies. If P(b) is identified solely with the probability of ionisation, the total ionisation cross section is given by

$$\sigma_I = 2\pi \int_0^{b_c} P(b)bdb$$

and the contribution calculated over the region of b sampled by the experiment is $13A^{o2}$. No results have been reported for the ionisation cross section of potassium on collision with SF_6. Ion production experiments have been reported (YAN 74) for the related system Cs/SF_6 but only the relative intensities of the various negative ions produced were measured.

The absence of observed structure may be related to the apparent deviation from the Landau Zener approximation indicated above. The approximation is only valid for structureless particles whereas SF_6^- might well change its structure in the interval between crossing points. If this resulted in reduced probability of crossing back to the neutral surface, the ionisation cross section would be enhanced and the interference structure reduced in amplitude. Since the duration of the collisions are so short ($\sim 2 \times 10^{-14}$ secs) vibration of SF_6^- is unlikely to be responsible but perturbation of the electronic structure by the K^+ ion might be. Vibrational excitation of SF_6 would also reduce the amplitude of any structure as the coherence of the scattered wave front would be destroyed. The best experimental approach would be direct measurement of the ions produced either as a function of angle or energy.

4.8 Potassium/Methyl Iodide

A crossing to an ionic surface is expected for this system, and recent Monte Carlo studies used such a surface to reproduce many of the experimentally observed features at thermal energies. The reaction cross section has a maximum at a collision energy of .18eV and reaction is not expected to be important in the 100eV region. Nevertheless the presence of a crossing to an ionic surface should produce structure in the observed cross section as described in section 4.5. Unfortunately the experimental results are of rather poor quality and no structure has been observed. The large scatter in the data is also evident in the error in the value obtained for the power dependence of the potential, $s = 8 \pm 3$. The rather low value of the mean suggests that the envelope may be perturbed by ionisation as described for the case of K/SF_6.

4.9 Potassium/Nitrogen

Despite the large amount and relatively high quality of this data, no reproducible structure or features have been observed. Therefore the production of excited potassium by collision with N_2 cannot proceed by the mechanism of a single repulsive wall crossing as described in 4.4. The absence of structure is in agreement with the results of Pauly for the elastic scattering cross section at 100 and 150eV, although there is some suggestion of structure in some of the

inelastic channels. These results also show the amplitude in the inelastic channels to be about .1 of that in the elastic channel. This indicates that $P_c \simeq .3$ which by the criterion of 4.3 would result in structure in the elastic channel being of large enough amplitude to be observable. For small enough impact parameters 'washing out' of the structure due to the accessibility of several states is possible but the absence of features corresponding to the thresholds is still a puzzle. Although the potentials are expected to be strongly anisotropic at such small separations, their relative values are unlikely to change sufficiently to affect the structure as shown in 4.4.

The result for the power dependence of the potential, s = 7, is anomalously low for such hard collisions. This result agrees with that estimated from the elastic differential cross sections of Pauly, and suggests the use of an opacity analysis as for SF_6. Again the removal mechanism is expected to be ionisation but there are no reported measurements of ion production in K/N_2 collisions to confirm this. If substantial ionisation is occurring the question of the absence of structure due to the ionic surface arises. The effect of such a crossing in an atom/diatom collision has been considered by M.S. Child (CHI 73). The crossing takes place between two sets of potential surfaces corresponding to the vibrational levels of the ionic and neutral diatom. Vertical, Frank Condon transitions are possible if the collision velocity is sufficiently high, so a considerable degree of vibrational excitation is possible. This would destroy the coherence of the scattering and could wash out any structure. High resolution time of flight experiments might reveal this effect and measurements of ion production would be interesting.

CHAPTER 5

CLASSICAL TRAJECTORY STUDY OF K/I_2

A classical trajectory study of the collision system K/I_2 at energies from .087 to 87eV has been carried out by McDonald, Fluendy and Lawley (McD 73). Only preliminary results were reported and in this chapter the method will be described briefly and a more detailed report given.

5.1 Collision System and Potential Surface

The reaction $K + I_2 \rightarrow KI + I$ has been much studied. The large reaction cross section and negligibly small activation energy led to the harpooning model in which reaction is assumed to take place via an electron jump at large internuclear separations. Molecular beam experiments (HER 66) revealed other features of this type of reaction: strong forward peaking of the product intensity and high internal excitation of the product molecule. These features are characteristic of the stripping mechanism for chemical reaction and a simple model assumes that one iodine atom takes no part in the reaction, acting merely as a spectator. In order to test the validity of the harpooning model, classical Monte Carlo trajectory calculations were carried out by Blais (BLA 68) in which the electron jump is represented by a transition from the neutral potential surface to the ionic one at the point at which they cross. The spectator model was shown to be inadequate as the ion induced dipole term between the I atom and the departing K^+I^- was found to be important in reproducing the observed energy distribution. The potential surface of Blais, based on spectroscopic values and fitting the observed results, is used in the

present calculations with the small modification that the repulsive terms have been strengthened slightly to prevent unphysical penetration at the high collision energies investigated. The potential surface used is

$$V_{covalent} = DI_2(\{1 - \exp - \beta(R_2-R_{20})\}^2 - 1)$$

$$+ A\exp - R_1/\rho + A\exp - R_3/\rho$$

ie a Morse potential for the I/I interaction plus exponential K/I repulsion

$$V_{ionic} = -\ell^2/R_1 - (\alpha_1+\alpha_2)\ell^2/2R_1^4 + A\exp - R_1/\rho + \delta$$

$$- \tfrac{1}{2}\alpha_3 q^2\{1/R_2^4 + 1/R_3^4 - (R_2^2+R_3^2-R_1^2)/(R_2R_3)^2\}$$

$$+ D_2(R_{o2}/R_2)^{12} + D_3(R_{o3}/R_3)^{12}$$

ie a Rittner potential for K^+I^- plus an induced dipole term plus repulsion terms for K^+I and I^-I.

The constants are

$$DI_2 = 1.5417eV,\ \beta = .642\overset{o}{A},\ R_{20} = 2.66\overset{o}{A}$$

$$A = 20700eV,\ \rho = .311\overset{o}{A}$$

$$\alpha_1 = .84\overset{o}{A}^3,\ \alpha_2 = 7.16\overset{o}{A}^3,\ \alpha_3 = 5.0\overset{o}{A}^3,$$

$$\delta = 1.345eV,\ q^2 = 100eV\overset{o}{A},\ D_2 = .82eV$$

$$D_3 = 1.084\text{eV}, \; R_{o2} = 2.84\text{A}^o, \; R_{o3} = 2.00\text{A}^o$$

The probability that a transition will occur between two surfaces with a crossing at R is given by the Landau Zener formula

$$P_{12} = \exp(-v^*/v_R)$$

where v_R is the radial velocity and

$$v^* = 2\pi H_{12}^2/(h|\frac{dV_i}{dR} - \frac{dV_c}{dR}|)$$

H_{12} is the interaction matrix element between the two surfaces. The value of H_{12} for K/I_2 has been estimated to be .04eV (MOU 71) and the crossing is at R =13.6 a.u. P_{12} evidently falls off with increasing collision energy but for the highest energy included in the calculations $P_{12}(b)>.7$ and the assumption of adiabatic motion for all trajectories will reproduce the main features of the interaction.

The purpose of extending the calculations to higher energies is to investigate the expected closure of the reactive channel and to observe the processes which may replace reaction. For motion on a single electronic surface, these are,

$$K + I_2 \rightarrow K + I_2 \quad \text{elastic}$$

$$\rightarrow K + I_2^* \quad \text{vib/rot excitation}$$

$$\rightarrow K + I + I \quad \text{dissociation}$$

A second objective is to consider the possibility of investigating these processes experimentally. The rainbow resulting from the ionic

well should be visible in the high energy elastic differential cross section and allow information to be obtained about the potential directly. The inelastic processes could be investigated by energy loss measurements.

5.2 Method

The co-ordinate system and equations of motion are as described by Bunker and Blais (BUN 64). The quasiclassical assumption is used to obtain the initial rotational and vibrational energies of the I_2 molecule from the most probable quantum states at room temperature. The initial and final separations are chosen such that the potential is virtually zero and the remaining parameters are chosen at random from their statistical distributions by established Monto Carlo procedures. The equations of motion are solved by stepwise numerical integration and conservation of energy and backwards integration to yield the starting values are used as checks on accuracy. The conservation of energy is found to be better than one part in 1000. 600 trajectories were calculated for each of the 8 collision energies and the final values of the dynamical variables were stored for subsequent analysis.

5.3 Results and Discussion

Reaction and Dissociation

The variation of total cross section with energy for the

various processes is shown in Figure 5.1. The closure of the reactive channel is clearly shown and is a consequence of the difficulty of transferring sufficient momentum to an iodine ion as the collision time decreases. As might be expected, the decrease in the reactive cross section coincides with an increase in the dissociative cross section. However, although dissociation eventually decreases with increasing energy, it does not fall to zero as in the reactive case but reaches a minimum value fairly independent of energy. This behaviour at high energy suggests that a hard sphere 'knock out' mechanism is operating for dissociation as well as the large impact parameter stripping mechanism which produces reaction and dissociation at lower energies. The hard sphere radius implied by the limiting value of the dissociation cross section is 2.7Å which compares with that for the K^+I^- potential of 2.55Å. This interpretation is confirmed by the plots of probability of dissociation against impact parameter for various energies, which are shown in Figure 5.2. Apart from that at 4.3eV where reaction is still important, the graphs are very similar at small b. At large b, there is significant probability of dissociation only for 4.3 and 8.7eV. The distinction between 4.3 and 8.7eV and the higher energies shows up clearly in the differential cross section for potassium scattered from dissociative collisions, plotted against Eθ in Figure 5.3. The cross sections for 43 and 87eV, which are not shown, are very similar to that for 17eV and show no sign of the forward peaking of the 4.3 and 8.7eV cases.

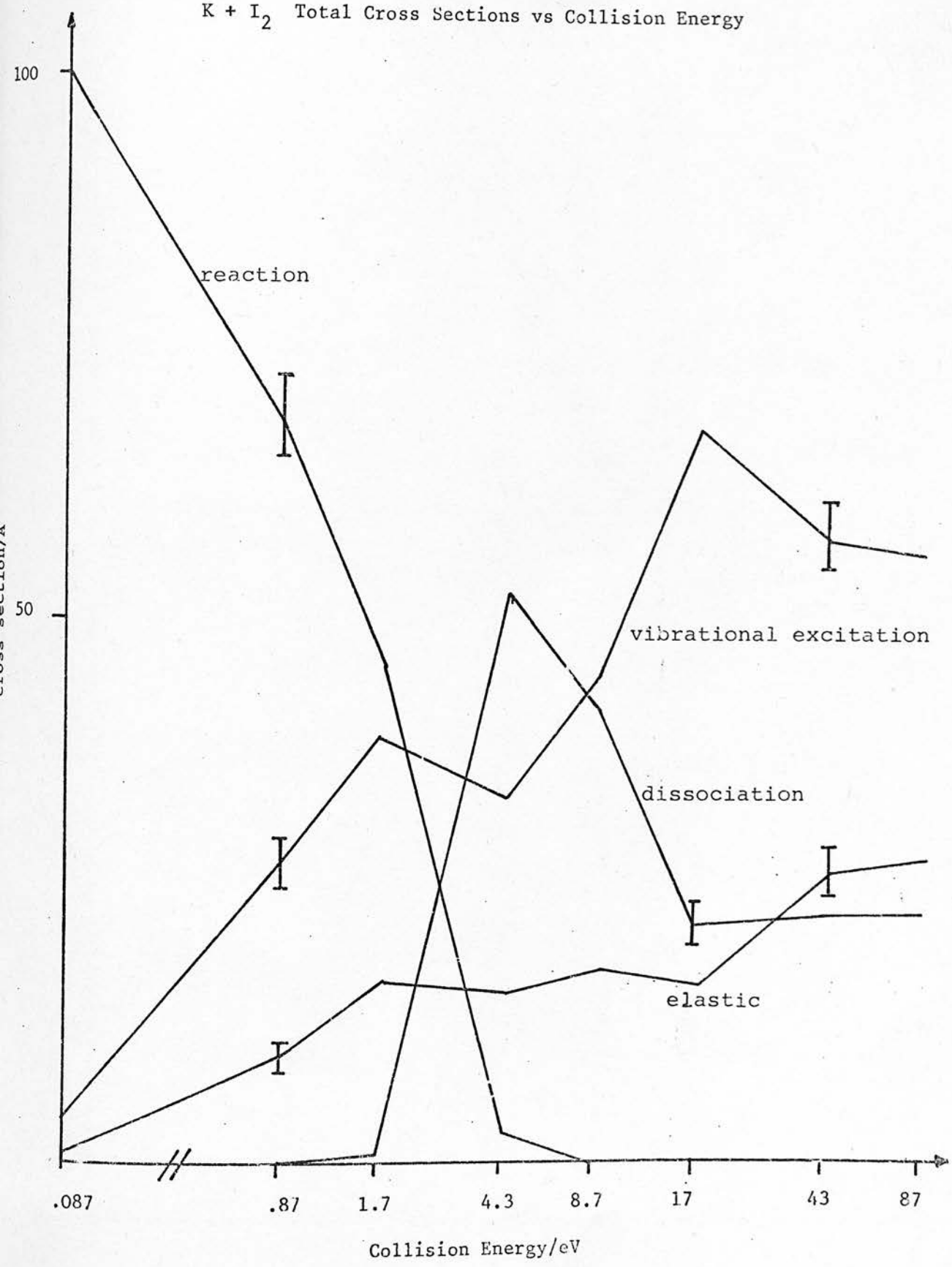
K + I2 Total Cross Sections vs Collision Energy
100
50
reaction
vibrational excitation
dissociation
elastic
.087
.87
1.7
4.3
8.7
17
43
87
Collision Energy/eV

FIGURE 5.1

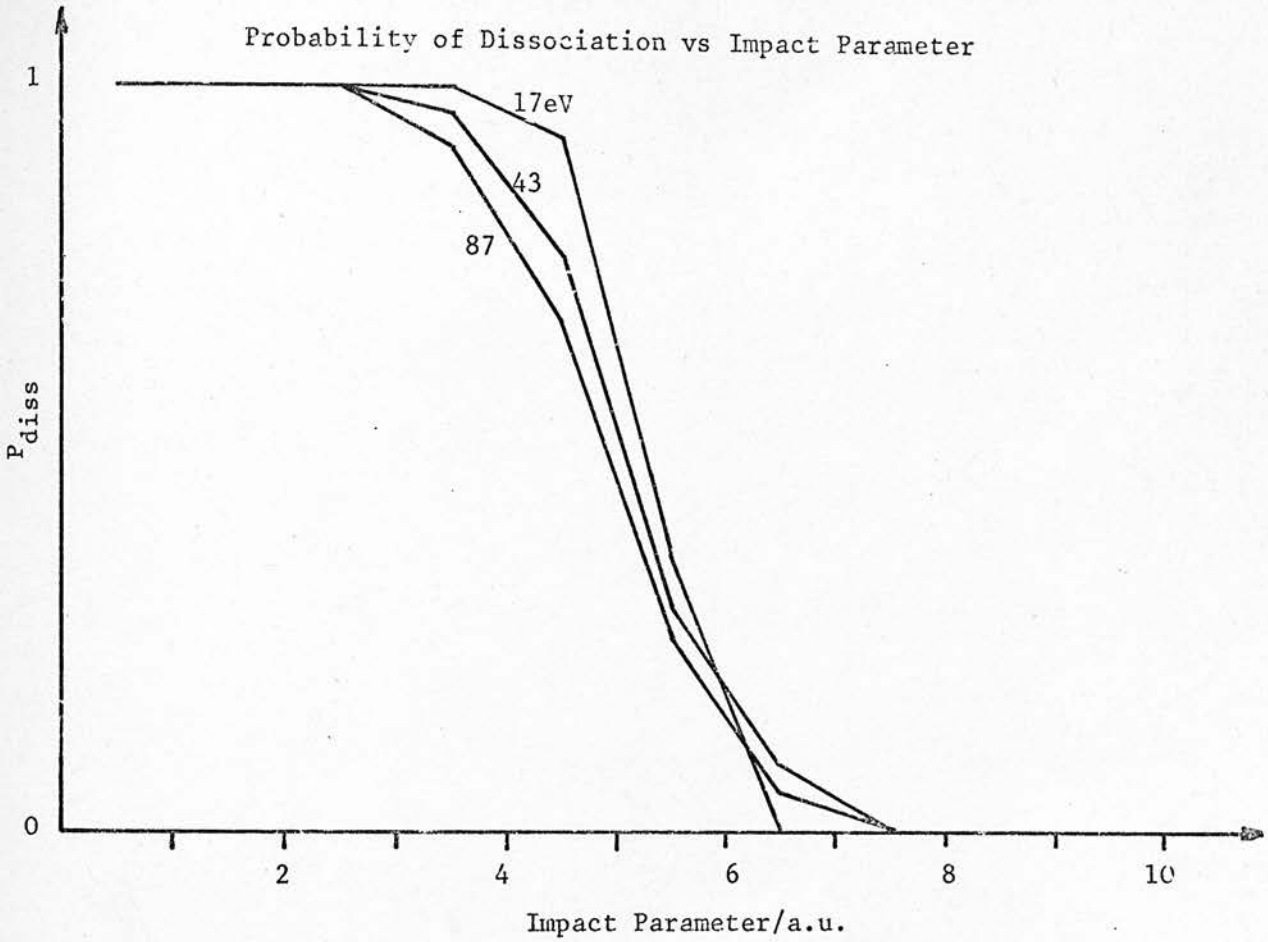
Probability of Dissociation vs Impact Parameter
1
0
P_{diss}
17eV
43
87
2
4
6
8
10
Impact Parameter/a.u.

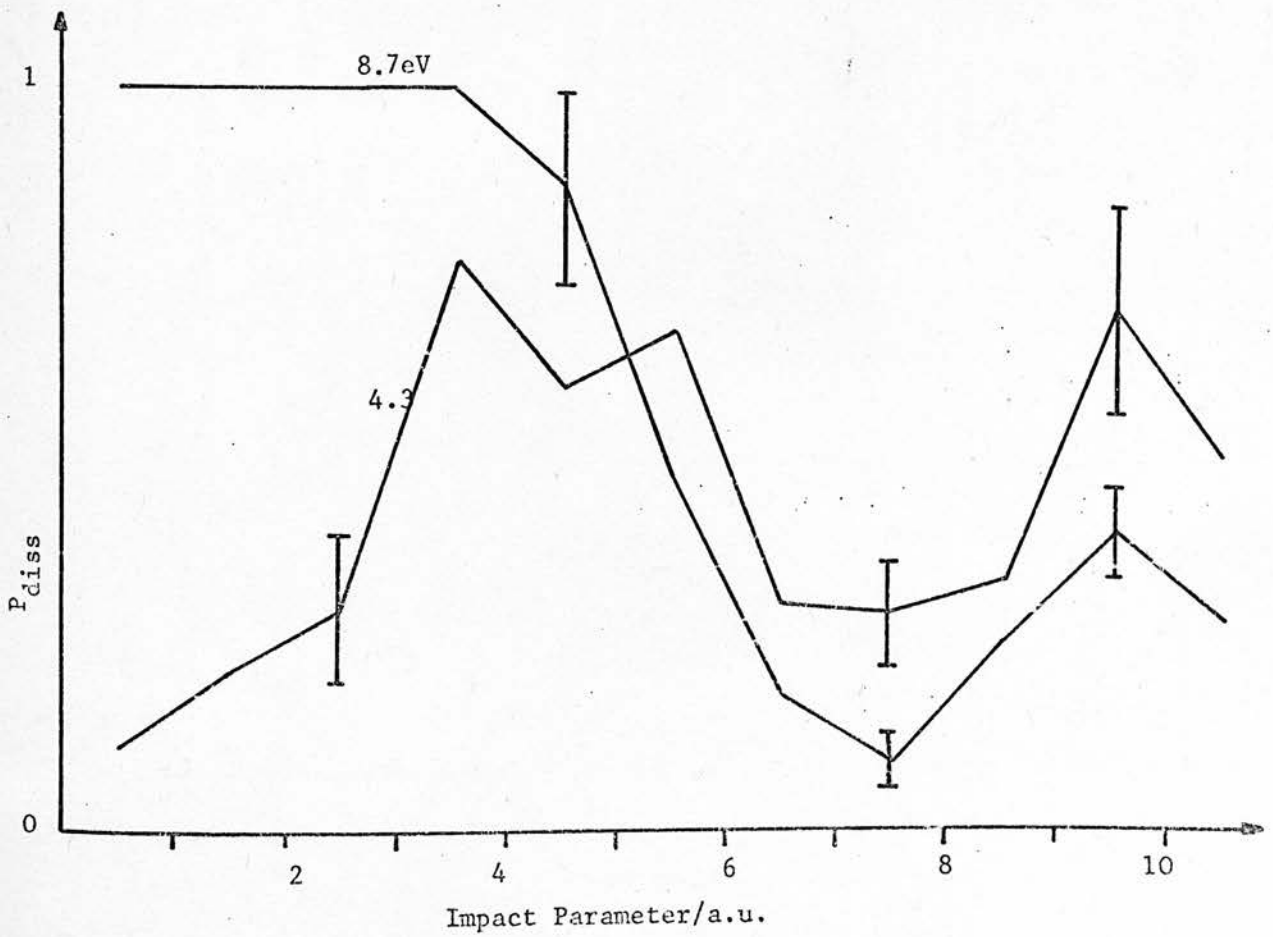
1
0
P_{diss}
8.7eV
4.3
2
4
6
8
10
Impact Parameter/a.u.

FIGURE 5.2

Differential K atom cross section

for dissociative collisions

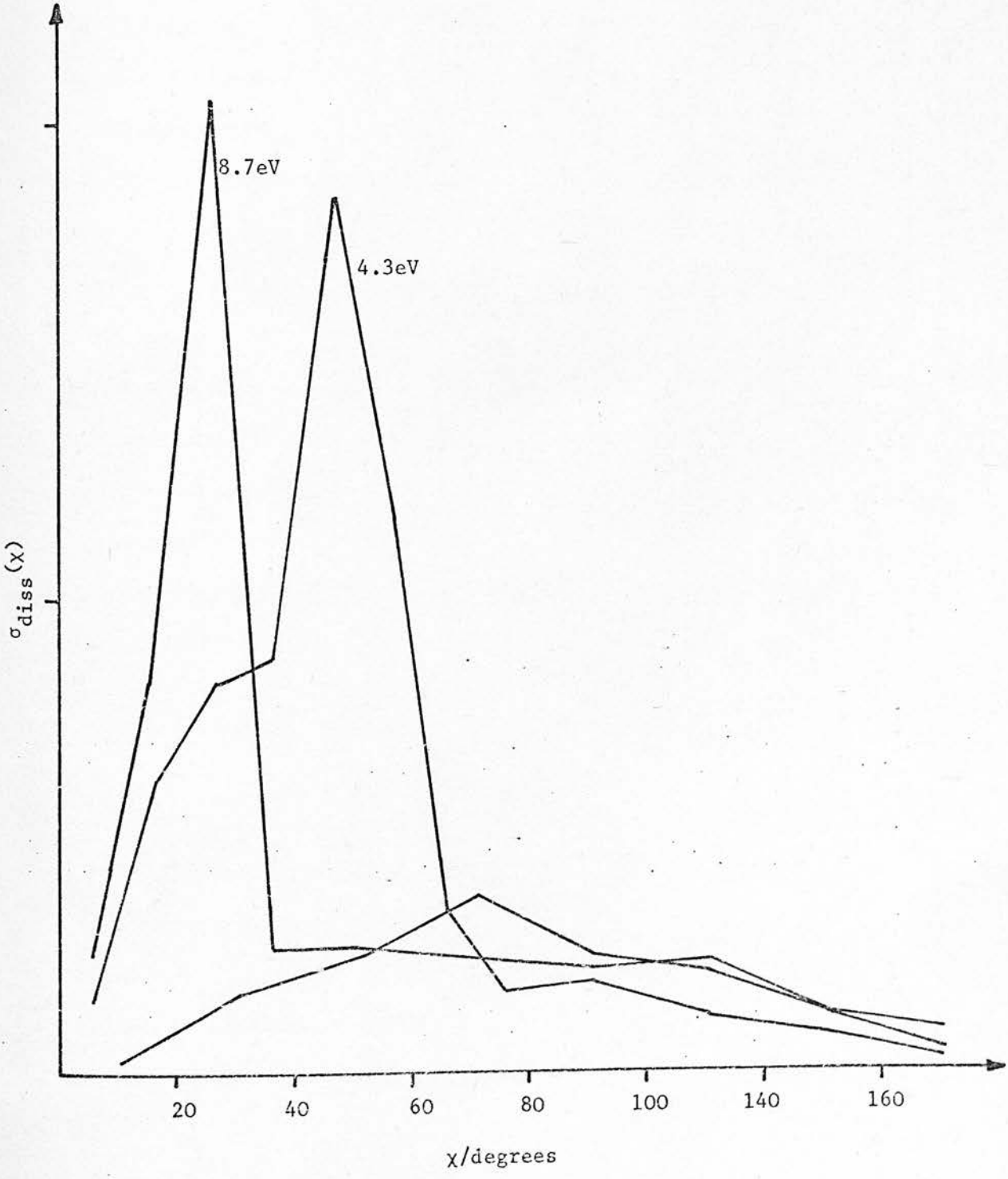

FIGURE 5.3

The increasing importance of small impact parameter collisions also results in the mean K atom energy loss for dissociative collisions increasing sharply with collision energy as shown in Figure 5.4. A curious feature of Figure 5.2 is the minimum in the curves at around 7Å in both the 4.3 and 8.7eV case. A similar 'window' is seen in the graphs of probability of reaction against impact parameter at .87 and 1.7eV shown with that for 4.3eV in Figure 5.5. The position of this minimum is independent of energy and must be a result of the particular form of the potential.

The effect of reaction on the elastic differential cross section is shown in Figure 5.6. The rainbow peak at around 130eV degrees is present for all cases except .87 and 1.7eV where the appropriate trajectories are obviously swallowed by reaction. The presence of the deep well rainbow above 4eV indicates the value of elastic differential scattering cross sections at high energies in investigating the potential.

5.4 Rotational and Vibrational Excitation

The cross section for vibrational excitation (σ_{vib} of Figure 5.1) was calculated from those trajectories for which the vibrational energy of I_2 increased by .027eV or more. This is the energy required to excite the first vibrational level as all trajectories were started with I_2 having vibrational energy corresponding to the ground state.

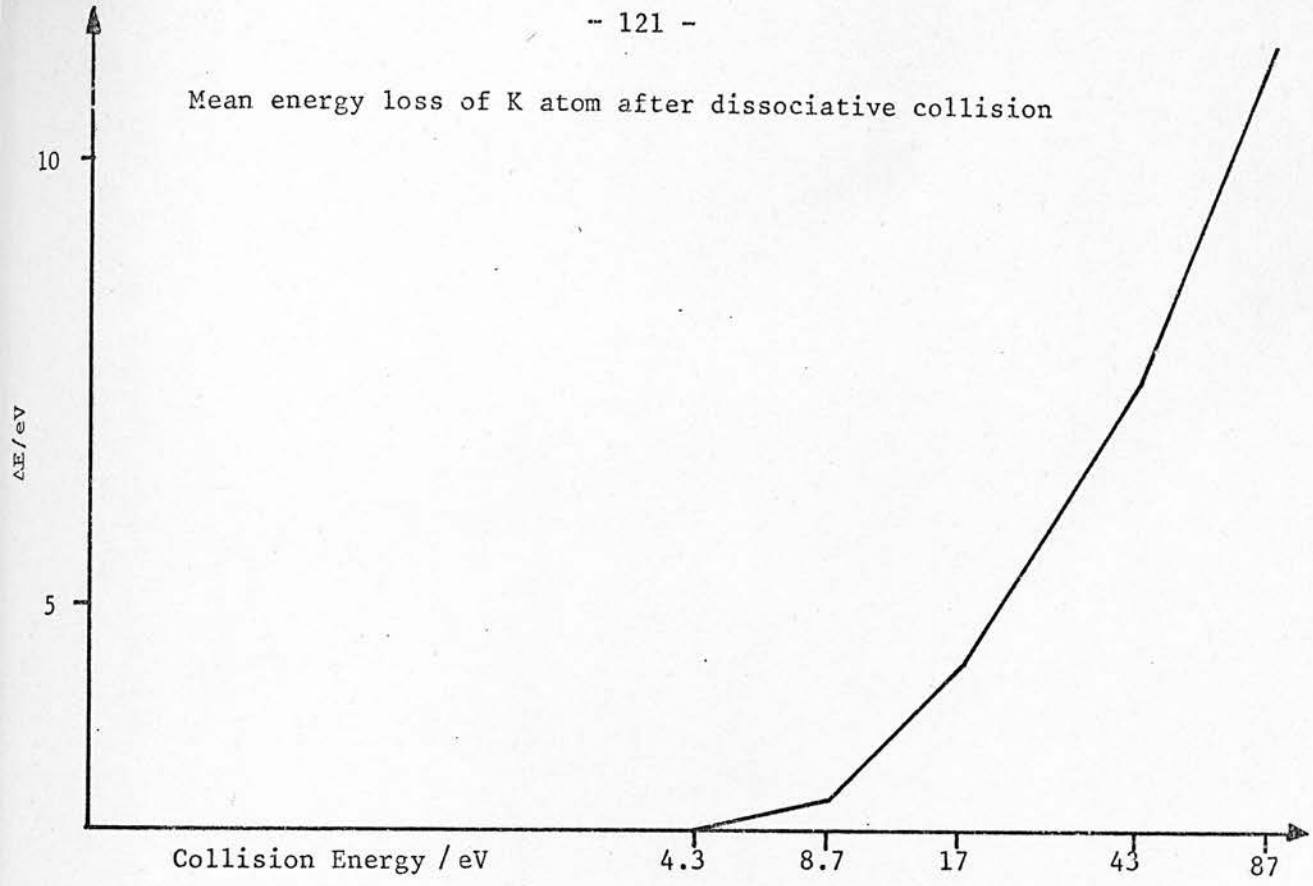
Mean energy loss of K atom after dissociative collision
10
5
ΔE/eV
Collision Energy / eV
4.3
8.7
17
43
87

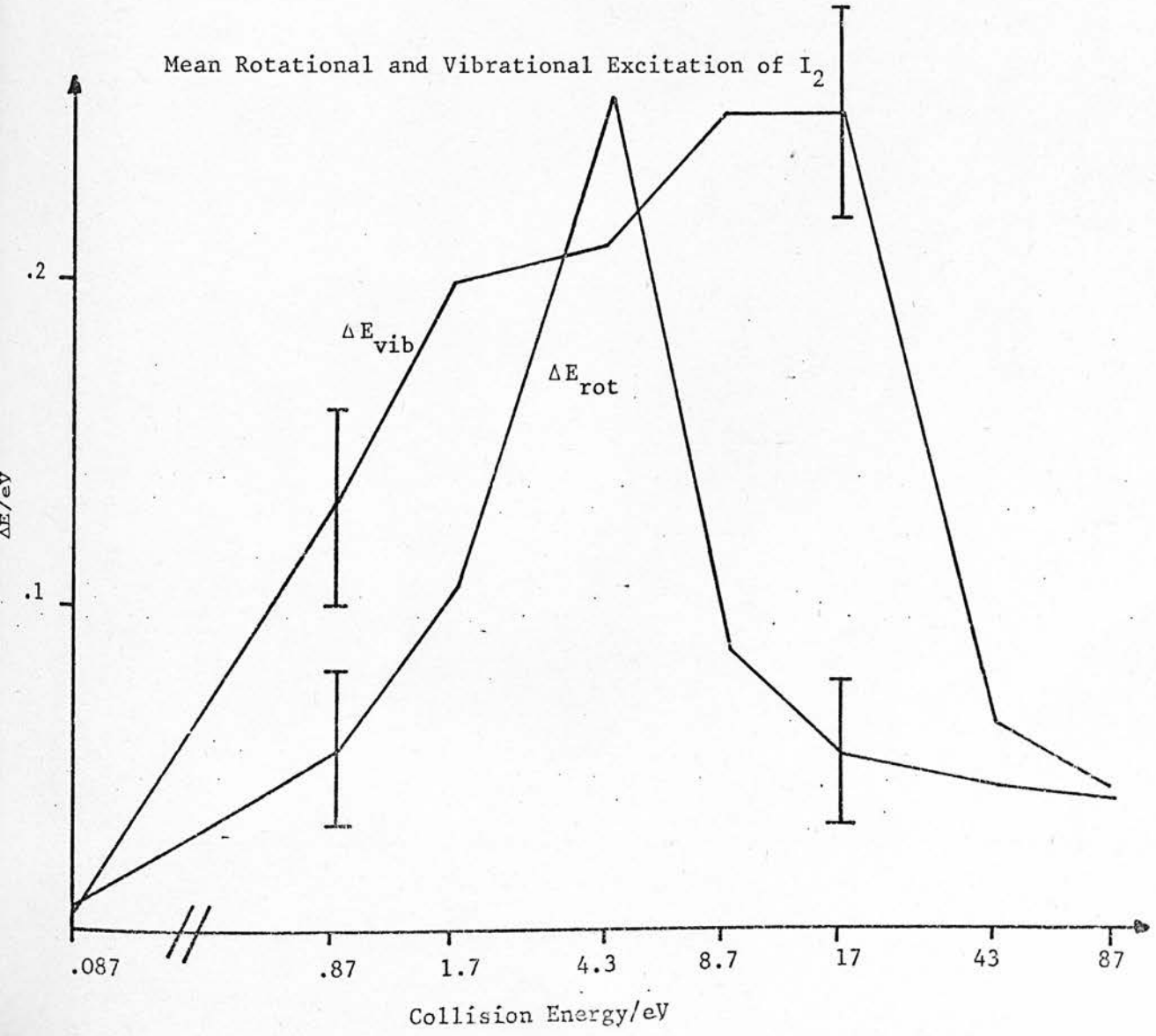
Mean Rotational and Vibrational Excitation of I_2
.2
.1
ΔE/eV
ΔE_{vib}
ΔE_{rot}
.087
.87
1.7
4.3
8.7
17
43
87
Collision Energy/eV

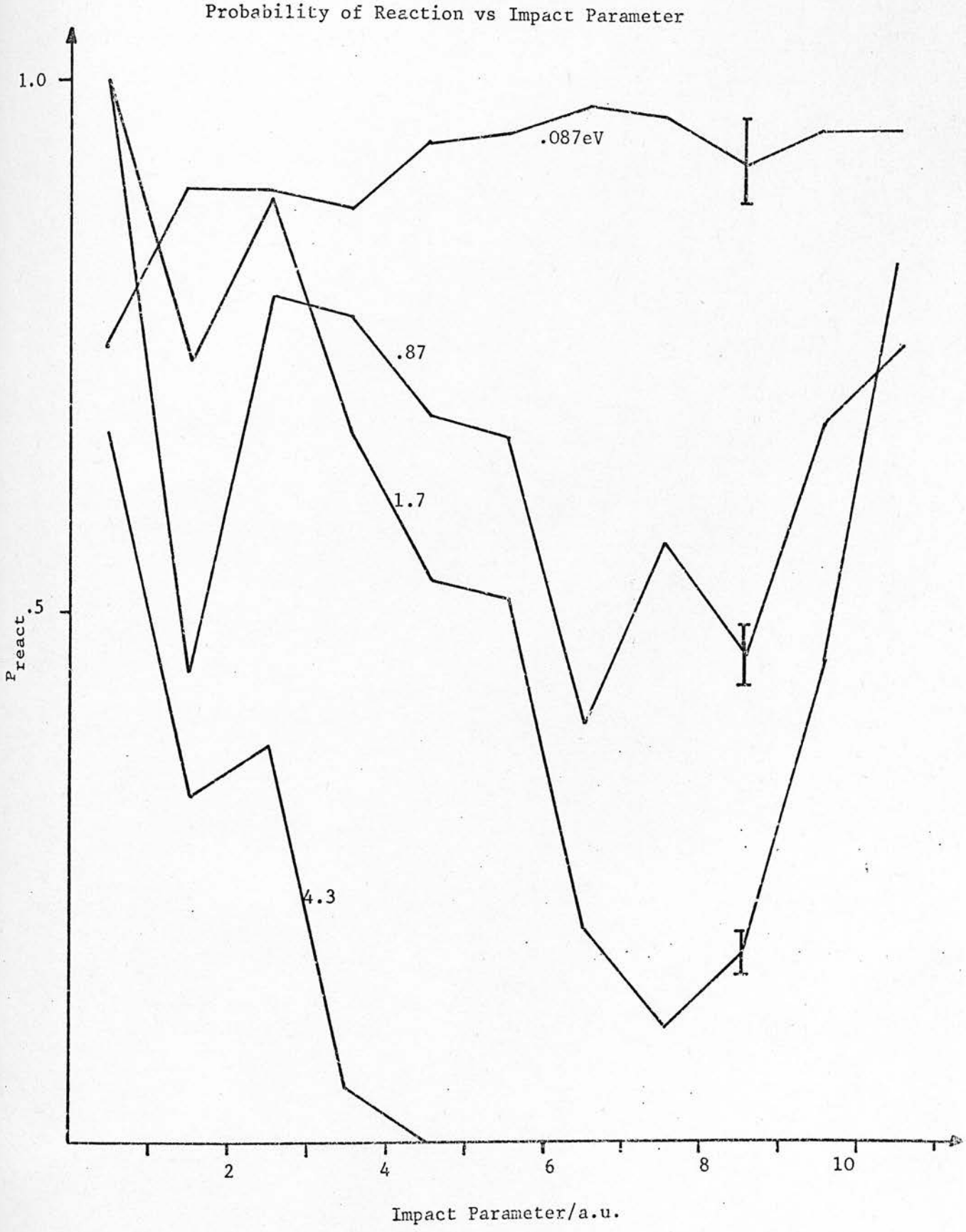
Probability of Reaction vs Impact Parameter
1.0
.5
P_{react}
.087eV
.87
1.7
4.3
2
4
6
8
10
Impact Parameter/a.u.

FIGURE 5.5

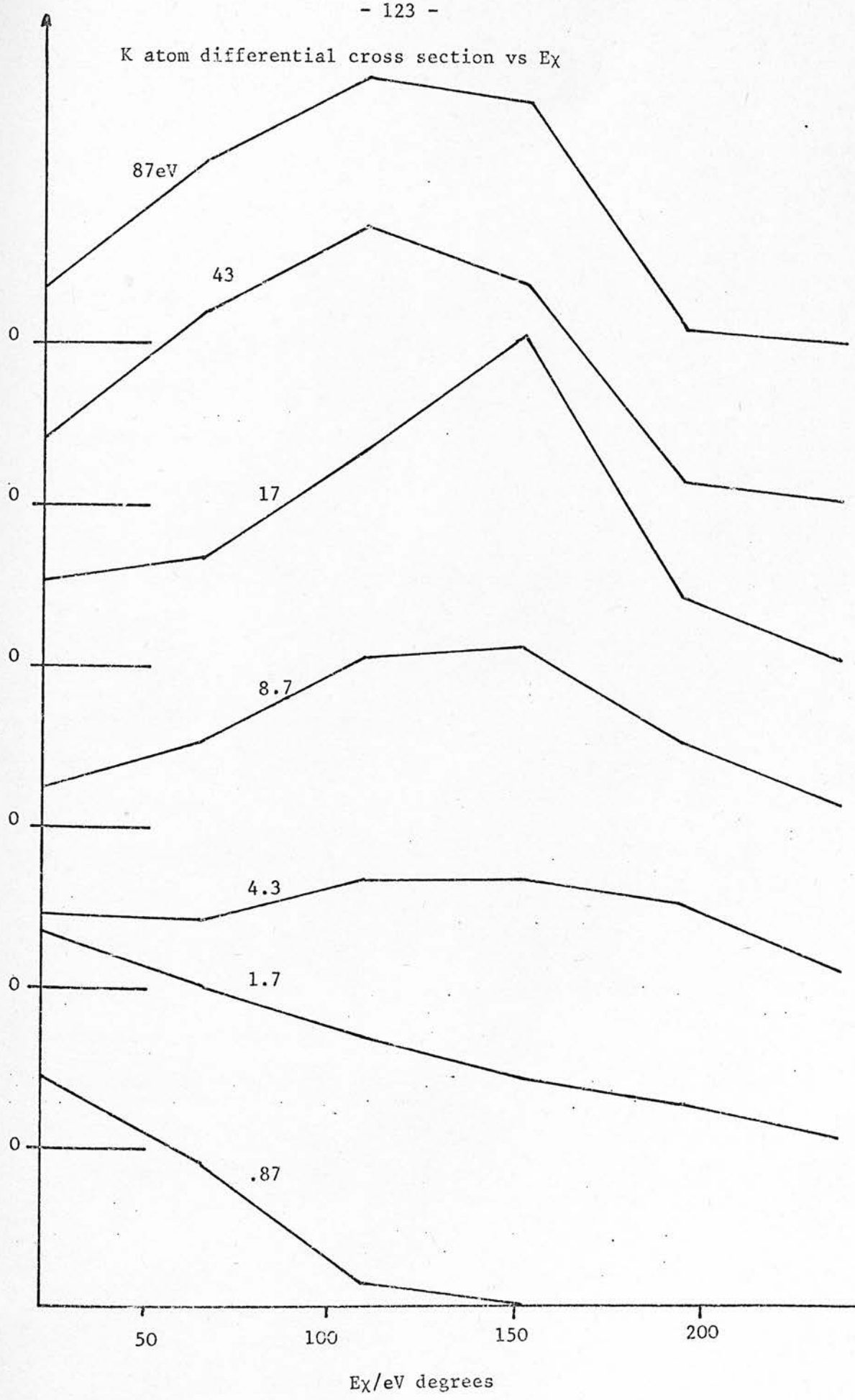
K atom differential cross section vs Eχ
87eV
43
17
8.7
4.3
1.7
.87
0
0
0
0
0
0
50
100
150
200
Eχ/eV degrees

FIGURE 5.6

All remaining trajectories were labelled elastic irrespective of the degree of rotational excitation. σ_{vib} and $\sigma_{elastic}$ increase with collision energy except for a small fall off in σ_{vib} at 43 and 87eV. The variation of the mean energy transferred to vibration and rotation of I_2 with collision energy is shown in Figure 5.4 and the steep fall off at high energies is pronounced. Again this can be attributed to the difficulty of momentum transfer in collisions of very short duration. The rotational excitation is much more strongly tuned to the value of collision energy but the two curves are broadly similar in shape. This can be contrasted with the behaviour of $\overline{\Delta E}_{vib}$ and $\overline{\Delta E}_{rot}$ as functions of K atom scattering angle as shown in Figure 5.7. It is evident that vibrational excitation is a small impact parameter process whereas rotational excitation occurs at large impact parameters. A clear distinction between the mechanism for inelastic events at small and large impact parameters is shown in the plots of total energy loss against b in Figure 5.8. The small b 'clouting' mechanism results in ΔE increasing with E whereas the position is exactly reversed for the large impact parameter 'clutching' mechanism. Finally the degree of vibrational and rotational excitation is plotted against K atom scattering angle is an experimentally accessible region of θ for 43 and 87eV in Figure 5.9. Excitation of one or two vibrational quanta and a large degree of rotational excitation is predicted.

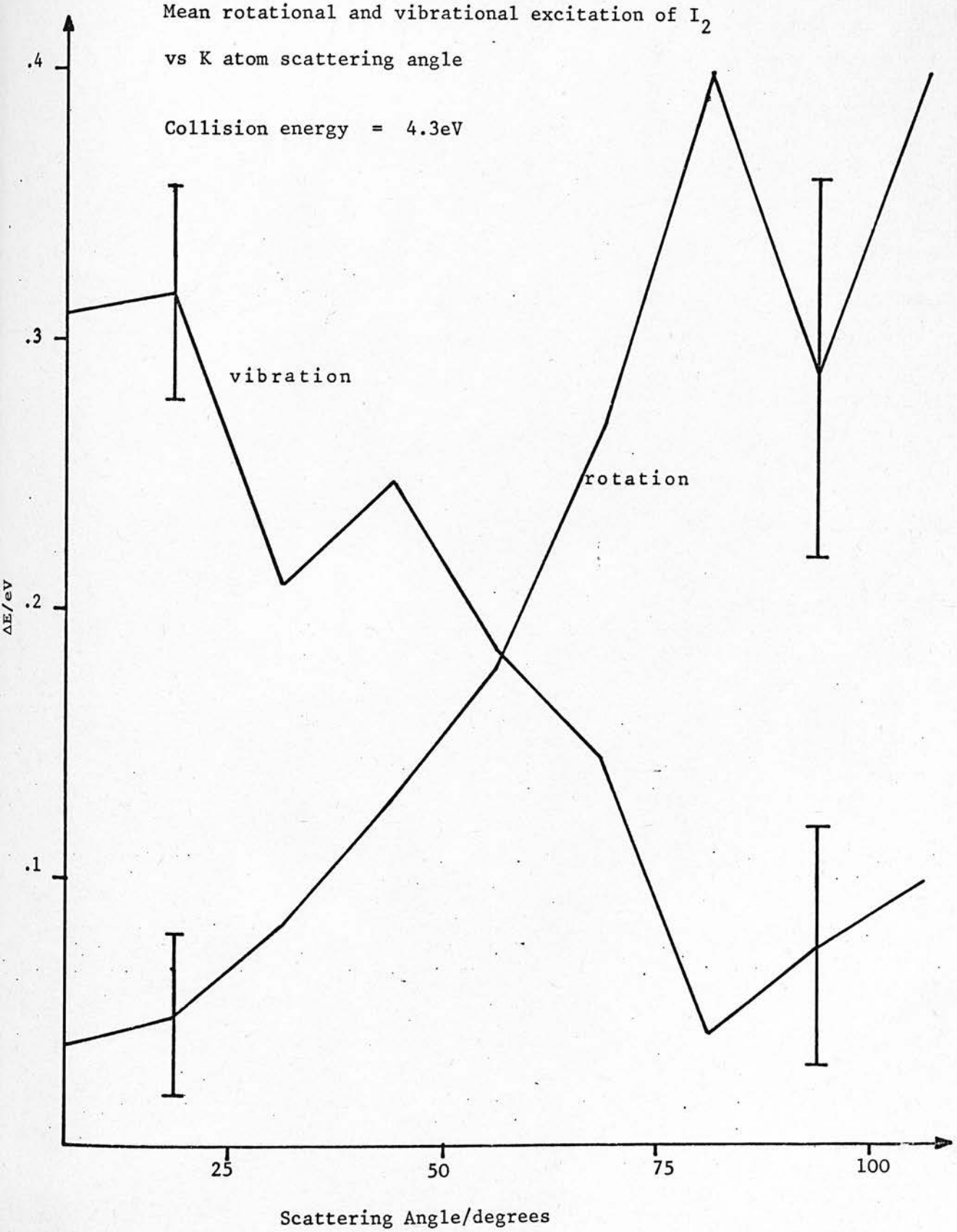
Mean rotational and vibrational excitation of I_2
vs K atom scattering angle
Collision energy = 4.3eV
.4
.3
.2
.1
ΔE/eV
vibration
rotation
25
50
75
100
Scattering Angle/degrees

FIGURE 5.7

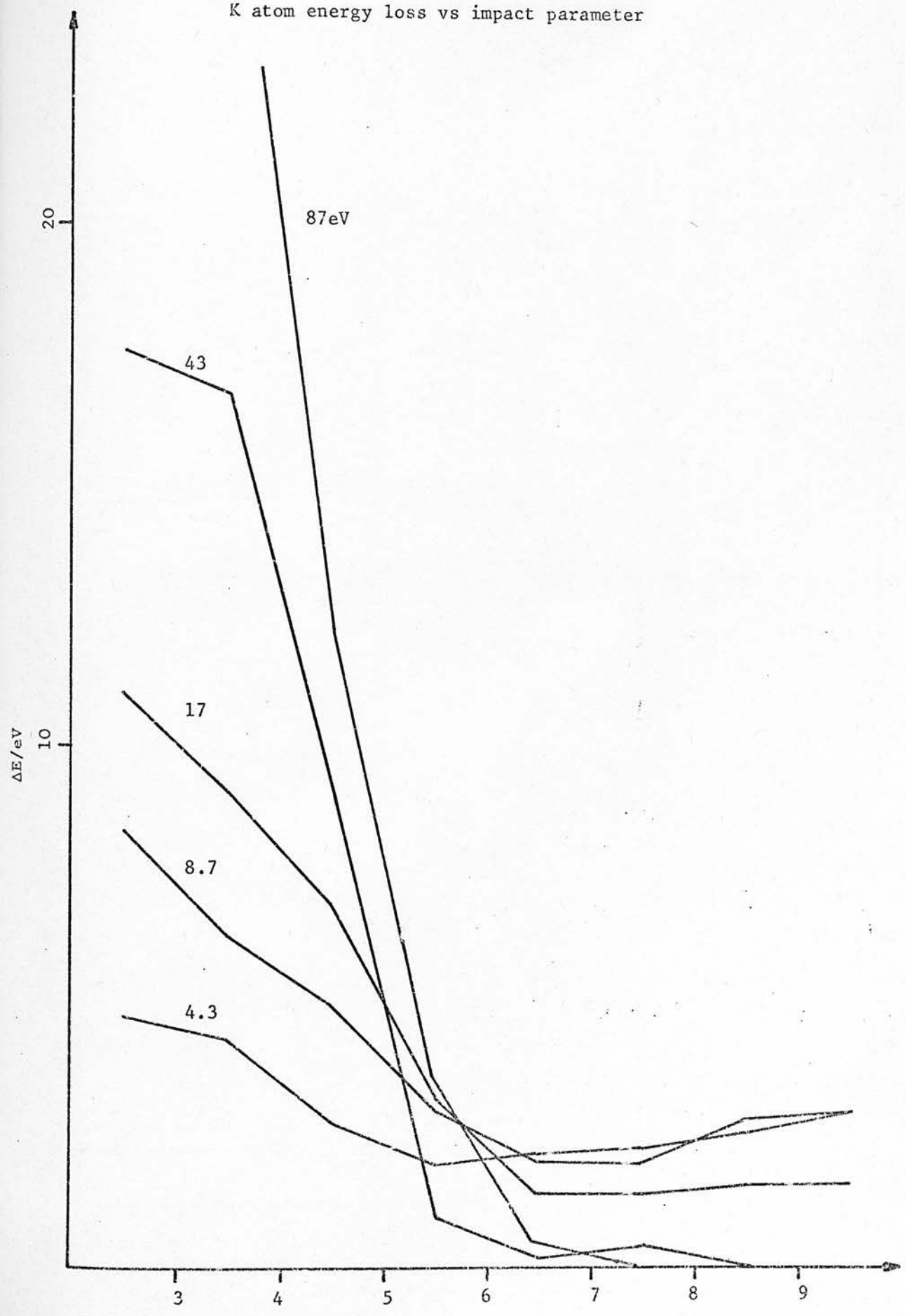
K atom energy loss vs impact parameter
87eV
43
17
8.7
4.3
20
10
ΔE/eV
3
4
5
6
7
8
9
Impact Parameter/a.u.

FIGURE 5.8

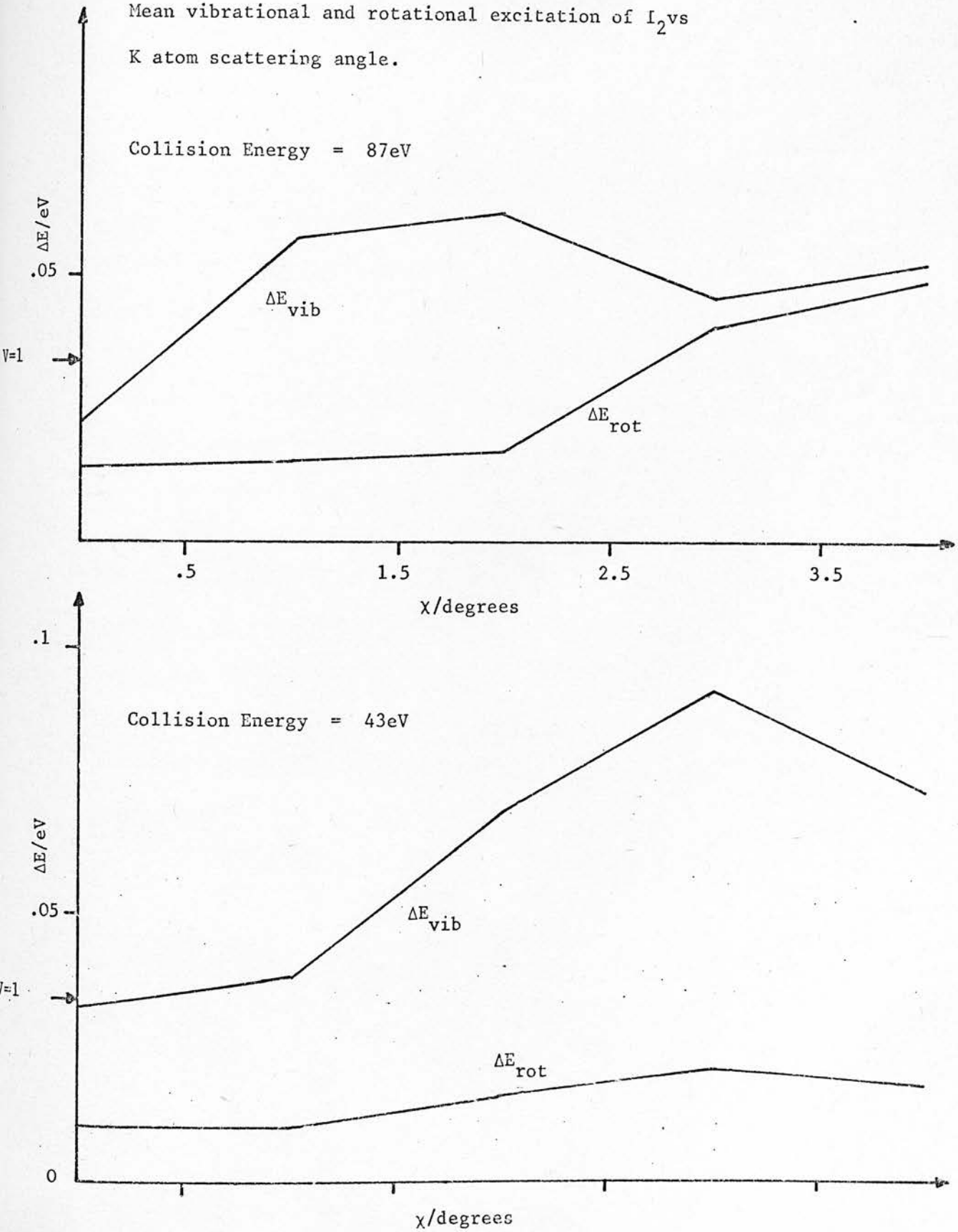
Mean vibrational and rotational excitation of I_2 vs
K atom scattering angle.
Collision Energy = 87eV
ΔE/eV
.05
V=1
ΔE_{vib}
ΔE_{rot}
.5
1.5
2.5
3.5
χ/degrees
.1
Collision Energy = 43eV
ΔE/eV
.05
V=1
ΔE_{vib}
ΔE_{rot}
0
χ/degrees

FIGURE 5.9

5.5 Conclusions

The fall off in reactive cross section with increasing collision energy is in agreement with experimental results for the system K/CH_3I which have also been duplicated by Classical trajectory calculations (LAB 73). The same fall off is seen in the dissociative cross section except that the value levels off at high energies. This is attributed to a small impact parameter 'knock on' mechanism. The mean vibrational and rotational excitation increase similarly with collision energy in agreement with the results of Brown (BRO 74) for Li^+/H_2 trajectory calculations. However both decrease sharply as energy is further increased, rotational more sharply than vibrational. The calculations indicate that elastic differential cross sections at high energies would yield information on the ionic potential and energy loss differential cross sections would be useful in examining the change in dissociation mechanism with energy and the different dependence of rotational and vibrational energy transfer on impact parameter.

REFERENCES

ABR 63 - A.A. Abrahamson, Phys. Rev. 130 p693 (1963)

AIR 67 - J.R. Airey, E.F. Green, G.P. Reck and J. Ross, J. Chem. Phys. 46 p3295 (1967)

AND 69 - R.W. Anderson, V. Aquilanti and D.R. Herschbach Chem. Phys. Letts. 4 p5 (1969)

AMD 66 - I. Amdur and J.E. Jordan, Adv. Chem. Phys. 10 p29 (1966)

BEC 62 - D. Beck, J. Chem. Phys. 37 p2884 (1962)

BER 73 - R.B. Bernstein and A.M. Rulis, Disc. Faraday Soc. 55 p293 (1973)

BER 73 - P.J. Bertoncini and A.C. Wahl, J. Chem. Phys. 58 p1259 (1973)

BLA 68 - N.C. Blais, J. Chem. Phys. 41 p9 (1968)

BLY 64 - A.R. Blythe, A.E. Grosser and R.B. Bernstein J. Chem. Phys. 41 p1917 (1964)

BRO 74 - N.J. Brown, J. Chem. Phys. 60 p2958 (1974)

BUC 47 - R.A. Buckingham and J. Corner, Proc. Roy. Soc. (London) Ser. A 189 p118 (1947)

BUC 71 - U. Buck, J. Chem. Phys. 54 p1923 (1971)

BUC 71 - U. Buck and H. Pauly, J. Chem. Phys. 54 p1929 (1971)

BUN 64 - D.L. Bunker and N.C. Blais, J. Chem. Phys. 41 p2377 (1964)

CHI 73 - M.S. Child, Disc. Faraday Soc. 55 p30 (1973)

COM 73 - R.N. Compton and C.S. Cooper, J. Chem. Phys. 59 p4140 (1973)

COU 72 - C.A. Coulson, "Valence", Clarendon Press, Oxford (1972)

DAL 67 - A. Dalgarno, Adv. Chem. Phys. 12 p143 (1967)

DAV 71 - R. David, M. Faubel, P. March and J.P. Toennies, Proc. 7th I.C.P.E.A.C. p252 (1971)

DEL 74 - C.A.L. Delvigne and J. Los , Physica (to be published)

DUC 71 - B.S. Duchart, PhD. Thesis, Edinburgh (1971)

FIR 53 - O.B. Firsov, Zh. Eksp. Teor. Fiz. 24 p279 (1953)

FIT 66 - D.D. Fitts, Ann. Rev. Phys. Chem. 17 p59 (1966)

FLU 73 - M.A.D. Fluendy and K.P. Lawley, "Chemical Applications of Molecular Beam Scattering", Chapman and Hall, London (1973)

FOR 59 - K.W. Ford and J.A. Wheeler, Ann. Phys. 7 p259 (1959)

GER 73 - E. Gersing, H. Pauly, E. Schadlich and M. Vonderschen, Disc. Faraday Soc. 55 p211 (1973)

GIN 65 - M.L. Ginter and R. Battino, J. Chem. Phys. 42 p3222 (1965)

HAS 62 - J.B. Hasted, in "Atomic and Molecular Processes" Ed. D.R. Bates, Academic Press, London (1962)

HER 66 - D.R. Herschbach, "Molecular Beams", in Adv. Chem. Phys. 10 (I. Prigogine, Editor)

HER 73 - D.R. Herschbach, Disc. Faraday Soc. 55 p233 (1973)

KEM 70 - V. Kempter, W. Mecklenbrauk, M. Menzinger, G. Schuller, D.R. Herschbach and Ch. Schlier, Chem. Phys. Letts. 6 p106 (1970)

KEN 38 - E.H. Kennard, "Kinetic Theory of Gases", Int. Ser. in Physics, New York (1938)

KEN 69 - M. Kennedy and F.T. Smith, Mol. Phys. 16 p131 (1969)

KRA 65 - M. Kraus and F.H. Mies, J. Chem. Phys. 42 p2703 (1965)

LAB 73 - R.A. Labudde, P.J. Kuntz, R.B. Bernstein and R.D. Levine, J. Chem. Phys. 59 p6286 (1973)

LAC 70 - K. Lacmann and D.R. Herschbach, Chem. Phys. Letts. 6 p106 (1970)

LAN 32 - L.D. Landau, Phys. Z. Sowjet 2 p46 (1932)

MAH 68 - B.H. Mahan, W.R. Gentry and Y. Lee, J. Chem. Phys. 49 p1758 (1968)

MAL 70 - C.J. Malerich and R.J. Cross, J. Chem. Phys. 52 p386 (1970)

MAR 69 - H. Margenau and N.R. Kestner, "Theory of Intermolecular Forces", Int. Ser. Monogs. in Nat. Phil, Pergamon, Oxford (1969)

McD 73 - D.R. McDonald, M.A.D. Fluendy and K.P. Lawley, Proc. 8th I.C.P.E.A.C. p56 (1973)

MIL 68 - W.H. Miller, J. Chem. Phys. 48 p464 (1968)

MOR 62 - F.A. Morse, R.B. Bernstein and H.U. Hostettler, J. Chem. Phys. 36 p1947 (1962)

MOU 71 - A.M.C. Moutinho, Post Doctoral Report, Amsterdam (1971)

NEW 66 - R. Newton, "Scattering Theory of Waves and Particles", Mcgraw Hill, New York (1966)

NIK 72 - E.E. Nikitin and M.Ya. Ovchinnikova, Soviet Phys. Uspekhi 14 p394 (i972)

OLS 71 - R.E. Olson and F.T. Smith, Phys. Rev. A3 3 p1607 (1971)

PAU 65 - H. Pauly and J.P. Toennies, Adv. At. Mol. Phys. 1 p195 (1965)

POL 70 - J. Politiek, J.J.M. Schiffer and J. Los , Physica 49 p165 (i970)

RED 73 - J.F. Reddington, PhD Thesis, Edinburgh (1973)

ROT 63 - E.W. Rothe, P.K. Rol and R.B. Bernstein, Phys. Rev. 130 p2333 (1963)

SMI 67 - F.T. Smith, R.P. Marchi, W. Aberth and D.C. Lorents, Phys. Rev. 161 p31 (1967)

SIS 70 - P.E. Siska, J.M. Parson, T.P. Schafer, F.P. Tully, Y.C. Wong and Y.T. Lee, Phys. Rev. Letts. 25 p271 (1970)

THO 63 - W.R. Thorson, Proc. 3rd I.C.P.E.A.C. p964 (1963)

TOE 65 - J.P. Toennies, Z. Phys. 182 p257 (1965)

USD 71 - H. Usdeth, U.F. Giese and W.R. Gentry, J. Chem. Phys. 54 p3642 (1971)

YAN 74 - S.Y. Yang, E.W. Rothe and G.P. Reck, Int. Journal of Mass Spectronomy ans Ion Physics 14 p79 (1974)

ZEN 32 - C. Zener, Proc. Roy. Soc. A 137 p696 (1932)

APPENDIX

Listing Of Data Collection Program

```
%BEGIN
%CONTROL 4  ; ! FORGET LINE NUMBERS
%INTEGERMAP INTEGER(%INTEGER AD)
%RESULT=AD
%END
%REALFN GETREAL(%INTEGER AD)
   ! READS REAL QUANTITY FROM COMMON AREA
%REAL X
*MOV…14.(R1),R2    ; ! R2 POINTS TO REAL IN COMMON AREA
*MOV…#36.,R3
*ADD…R1,R3         ; ! R3 POINTS TO X
*MOV…(R2)+,(R3)+
*MOV…(R2)+,(R3)+
%RESULT=X
%END
%REALFN MOD(%REAL x)
*…BIC…#100000,14.(R1)
%RESULT=X
%END; !MOD
%ROUTINE PRINT(%REAL Y,%INTEGER N,M)
%ROUTINESPEC PRINTFL(%REAL X,%INTEGER N)
%OWNINTEGER IMAX=32767; !MAX INTEGER IN ONE WORD.
%REAL Y,Z,ROUND
%INTEGER I,J,L,SIGN,DP;          ! DP =DECIMAL POINT
N=4 %IF N>4; DP=0;                    ! DEAL WITH STUPID PARAMS
%IF N<=0 %THEN N=1;              ! DEAL WITH STUPID PARAMS
Y=MOD(X);                        ! ALL WORK DONE WITH Y
ROUND= (1/2)/10**N;                ! ROUNDING FACTOR
%IF Y>IMAX %THEN %START
PRINTFL(X,M); %RETURN; %FINISH
I=0;Z=1; Y=Y+ROUND;
COUNT LEADING PLACES:
                                 ! NO DANGER OF OVERFLOW HERE
I=I+1;Z=10*Z;
%IF Y>=Z %THEN => COUNT LEADING PLACES
SPACES(N-I);                     ! O.K FOR ZERO OR -VE SPACES
SIGN=' ';                        ! '+' IMPLIED
%IF X<0 %THEN SIGN='-'
PRINT SYMBOL(SIGN)
J=I-1; Z=10**J
NEXT DIGIT:
                                 ! OBTAIN NEXT DIGIT
L=INT PT(Y/Z);                     ! AND REDUCE TOTAL
Y=Y-L*Z;Z=Z/10;
PRINT SYMBOL(L+'0')
J=J-1
%IF J>=0 %THEN => NEXT DIGIT
```

```
%IF M=0 %THEN %RETURN;          ! NO DECIMAL PART TO BE O/P
%IF DP=0 %THEN %PRINTTEXT'.'
DP=1; J=0; Z=1
Y=10*Y; M=M-1; -> NEXT DIGIT
%ROUTINE PRINTFL(%REAL X,%INTEGER N)

%REAL SIGN,ROUND,FACTOR
%INTEGER COUNT,INC
ROUND=.5/10**N
SIGN=1
%IF X=0 %THEN -> ZERO
%IF X < 0 %THENSTART
X=-X; SIGN=-SIGN; %FINISH
INC=1; COUNT=0; FACTOR=1/10
%IF X <= 1 %THENSTART
FACTOR=10; INC=-1; %FINISH
SCALE: %IF 1<=X+ROUND %AND X+ROUND<10 %THEN -> PRINTOUT
X=X*FACTOR; COUNT=COUNT+INC
-> SCALE
ZERO: COUNT=-99
PRINTOUT: PRINT(SIGN*X,1,N)
%PRINTTEXT'@'
WRITE(COUNT,2)
%END
%END
%INTEGERFN VOLT(%INTEGER CHAN,GAIN)
LACC(CHAN<<8+GAIN<<3)
*EMT…363
%RESULT=ACC
%END
%REALFN TIME
%INTEGER A,B
*MOV…R1,-(SP)
*EMT…321 ;          ! GET TIME IN R0, R1
*MOV…R1,R5
*MOV…(SP)+,R1 ;     ! RESTORE IMP R1
*MOV…R0,34.(R1) ;   ! SET HIGH ORDER TIME IN A
*MOV…R5,36.(R1) ;   ! SET LOW ORDER TIME IN B
A=A+1 %IF B < 0 ;   ! COMPENSATE FOR POSSIBLE SIGN BIT
%RESULT=(A*65536.+B)/3000  ; ! 50 TICKS PER SECOND
%END
%INTEGERFN READBIN
*EMT…337
*MOV…12.(R1),R1
*RTS…PC
%END
%ROUTINE SETPOT (%INTEGER X)
 ! X=1 MEANS SWITCH ON, X=0 MEANS SWITCH OFF
*MOV…R1,-(SP)     ; ! SAVE R1
*MOV…14.(R1),R0   ; ! GET PARAMETER
*MOV…#1,R1        ; ! SPECIFY RELAY 0
*EMT…352          ; ! WHAM
*MOV…(SP)+,R1     ; ! RESTORE R1
%END
%ROUTINESPEC MEANANDSD (%REALARRAYNAME D1,%REAL M1,LIM, %C
%REALNAME MEAN,SIGMA, %INTEGERNAME N1)

%ROUTINESPEC CHECKUP
%ROUTINESPEC RECORD ERROR (%INTEGER PN,EN)
%ROUTINESPEC PROCESSDATA
%REALFNSPEC SQRT(%REAL X)
%ROUTINESPEC CHOOSE ANGLE
%ROUTINESPEC GETVARIABLES
%ROUTINESPEC DRIVE STEPPER
%ROUTINESPEC DRIVE MOTOR(%INTEGER UNIT,STEPS)
%ROUTINESPEC READIN
```

```
%ROUTINESPEC DECODE
%ROUTINESPEC DISC WRITE
%ROUTINESPEC FILL BLOCK
%ROUTINESPEC RING BELL
%INTEGERARRAY ERROR(1:30)
%INTEGERARRAY D(1:32)
%REALARRAY A(1:14)
%REALARRAY NS(1:200)
%REALARRAY N(1:200)
%INTEGERARRAY X(1:200)
%INTEGER MAXANGLE,MINANGLE,CENTRE,ANGLECOUNT,MBCHECK,ENTRY,NEWANGLE
%INTEGER ACOUNT,ASENT,RSENT,MRTE,AF,R,FIXUP,STEPS
%INTEGER P,ENOUGH,OUTRTE,MB,I,OLDMDE,OLDANG,RTE,ICOUNT,ANGLE,EACC,SENT
%INTEGER FLAG,OLDFLAG,SC,MODE,IB,JB,XBEAM,II,IC,NBLOCK,DATA
%INTEGER J,JREAD,CF,CC,NUM,NN,NXS,NSIG,N2,IA,JA,TCOUNT,SENSE,POT
%INTEGER ION,OLDION.
%REAL NOW,DTD,TD,RRATE,THEN,PERIOD,TSENT,OLDBEAM
%REAL MSN,ATT,GOODNESS,ST,Y,TGRAD,DX,DN,DS,DXS
%REAL MXR,EX,EN,ES,EXS,MN,MS,MXS,MX,MNR,MSR,MXSR,LL,MM
%REAL ACC,COUNTA,COUNTB,OLDMX,RAT,RAT1,OLDATT
OLDFLAG=0
CF=1
AF=280
IB=0
SC=0
OLDION=0
OLDATT=0
OLDBEAM=0.
DATA=0
FIXUP=0
MODE=1
ANGLE=0
NBLOCK=1
RTE=3
EACC=0                    ; ! ERROR COUNTER
SENT=0                    ; ! SENTENCE COUNTER
ASENT=0                    ; ! GOOD SENTENCES PER BLOCK
RSENT=0                    ; ! SENTENCES PER BLOCK REJECTED BY MEANANDSD
R=0
TCOUNT=0
ACOUNT=0
CC=0
ENOUGH=16          ; ! NO. OF SENTENCES TO PROCESSDATA
OUTRTE=0                ; ! OUTPUT CHANNEL FOR PROCESSDATA
SENSE=0
RAT=1.0
SELECT OUTPUT(4)
%PRINTTEXT'
   CHECKING ONLY. GIVE EXPERIMENTAL AND CONTROL VARIABLES TO CHE2
   BEFORE SETTING FLAG = 110 OR 100
'
J=1
1: READIN
->2 %IF D(1) = 13 %AND D(26) = 14 %AND D(22)!8 = 14
 ! LOCK ON TO START CODE, END CODEAND SCALER B IDENTITY
 ! AT CORRECT SEPARATIONS
R=0
RECORD ERROR(1,1)  ; ! SLIPPED OUT OF PHASE
%CYCLE I=3,1,31
%IF D(I) = 13 %THENSTART  ; ! FIND POSSIBLE START CODE
%CYCLE II=I,1,32
D(II-I+1)=D(II)            ; ! SHIFT ARRAY TILL START CODE IN ELEMENT 1
%REPEAT
J=(33-I)//2+1          ; ! J POINTS TO ELEMENTS OF D NEEDING REFILLED
->1                        ; ! GO AND FILL THEM
%FINISH
```

```
%REPEAT
->1                          ; ! WHOLE NEW SENTENCE REQUIRED
2: DECODE
->1
%ROUTINE DECODE
 ! FLAG = 7 => READ COMMON APEA AND START NEW BLOCK
 ! FLAG = 6 => START SWEEP
 ! FLAG = 5 => END SWEEP
 ! FLAG = 4 => TUNE UP
 ! FLAG = 3 => STOP
 ! FLAG = 2 => READ COMMON AREA
 ! RTE=3 => LOOK FOR STARTSWEEP
 ! RTE=2 => WAIT TILL ANGLE STEADY
 ! RTE=1 => COLLECT DATA
 ! PROCESSDATA IS CALLED WHEN ANGLE CHANGED OR END SWEEP ENCOUNTERED.
%SWITCH S(1:3)
OLDANG=ANGLE
OLDMDE=MODE
XBEAM=4095-D(23)-16*D(24)-256*D(25)   ; ! XBEAM OUTPUT IS INVERTED BINARY
FLAG=D(13)>>1
MODE=D(13)&1
CC=CC+1
%IF CC = CF %THENSTART
CHECKUP
CC=0
%FINISH
COUNTA=0
SENT=SENT+1              ; ! TOTAL SENTENCE COUNTER
COUNTB=0
%CYCLE I=6,-1,2
COUNTA=COUNTA*10+D(I)
COUNTB=COUNTB*10+D(12+I)
%REPEAT
ANGLE=0
%CYCLE I=12,-1,9
ANGLE=ANGLE*10+15-D(I)        ; ! ANGLE OUTPUT IS INVERTED BCD
%REPEAT
%IF FIXUP = 2 %THENSTART
FIXUP = 0
%IF MOD(ANGLE-NEWANGLE) > 3 %THENSTART
%PRINTTEXT'   MISSED '
WRITE(NEWANGLE,6)
NEWLINE
%FINISH
%FINISH
%IF FIXUP = 1 %AND MOD(ANGLE-NEWANGLE) > 1 %THENSTART
%IF MOD(ANGLE - NEWANGLE) > 20 %THENSTART ; ! LARGE FIXUP NOT ALLOWED
RING BELL
%PRINTTEXT'
TELETRAK OR MOTOR FAULT'
WRITE(NEWANGLE,6)
NEWLINE
FIXUP=0; RTE=2
%RETURN; %FINISH
DRIVE STEPPER
FIXUP = 2
%FINISH
-> S(RTE)
S(3): SC=SC+1
%RETURN %UNLESS SC=5
SC=0
-> FLAG FIXED %IF FLAG = OLDFLAG
OLDFLAG=FLAG
%RETURN
FLAG FIXED: %IF FLAG = 4 %THENSTART        ; ! TUNE UP REQUIRED
RTE=2
```

```
%IF ANGLE > 4900 %AND ANGLE < 5100 %THENSTART    ; ! IN MAIN BEAM
%PRINTTEXT'
MAIN BEAM    ERROR    ATTENUATION    ION CURRENT
'
ENOUGH=42; MB=1; %FINISH %ELSE %START
%PRINTTEXT'
SIGNAL  SIGNAL/S.D.  BACKGROUND
'
ENOUGH=60; MB=0; %FINISH      ; ! OUT OF MAIN BEAM
OUTRTE=1; %FINISH
%IF FLAG = 7 %OR FLAG = 3 %THENSTART  ; ! READIN OR STOP
FILL BLOCK %UNLESS DATA = 0
%IF FLAG = 3 %THENSTART
%PRINTTEXT'POSITION IN ANGLE SCAN IS '
WRITE(IB,4);WRITE(JB,4)
NEWLINE
%STOP
%FINISH
%PRINTTEXT'WAITING FOR FLAG = 110
'
%FINISH
GETVARIABLES %IF FLAG = 2 %OR FLAG = 7
 %RETURN %UNLESS FLAG=6
THEN=TIME          ; ! STARTING TIME
RTE=2
GETVARIABLES %IF NBLOCK = 1      ; ! NEW EXPERIMENTAL VARIABLES
%RETURN %IF RTE=3
%PRINTTEXT'COLLECTING DATA
'
S(2): %IF MOD(ANGLE-OLDANG)>1 %THEN %RETURN
%IF SENSE = 0 %THENSTART
 ! SETTING MASS SPEC RELAY UNLESS IT IS BEING CHECKED IN TUNE UP
%IF MOD(ANGLE-CENTRE) > 30 %THENSTART
SETPOT(0); POT=0
%FINISH %ELSE %START
SETPOT(1); POT=1
%FINISH; %FINISH
RTE=1
ICOUNT=0
S(1):  -> TEST FLAG %IF MODE = OLDMDE    ; ! REJECT SENTENCE IF MODE NOT
%IF MOD(ANGLE-OLDANG) > 2 %THENSTART
 RTE=2
PROCESSDATA
DISC WRITE
%RETURN
%FINISH
TCOUNT=TCOUNT+1
ICOUNT=ICOUNT+1      ; ! 'GOOD' SENTENCE COUNTER
X(TCOUNT)=XBEAM
%IF MODE=0 %THENSTART          ; ! IF MODE = 0
NS(TCOUNT)=COUNTA          ; ! NOISE + SIGNAL IN COUNTER A
N(TCOUNT)=COUNTB          ; ! NOISE IN COUNTER B
%FINISH %ELSE %START          ; ! IF MODE = 1
NS(TCOUNT)=COUNTB          ; ! VICE VERSA.
N(TCOUNT)=COUNTA
%FINISH
ACOUNT=ACOUNT+1
-> TEST FLAG %UNLESS ICOUNT = ENOUGH %OR TCOUNT = 200 ; ! ANGLE TO BE C
RTE=2
PROCESSDATA
-> TEST FLAG %IF OUTRTE = 1  ; ! NO ANGLE STEPPING IN TUNE UP
-> MOVE %IF TCOUNT=200  ; ! MUST MOVE IF ARRAYS FULL
%IF MOD(MSR/ES) > ACC %OR ACOUNT > AF %THENSTART
 ! CHANGE ANGLE IF DESIRED ACCURACY REACHED OR THE MAXIMUN
 ! NUMBER OF SENTENCES HAS BEEN EXCEEDED.
   MOVE:
```

```
DISC WRITE
-> TEST FLAG %IF RTE = 3
CHOOSE ANGLE
DRIVE STEPPER
FIXUP = 1
ACOUNT=0
%FINISH
   TEST FLAG:  %RETURN %UNLESS FLAG=5
%IF OUTRTE = 1 %THENSTART
%RETURN %IF SENSE = 1
-> EXIT %IF SENSE = 2
 ! ON EXIT FROM TUNE UP, DRIVE TO NEAR MAIN BEAM TO CHECK THE RATIO
 ! OF THE SIGNALS FO THE TWO POTIENTIOMETER SETTINGS ON THE MASS SPEC
SENSE=1; RTE=2
NEWANGLE=CENTRE+50
DRIVE STEPPER
FIXUP=1
SETPOT(0)
%RETURN; %FINISH
   EXIT: %PRINTTEXT'DATA BEING CHECKED BUT NOT COLLECTED
'
RTE=3
PROCESSDATA
DISC WRITE
ENOUGH=16; ACOUNT=0
OUTRTE = 0; SENSE=0
%END
%ROUTINE CHECKUP
%INTEGER IS
IS=2              ; ! COUNTER A
TESTING COUNTERS:%CYCLE I=IS,1,IS+6
%IF D(I) > 9 %THEN RECORD ERROR(I,5)  ; ! DIGIT > 9 ?
%REPEAT
RECORD ERROR(IS+5,7) %IF D(IS+5) > 0  ; ! OVERFLOW ?
RECORD ERROR(IS+6,7) %IF D(IS+6) > 0  ; ! OVERFLOW ?
%IF IS = 2 %THENSTART
IS=14             ; ! COUNTER B
-> TESTING COUNTERS
%FINISH
%CYCLE I=12,-1,9          ; ! ANGLE
RECORD ERROR(I,5) %IF D(I) < 6    ; ! DIGIT > 9 ?
%REPEAT
IS=D(2)&1+2*(D(14)&1)+4*(D(9)&1)
RECORD ERROR(21,4) %UNLESS D(21)= IS    ; ! BIT CHECK OK ?
RECORD ERROR(13,9) %IF MODE = OLDMDE    ; ! MODE CHANGED ?
R=0
%END
%ROUTINE RECORD ERROR(%INTEGER PN,EN)
R=R+1
%RETURN %IF R > 3
EACC=EACC+3   ; ! DO NOT RECORD MORE THAN 3 ERRORS PER SENTENCE
ERROR(EACC-2) = SENT          ; ! SENTENCE NO.
ERROR(EACC-1) = PN            ; ! PATTERN NO.
ERROR(EACC) = EN              ; ! ERROR NO.
%IF EACC = 30 %THENSTART
NEWLINE
%CYCLE IC=0,1,2
%CYCLE II=1,3,28
WRITE(ERROR(II+IC),3)
%REPEAT; NEWLINE; %REPEAT
EACC=0
%FINISH
%END
%ROUTINE READIN
%CYCLE I=J,1,16
IN=READBIN
```

```
D(2*I)=NN>>4
D(2*I-1)=NN&15
%REPEAT
J=1
%END
%ROUTINE PROCESSDATA
%REALARRAY W1(1:100)
%REALARRAY W2(1:100)
%RETURN %IF TCOUNT < 4
NUM=TCOUNT//2
%CYCLE I=1,1,NUM
MM=(N(2*I-1)+N(2*I))/2        ; ! NOISE
W1(I)=(NS(2*I-1)+NS(2*I))/2-MM    ; ! SIGNAL
W2(I)=MM          ; ! NOISE
%REPEAT
MM=0.          ; ! ESTIMATED MEAN AND LIMIT SET SUCH THAT
LL=100000.    ; ! NO DATA IS REJECTED ON FIRST PASS.
MRTE=1
MEANANDSD(W1,MM,LL,MS,DS,N2)
MEANANDSD(W2,MM,LL,MN,DN,N2)
DS=2.*DS       ; ! LIMITS SET AT TWICE STANDARD ERROR.
DN=2.*DN
MRTE=2
MEANANDSD(W1,MS,DS,MSR,ES,NSIG)
MEANANDSD(W2,MN,DN,MNR,EN,NN)
%CYCLE I=1,1,NUM
II=X(2*I-1)+Y(2*I)
MM=II/2.     ; ! CROSS BEAM SIGNAL
%IF MM < 10. %THEN MM = 2048.
W1(I)=NS(2*I-1)+NS(2*I)-N(2*I-1)-N(2*I)
W1(I)=1500.*W1(I)/MM              ; ! NORMALISED SIGNAL
W2(I)=MM                          ; ! CROSS BEAM INTENSITY
%REPEAT
MM=0.
LL=200000.
MRTE=1
MEANANDSD(W1,MM,LL,MXS,DXS,N2)
MEANANDSD(W2,MM,LL,MX,DX,N2)
DXS=2.*DXS
DX=2.*DX
MRTE=2
MEANANDSD(W1,MXS,DXS,MXSR,EXS,NXS)
MEANANDSD(W2,MX,DX,MXR,EX,N2)
EN=EN/SQRT(NN)        ; ! STANDARD DEVIATIONS
ES=ES/SQRT(NSIG)
EXS=EXS/SQRT(NXS)
EX=EX/SQRT(N2)
MSN=MS+MN
%IF POT = 1 %THENSTART
 ! CORRECTING FOR DETUNED MASS SPEC IN MAIN BEAM
MSR=MSR*RAT; ES=ES*RAT
MNR=MNR*RAT; EN=EN*RAT
MXS=MXS*RAT; EXS=EXS*RAT
%FINISH
DTD=0
ST=0
NOW=TIME
ASENT=ASENT+NUM
RSENT=RSENT+NUM-NSIG
%RETURN %UNLESS OUTRTE = 1   ; ! IN TUNE UP, WRITE TO TELETYPE
TCOUNT=0
%IF SENSE = 1 %THENSTART
 ! MASS SPEC SIGNAL AT FULL STRENGTH
RAT1=MNR; SENSE=2
SETPOT(1)
%RETURN; %FINISH
```

```
%IF SENSE = 2 %THENSTART
 ! DETUNED SIGNAL
RAT=1000.00
RAT=RAT1/MNR %UNLESS MNR < 0.1
%PRINTTEXT'
RATIO OF SIGNALS FROM MASS SPEC (TUNED/DETUNED) ='
PRINT(RAT,4,2); NEWLINE
FLAG=5
%RETURN; %FINISH
%IF MR = 1 %THENSTART          ; ! MAIN BEAM
%IF MNR = 0 %THEN ATT = 0 %ELSE ATT=-100.*MSR/MNR          ; ! % ATTENUATI
PRINT(MNR,6,2)
PRINT(EN,6,1)
PRINT(ATT,6,1)
WRITE(VOLT(0,1),8)
NEWLINE
%FINISH %ELSE %START
GOODNESS = MSR/ES          ; ! SIGNAL/STD DEVIATION
PRINT(MSR,6,2)
PRINT(GOODNESS,6,1)
PRINT(MNR,6,2)
NEWLINE
%FINISH; %RETURN; %END
%ROUTINE DISC WRITE
%RETURN %IF OUTRTE=1  ; ! NO DISC WRITING IN TUNE UP
TCOUNT=0
%IF MX > 4000 %THEN  %PRINTTEXT'CROSS BEAM OUTPUT CLOSE TO SATURATION
'
-> DISCO %UNLESS MOD(OLDANG-CENTRE) < 3 ;  ! CENTRE OF MAIN BEAM
%IF MNR = 0 %THEN ATT = 0 %ELSE ATT = -100*MSR/MNR
%IF OLDATT-ATT > OLDATT/10 %THENSTART  ; ! ATTENUATION FALLING OFF ?
RING BELL
%PRINTTEXT'ATTENUATION FALLEN FROM '; PRINT(OLDATT,4,1)
%PRINTTEXT' TO '; PRINT(ATT,4,1)
NEWLINE
%FINISH
%IF OLDBEAM - MNR > OLDBEAM/20 %THENSTART;  ! BEAM FALLING OFF ?
RING BELL
%PRINTTEXT'BEAM INTENSITY DOWN FROM '
PRINT(OLDBEAM,6,1)
%PRINTTEXT' TO '
PRINT(MNR,6,1)
%PRINTTEXT'
ATTENUATION IS '; PRINT(ATT,4,1)
NEWLINE
%FINISH
%IF OLDBEAM-MNR > OLDBEAM/6 %OR OLDATT-ATT > OLDATT/5 %THENSTART
RING BELL
%PRINTTEXT' DRASTIC FALLOFF IN BEAM/ATTENUATION, DATA COLLECTION'
%PRINTTEXT' STOPPED
'; RTE=3
%FINISH
OLDATT=ATT
OLDBEAM=MNR          ; ! UPDATE OLDBEAM
   DISCO:  SELECT OUTPUT(1)
DATA=DATA+1
NEWLINE
PRINT(NOW,5,2)
WRITE(VOLT(0,1),6)
PRINT(MSR,6,2)
PRINT(ES,6,2)
WRITE(NSIG,3)
NEWLINE
PRINT(MXSR,6,2)
PRINT(EXS,6,2)
WRITE(NXS,3)
```

```
PRINT(MNR,6,2)
PRINT(EN,6,2)
NEWLINE
WRITE(NN,3)
PRINT(MXR,6,2)
PRINT(EX,6,2)
WRITE(OLDANG,5)
WRITE(DATA,3)
WRITE(NBLOCK,4)
SELECT OUTPUT(4)
FILL BLOCK %IF DATA = 15
%END
%ROUTINE FILL BLOCK
%IF MOD(OLDMX-MXR) > 200 %THENSTART
  ! SIGNIFICANT CHANGE IN CROSSS BEAM SINCE LAST BLOCK ?
RING BELL
%PRINTTEXT'
CROSS BEAM INTENSITY CHANGED FROM'
PRINT(OLDMX/27.3,6,1)
%PRINTTEXT'  TO'
PRINT(MXR/27.3,6,1)
NEWLINE
%FINISH
OLDMX=MXR
ION=VOLT(0,1)
%IF MOD(ION-OLDION) > 100 %THEN %PRINTTEXT'
 ION CURRENT DRIFT
'
OLDION=ION
SELECT OUTPUT(1)
%IF DATA < 15 %THENSTART    ; ! FILL BLOCK WITH ZEROES
%CYCLE I=DATA+1,1,15
NEWLINE
%CYCLE J=1,1,16
%PRINTTEXT'0,0 '
%REPEAT; %REPEAT
%FINISH
NEWLINE
%CYCLE I=1,1,14
PRINT(A(I),6,2)
NEWLINE %IF I = 7
%REPEAT
%PRINTTEXT'
 16'
WRITE(NBLOCK,4)
SELECT OUTPUT(4)
NEWLINE
WRITE(NBLOCK,6)
%PRINTTEXT' BLOCKS ON DISC, % REJECTION ='
RRATE=100.*RSENT/ASENT %UNLESS ASENT = 0
PRINT(RRATE,3,1)
NEWLINE
ASENT=0
RSENT=0
SENT=0
NBLOCK=NBLOCK+1
DATA=0
%END
%ROUTINE MEANANDSD(%REALARRAYNAME D1, %REAL M1,LIM, %C
%REALNAME MEAN,SIGMA, %INTEGERNAME N1)
  ! CALCULATES MEAN AND STANDARD ERROR OF ELEMENTS OF ARRAY D1
  ! AFTER REJECTING ANY ELEMENTS MORE THAN LIM FROM ESTIMATED MEAN M1.
  ! ON FIRST ENTRY (MRTE=1), THE N POINTS FARTHEST FROM THE MEAN ARE
  ! DISCARDED, WHERE N=((NUM-20)//20)*2. ON SECOND ENTRY (MRTE=2),
  ! THEY MAY BE REINSTATED.
%INTEGER NA,NB,IMIN,IMAX,C
```

```
%REAL E,MIN,MAX,M2,SD
NA=1
NB=NUM
-> NO REJECTION %IF NRTE = 2 %OR NUM <= 20
C=0
AGAIN: MIN=D1(NA)
MAX=MIN
IMIN=NA
IMAX=NA
%CYCLE I=NA,1,NB
E=D1(I)
%IF E < MIN %THENSTART
MIN=E; IMIN=I
%FINISH
%IF E > MAX %THENSTART
MAX=E; IMAX = I
%FINISH
%REPEAT
D1(IMIN)=D1(NA)
D1(NA)=MIN
D1(IMAX)=D1(NB)
D1(NB)=MAX
NA=NA+1
NB=NB-1
C=C+1
-> AGAIN %IF C < NUM//20
   NO REJECTION: M2=0.
SD=0.
C=0
%CYCLE I=NA,1,NB
E=D1(I)
%IF MOD(E-M1) < LIM %THENSTART
M2=M2+E
C=C+1       ; ! COUNTS ACCEPTED ELEMENTS
%FINISH
%REPEAT
M2=M2/C   ; ! NEW ESTIMATE OF MEAN
%CYCLE I=NA,1,NB
E=D1(I)    ; ! SUBTRACTING MEAN TO AVOID LOSS OF PRECISION
%IF MOD(E-M1) < LIM %THEN SD=SD+(E-M2)*(E-M2)
%REPEAT
-> OK %UNLESS C = 0
%PRINTTEXT'
DIVISION BY ZERO IN MEANANDSD
'
WRITE(C,4); WRITE(NRTE,4); WRITE(NUM,4); WRITE(NA,4); WRITE(NB,4)
NEWLINE
PRINT(M1,6,2); PRINT(LIM,6,2); PRINT(E,6,2); PRINT(MAX,6,2)
PRINT(MIN,6,2)
MEAN=0; SIGMA=0; NEWLINE; %RETURN
OK; N1=C
MEAN=M2
SIGMA=SQRT(SD/(C-1))    ; ! STANDARD ERROR
%END
%ROUTINE GETVARIABLES
 ! TAKES EXPERIMENTAL AND CONTROL VARIABLES FROM COMMON AREA
%INTEGER AD
AD=-8192          ; ! STARTING ADDRESS OF COMMON AREA
%CYCLE I=1,1,14
A(I) = GETREAL(AD)     ; ! EXPERIMENTAL VARIABLES
AD = AD + 4            ; ! POINTS TO NEXT REAL
%REPEAT
ACC = GETREAL(AD)
AD = AD + 4            ; ! INTEGERS FROM NOW ON
CF = INTEGER(AD)
AD=AD+2
```

```
AF=INTEGER(AD); AD=AD+2
MAXANGLE=INTEGER(AD); AD=AD+2
MINANGLE=INTEGER(AD); AD=AD+2
MBCHECK=INTEGER(AD); AD=AD+2
IA=INTEGER(AD); AD=AD+2
JA=INTEGER(AD)

%PRINTTEXT'NEW VARIABLES READ IN
'
ACOUNT=0; ANGLECOUNT=0
CENTRE=INT PT(A(9))
%RETURN %IF A(1) = 16
%PRINTTEXT'
ERROR IN EXPERIMENTAL VARIABLES
'
%CYCLE I=1,1,14
PRINT(A(I),6,2)
NEWLINE %IF I = 7
%REPEAT
NEWLINE
PRINT(ACC,6,2)
WRITE(CF,5)
WRITE(AF,5)
WRITE(MAXANGLE,6)
WRITE(MINANGLE,6)
WRITE(MBCHECK,6)
WRITE(IA,4)
WRITE(JA,4)
NEWLINE
RTE=3
%END
%ROUTINE DRIVE MOTOR(%INTEGER UNIT,STEPS)
%RETURN %IF STEPS = 0
*MOV…R1,-(SP)      ; ! SAVE R1
*MOV…14.(R1),R0    ; ! UNIT NUMBER
*MOV…16.(R1),R1    ; ! NUMBER OF STEPS
*EMT…354           ; ! DRIVE MOTOR IN GROUP 1
*MOV…(SP)+,R1      ; ! RESTORE R1
%END
%ROUTINE DRIVE STEPPER
%IF NEWANGLE > 7500 %OR NEWANGLE < 2500 %THENSTART
%PRINTTEXT'   ANGLE OUT OF RANGE, ='
WRITE(NEWANGLE,6)
NEWLINE
%RETURN; %FINISH
STEPS=NEWANGLE-ANGLE
DRIVE MOTOR(4,STEPS)
%END
%ROUTINE CHOOSE ANGLE
%OWNINTEGERARRAY A(1:25)=0,1,2,3,4,5,6,7,8,9,10,11,12,13,14,15,16,17,18
     19,20,21,22,23,24
%OWNINTEGERARRAY B(1:25)=84,80,60,0,72,40,8,88,28,44,4,68,76,36,32,56,
     96,12,52,24,92,16,20,64,48
%OWNINTEGER IB=1
%OWNREAL RANGE
%IF ENTRY = 2 %THEN -> NORMAL STEPPING
IB=IB+1            ; ! MAIN BEAM PROFILE
ENOUGH=60          ; ! SHORT OBSERVATION TIME
NEWANGLE = CENTRE-48+B(IB)
%IF IB = 25 %OR IA#0 %OR JA#0 %THENSTART     ; ! MAIN BEAM PROFILE COMPL
IB=IA; JB=JA       ; ! STARTING POINT OF ANGLE SEQUENCE
 ENTRY=2
RANGE=(MAXANGLE - MINANGLE)/2500.
%FINISH; %RETURN
     NORMAL STEPPING:
ANGLECOUNT=ANGLECOUNT+1
```

```
%IF ANGLECOUNT=MBCHECK %THENSTART  ; ! TIME FOR A MAIN BEAM READING ?
ANGLECOUNT=0
ENOUGH=40
NEWANGLE=CENTRE
%RETURN; %FINISH
ENOUGH=16       ; ! NORMAL OBSERVATION TIME
IB=IB+D
%IF IB = 26 %OR IB = 0 %THENSTART
D=-D; IB=IB+D      ; ! START AGAIN GOING OTHER WAY
JB=JB+1-D          ; ! AND SHIFT B BY ONE
%FINISH
JB=JB+D
JB = 1 %IF JB = 26
JB = 25 %IF JB = 0
II=100*A(IB)+B(JB)
NEWANGLE=MINANGLE+INT PT(RANGE*II)
%RETURN
%END
%REALFN SQRT(%REAL X)
%REAL A1,A2
%IF X < 0 %THENSTART
%PRINTTEXT'NEGATIVE ARGUMENT OF SQRT'
PRINT(X,6,6)
NEWLINE
X=-X; %FINISH
A2=1.
1:A1=A2
A2=.5*(A1+X/A1)
A1=MOD(A1-A2)
->1 %IF A1 > 0.0001 %AND A1 > .000001*A2
%RESULT=A2
%END
%ROUTINE RING BELL
%CYCLE I=1,1,50
PRINT SYMBOL(7)
   ! BELL (CTRL G) ON TELETYPE
%REPEAT
%END
%ENDOFPROGRAM
```

A C K N O W L E D G E M E N T S

This work was made possible by several people whose help I gratefully acknowledge. My supervisors, Malcolm Fluendy and Kenneth Lawley, were liberal with help, encouragement and champagne, and for the final year John McCall was an enthusiastic and capable colleague. Bill Stevenson provided mechanical know-how and much general assistance; Douglas Monroe did a tremendous job on the electronics side and Peter McInnes and Steven Hayes helped above and beyond the call of duty in the development of the computer system. I am also grateful to the Science Research Council for financial support and to Edinburgh University for laboratory, library and computing facilities.